P-11-28

Analysis of core material from the TRUE-1 site

Fracture mineralogy, fracture pore volume geometry and Cs sorption

Eva Hakami, Malin Johansson, Itasca Geomekanik AB

Johan Byegård, Geosigma AB

Henrik Drake, Isochrone Geoconsulting

Eva-Lena Tullborg, Terralogica

December 2014

Svensk Kärnbränslehantering AB
Swedish Nuclear Fuel
and Waste Management Co

Box 250, SE-101 24 Stockholm
Phone +46 8 459 84 00

SKB

ISSN 1651-4416
SKB P-11-28
ID 1390086
December 2014

Analysis of core material from the TRUE-1 site

Fracture mineralogy, fracture pore volume geometry and Cs sorption

Eva Hakami, Malin Johansson, Itasca Geomekanik AB

Johan Byegård, Geosigma AB

Henrik Drake, Isochrone Geoconsulting

Eva-Lena Tullborg, Terralogica

Abstract

The Tracer Retention Understanding Experiments (TRUE) project at the Äspö Hard Rock Laboratory comprise a number of field tracer and laboratory experiments performed in order to increase the understanding of transport of dissolved solids. The various experiments within the TRUE project have been performed in laboratory scale (< 0.5 m), detailed scale (5–10 m) and in block scale (10–50 m).

TRUE-1 Completion was performed, as a part of the TRUE-1 Continuation experimental programme, at the TRUE-1 site. The main activity within TRUE-1 Completion has been the injection of epoxy with subsequent overcoring of Feature A and A' and analysis of pore structure and identification of sorption sites. Furthermore, a number of complementary *in situ* experiments were performed prior to epoxy injection in order to collect important additional information about Feature A and the TRUE-1 site before the site is destructed by epoxy injection and overcoring.

This report describes analysis of core material in terms of fracture mineralogy, fracture pore volume geometry and Cs sorption. Core material from the overcoring of boreholes KXTT3 and KXTT4 were used in this study. After extraction of the drill cores it was noted that the epoxy had penetrated into the whole pore system of Feature A while the amount of epoxy was limited to the area close to the injection borehole in Feature A'.

Some of the core pieces including fracture surfaces of Feature A and A' were selected for further study. These samples were reinforced and cut into ca 1 cm thick slices which allowed studying epoxy layers in profiles. In total, 72 of the 244 slices were also studied using close-up images. About one third of the surface has simpler geometry with a single fracture plane without fragments and branches, while other parts show various degrees of a more complex pattern. The result of the aperture analyses for Feature A is that the mean cumulative aperture of the main fracture plane is about 0.45 mm and the aperture correlation distance is in the order of 75 mm. The results are similar when looking at Feature A in sample KXTT3 and KXTT4 separately.

Detailed investigations were carried out on the fracture coating material, where methods used included scanning electron microscope investigation and X-ray diffractometry. The samples from the two drill cores KXTT3 and KXTT4 generally show the same type of fracture mineral assemblies and deformation patterns, and the variation within the samples is generally larger than the variation between the different boreholes. Several generations of fracture coatings show that Feature A has been reactivated at several events and that it has been intermittently water-conducting for a very long time.

An extensive campaign was performed to measure the amount of sorbed radioactive tracer, Cs-137, on the overcored rock fracture surfaces from KXTT4, which was the injection borehole. The results of the measurements show that the distribution of Cs-137 is relatively homogeneous over the fracture surface of Feature A, while Cs-137 is found only in the vicinity of the injection borehole for Feature A'. The total amount of Cc-137 in the rock samples was estimated through the γ-spectrometry of the slices to 3 kBq for Feature A and 9 kBq for Feature A'. This may be compared to the 4.4 MBq which was the total amount not recovered in the pumping during tracer tests performed 10 years earlier.

Sammanfattning

TRUE-projektet (Tracer Retention Understanding Experiments) vid Äspölaboratoriet omfattar en serie spårämnesförsök och laboratorietester i syfte att öka förståelsen av transporten av lösta ämnen. De olika spårämnesförsöken inom TRUE har gjorts i laboratorieskala (< 0.5 m), detaljskala (5–10 m) och i blockskala (10–50 m).

TRUE-1 Completion utfördes, som en del av projektet TRUE-1 Continuation, vid experimentplatsen TRUE-1. Den huvudsakliga aktiviteten inom TRUE-1 Completion har varit injicering av epoxi och efterföljande överborrning av utvalda delar av de s.k. Feature A och A' samt analys av porstrukturen och identifiering av sorptionsplatser. Dessutom har ett antal fältexperiment gjorts före injiceringen av epoxi i syfte att säkerställa ytterligare information av Feature A innan försöksplatsen förstörs genom epoxiinjicering och överborrning.

Denna rapport beskriver analyserna av kärnmaterial i fråga om sprickmineralogi, sprickvolymer och sorption av Cs. Kärnmaterial från överborrningen av KXTT3 och KXTT4 användes vid dessa studier. Efter överborrning noterades att epoxi hade penetrerat i hela det överborrade sprickplanet av Feature A medan inträngningen av epoxi var begränsat till ett litet område vid injiceringshålet i Feature A'.

Några av de kärnbitar som gränsade till Feature A och A' valdes ut för att analyseras närmare. Sprickytan på dessa bitar förstärktes och kapades i ca 1 cm tjocka skivor, och epoxilagret kunde på detta sätt studeras i snittet längs profiler. Totalt 72 av de 244 skivorna studerades också genom närbilder. Cirka en tredjedel av den sprickytan har en enklare geometri på porvolymen med ett enda sprickplan utan fragment och förgreningar, medan övriga delar uppvisar ett komplext mönster av olika grad. Resultatet av sprickaperturstudierna visar att för Feature A är medelaperturen på huvudsprickplanet 0.45 mm och korrelationsavståndet i storleksordningen 75 mm. Resultaten är desamma om man ser på Feature A i prov från KXTT3 och KXTT4 var för sig.

Detaljerade studier har gjorts av sprickfyllnadsmaterialet på sprickorna, och de metoder som använts för detta är svepelektronmikroskopi och röntgendiffraktometri. Sprickproverna från de två borrkärnorna KXTT3 och KXTT4 uppvisar samma typ av sprickmineral och deformationsmönster, och variationen inom respektive provytor är större än variationen mellan borrhål. Ett flertal generationer av sprickfyllnader på ytorna visar att Feature A har reaktiverats vid ett antal tillfällen och att Feature A har varit intermittent vattenförande under en mycket lång tid.

En omfattande mätkampanj har utförts för att mäta mängden sorberat radioaktivt spårämne, Cs-137, på ytorna hos de överborrade bergsprickorna från KXTT4, vilket var det borrhål som använts som injektionshål i spårämnesförsöken. Resultatet av mätningarna visar att fördelningen av Cs-137 är förhållandevis konstant över provytan för Feature A medan Cs-137 finns endast i närheten av borrhålet vid Feature A'. Den totala mängden Cs-137 uppmättes genom γ-spektrometri av skivorna till ca 3 kBq från Feature A och 9 kBq från Feature A'. Detta kan jämföras med de 4.4 MBq som ej återfanns i pumpningen under spårförsöken utförda 10 år tidigare.

Contents

*Appendix 3 and 4 can be downloaded from www.skb.se/publications.
Direct link: http://www.skb.com/publication/2482382/

1 Introduction

1.1 Background

The Tracer Retention Understanding Experiments (TRUE) project included several field and laboratory tracer experiments performed in order to increase the understanding of transport of dissolved solids, especially sorbing radioactive tracers, in fractured rock. Processes that retard transport of solutes, such as diffusion and sorption, have been of particular interest. The various experiments within the TRUE project have been performed in laboratory scale (< 0.5 m), detailed scale (5–10 m) and in block scale (10–50 m). Presently, the First TRUE Stage (TRUE-1) (Winberg et al. 2000), and the TRUE Block Scale parts (Andersson et al. 2002a b, 2007, Poteri et al. 2002, Winberg et al. 2003) of the programme have been completed. A closely related project is the Long Term Diffusion Experiment (LTDE) (Widestrand et al. 2006, 2010, Byegård et al. 2010).

As part of the TRUE-1 Continuation experimental programme, it was decided that TRUE-1 Completion should be performed at the TRUE-1 site complementing already performed experiments. The TRUE-1 site is located at about 390 m depth in the Äspö Hard Rock Laboratory (Figure 1-1). At this site there in one main structure called Feature A. The main activity within TRUE-1 Completion is the injection of epoxy into this feature, which has previously been used for tracer tests, and subsequent overcoring of the fracture, analyses of pore structure and identification of potential sorption. Complementary in situ experiments were performed before the epoxy injection, made to secure important information from Feature A and the TRUE-1 area before destruction of the site (Nordqvist et al. 2015).

The borehole sections that were injected with epoxy resin and extracted by overcoring is KXTT3:S3 and KXTT4:T3 (Figure 1-2). These two borehole sections are connected through Feature A. The structural model established based on previous hydraulic and transport tests tells that Feature A consists of a single plane (Feature A) at the intersection of KXTT3:S3 and that this features has a splay (Feature A') such that two fracture planes intersects KXTT4:T3 (Figure 1-3). These flow paths, in Feature A and Feature A', are characterised from earlier investigations at the TRUE-1 site (Andersson et al. 2002c, Winberg et al. 2000).

This report describes how the rock cores were reinforced and cut into slices and how these slices were photographed and the images analysed. Pieces of the rock core have also been analysed by X-ray and microscopy and detection of Cs.

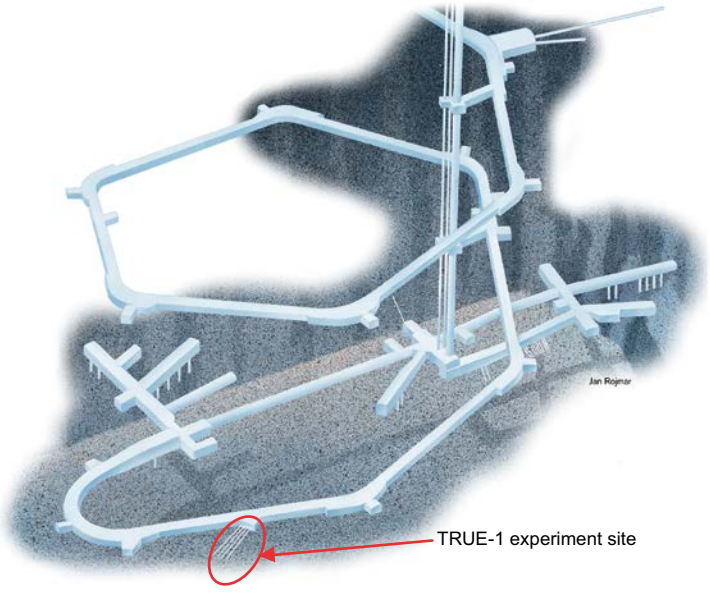

Figure 1-1. *View of Äspö HRL showing location of the TRUE-1 experiment site.*

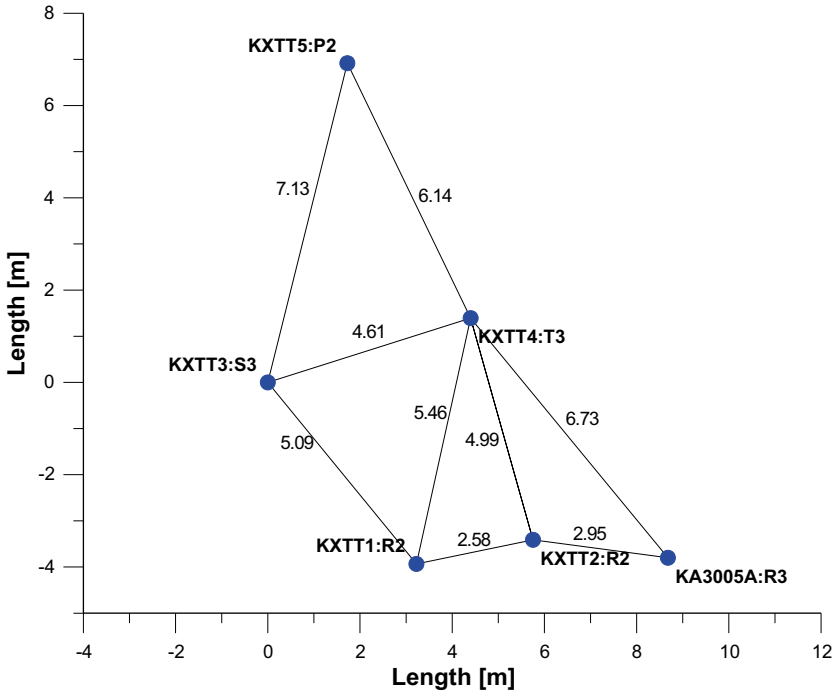

Figure 1-2. *Borehole intersection pattern with Feature A (as seen in the plane of the feature from the tunnel and inwards). Numbers between boreholes gives the Euclidian distance between borehole intersections. From Nordqvist et al. (2015) in which the tracer tests performed within TRUE-1 Completion are presented.*

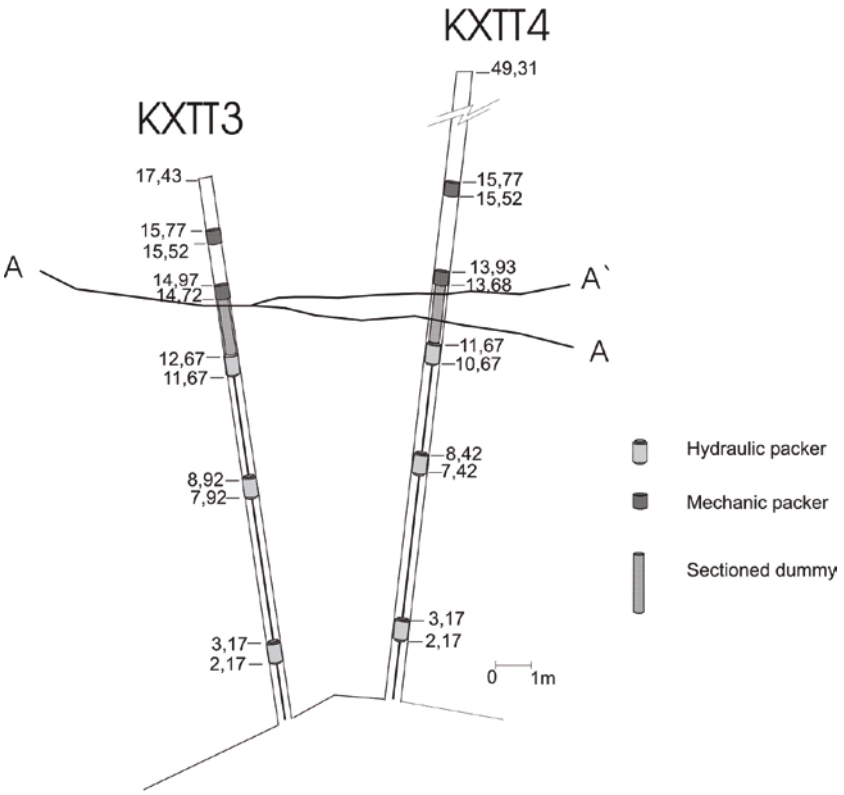

Figure 1-3. *Schematic drawing of the test sections and flow path used in the TRUE-1 completion campaign (Nordqvist et al. 2015).*

1.2 Objectives

1.2.1 General objectives

The general objectives of the TRUE-1 Completion are to:

1) improve the knowledge of the inner structure of Feature A and through epoxy injection and subsequent analyses, including improvement of the identification and description of the immobile zone(s) that are involved in observed retention effects.
2) perform complementary tests useful to the scientific understanding, including *in situ* K_d and SWIW tests.
3) improve the description of zones of immobile water that contributes to observed retention effects. The approach is identification and mineralogical-chemical characterisation of the sorption sites where Cs is found. Before overcoring the fracture, the Cs-signature must be enhanced.
4) update the conceptual microstructure and sorption models of Feature A.

1.2.2 Specific objectives

The specific objectives of the activities described in this report relate to the general objectives number 1 and 3 to enable update of the conceptual microstructure model and sorption models for Feature A.

The following questions were posed before the activities covered in this report started:

- How much, and what type of gouge material, is present in the feature?
- What does the aperture and porosity distribution look like?
- How much accessible fracture surface for sorption exists?
- Is it possible to prove channelised flow?
- What kind of differences may be found between intercepts of Feature A in KXTT3 and KXTT4?

1.2.3 Methodology

In order to provide data for answering the questions above, the specific goals for each step of the study were originally chosen to be the following:

1. to map Cs on open intact fracture surfaces in order to detect flow patterns during the tracer tests,
2. to photograph open fractures surfaces and analyse the images to detect the distribution of uranine tagged epoxy,
3. to prepare slices of rock, photograph them and analyse the images in order to quantify characteristics of the epoxy-filled pore geometry, which is expected to represent the (larger) pore geometry,
4. to prepare samples from the fracture surfaces and analyse them in order to detect and describe gouge material and fracture coating, and
5. to prepare rock samples in thin slices and analyse to describe mineral, texture, rim zone etc,
6. to prepare rock samples and analyse them for radioactive Cs in order to detect
   - flow patterns from previous tracer tests,
   - mineralogy connections to the sorption interaction surfaces.

1.3 Report structure

The description of where the drill samples were located in situ and how the cores were cut into smaller pieces is described in Chapter 2 and 3, respectively. In Chapter 4 the acquisition of images at different scales is presented. These images are used for image analysis and studies of the fracture aperture structure. This analysis methodology and associated results are presented in Chapter 5.

Chapter 6 deals with the mineralogical investigation which has been performed on samples from the fractures. This is followed by a reporting of the analysis of the radioactivity on the fracture surfaces in Chapter 7. The radioactivity emanates from the active Cs used in the tracer experiments previously performed at the site. A summary of the results from each of these investigations is given at the end of the corresponding chapter, and overall conclusions from the studies are drawn in Chapter 8.

2 Core samples location

2.1 Location of TRUE-1 site

The TRUE-1 site is located in conjunction with a niche of the access tunnel to the Äspö Hard Rock Laboratory at about 390 m depth (see also Figure 1-1). The structure studied, called Feature A, is a subvertical planar structure with an orientation of 331/79 (strike/dip) (Sigurdsson and Hjerne 2014), and A' is a subparallell fracture or splay to Feature A (see Figure 1-3). Epoxy was injected into two of the boreholes intersecting Feature A, KXTT3 and KXTT4 (Figure 1-2), and at these two intercepts a large diameter core (300 mm) was drilled to sample the feature around these two borehole intercepts. The techniques used to perform the epoxy injection and the overcoring is described in Sigurdsson and Hjerne (2014).

2.2 Structure geology of boreholes KXTT3 and KXTT4

According to earlier studies of the target sections in KXTT3 (12.67–14.92 m) and KXTT4 (11.67–13.68 m) (Sigurdsson and Hjerne 2014), the main rock type is medium to coarse grained, mainly massive Äspö diorite (porphyritic quartz monzonite to granodiorite) with minor amounts of fine-grained granite. The rock types are usually massive, with some deformation occurring in conjunction with Feature A. The main fracture filling mineral is chlorite, with lesser amounts of epidote and calcite. Chlorite and epidote occur in both open and closed fractures, while calcite only appears in open fractures within the target section of KXTT3.

The large diameter drill cores were mapped after the retrieval, and the results are shown in Figure 2-1. The map of KXTT3 and KXTT4 in Figure 2-1 shows the structures as they appear in the borehole wall, i.e. this map is directly comparable to the BIPS images from the original 56 mm pilot borehole. The notation at the right and left side of core refer to the directions when looking from the tunnel and inwards and top of core refers to the upward side of the drill core as oriented in the borehole according to the terminology presented in Sigurdsson and Hjerne (2014). From these maps it is noticeable where the main structure, Feature A, is located and where epoxy were found in fractures. The character of Feature A, having one major fracture plane, but also several minor fractures connected to the major plane may be understood from these mappings.

To enable keeping track of the different loose pieces of the core, each core piece was numbered as seen in Figure 2-1. In Figure 2-2 a close-up of the map at the section of Feature A in KXTT3 is shown. This map is a mirror image of the map in Figure 2-1, such that it show how the core looks like from outside (and not how the borehole wall looks like from the inside of the hole).

To enable further reference to the different part of the structure some name for the fracture planes were introduced. Without accurate knowledge of the apertures, one of the planes was selected as the main plane, Fracture 1, since it was judged on good grounds that this was the major fracture with evidences of shear displacement and with the largest aperture. The limitations of the study made it necessary to select only parts of the core for the detailed study. For this reason some of the pieces and some of the fractures surfaces were chosen for further study. In this report each fracture consists of two surfaces, *upper* and *lower*. The upper surface is the surface sitting on the piece closest to the tunnel (having the lowest length coordinate).

From Sigurdsson and Hjerne (2014) (cf. Appendix 1 and 2 therein) it is clear that several fractures in the target sections, also in the area around Feature A, may be interpreted as open since they contain epoxy. This character of Feature A, with several open fractures in the area of Feature A, has been kept in mind in the further studies and analysis of the results in subsequent chapters.

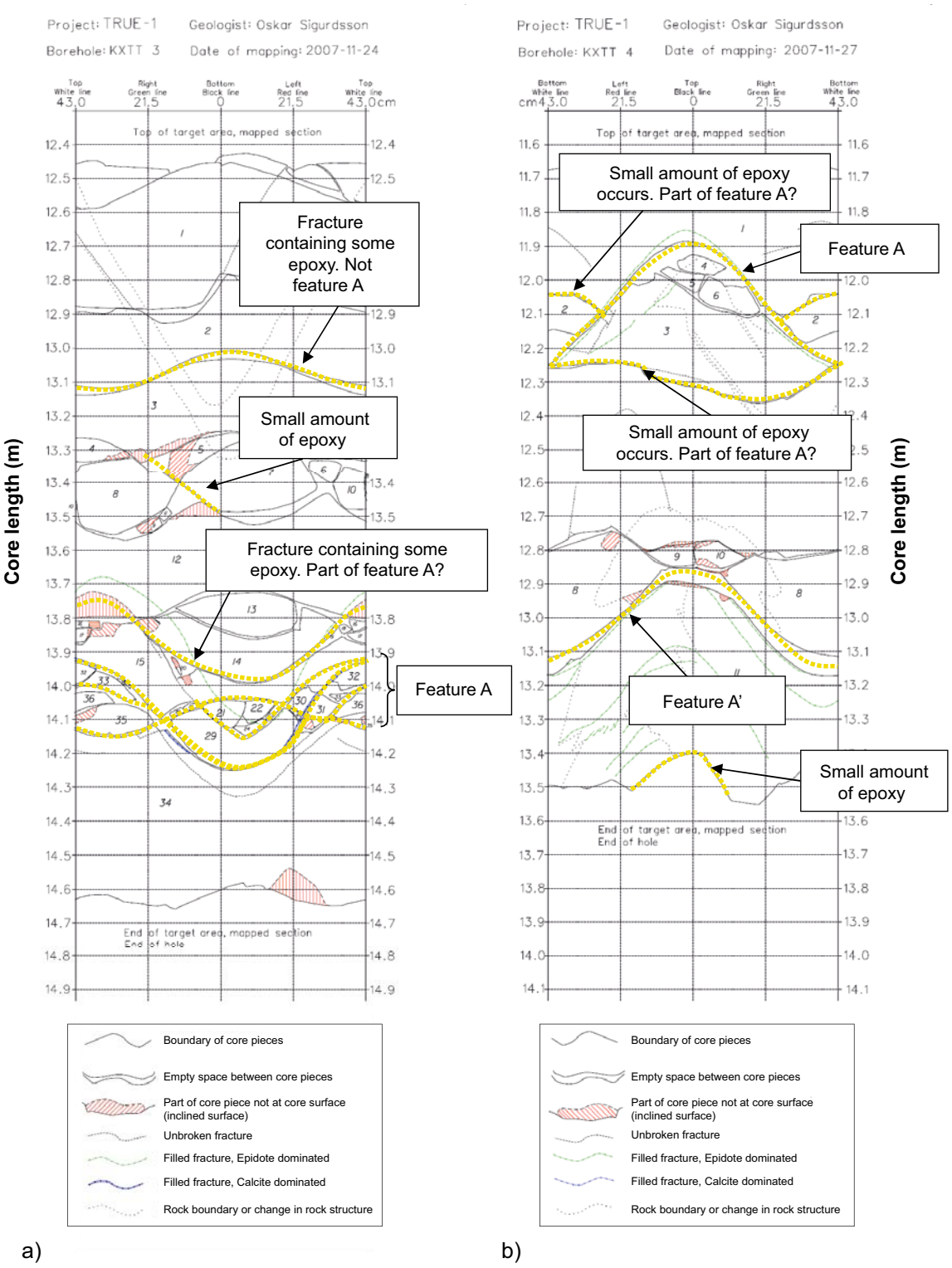

Figure 2-1. *a) KXTT3 b) KXTT4. These maps shows the structures as they appear in the borehole wall, i.e. this map is directly comparable to the BIPS images from pilot borehole. Dashed yellow lines indicate fractures containing epoxy. After Sigurdsson and Hjerne (2014).*

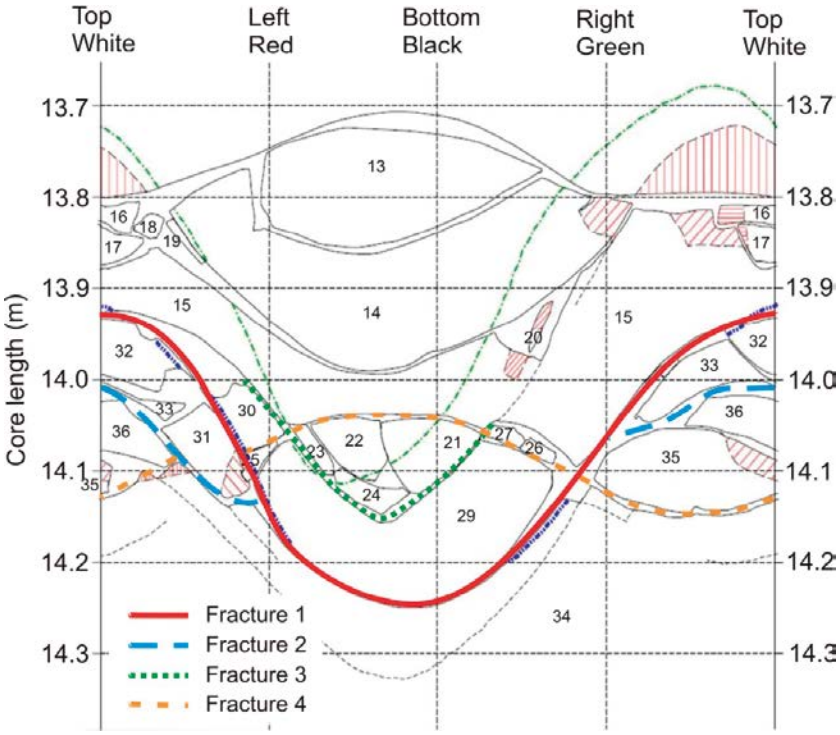

Figure 2-2. *Feature A in KXTT3. The picture shows how the drill core looked like (the map in Figure 2-1a shows the borehole wall and therefore this image is a mirror image). The numbers in the map is the core piece names. Modified from Sigurdsson and Hjerne (2014).*

2.3 General epoxy occurrence in KXTT3 and KXTT4

Since the epoxy was coloured with a strongly fluorescent dye it was easy to detect the epoxy occurrence using a UV (ultra violet) lamp. The epoxy occurrence on the open surface of the large diameter drill cores is reported, including many photographs, in Sigurdsson and Hjerne (2014). In the present study, overview photographs of some selected surfaces have been made. Examples from KXTT3 are given in Figure 2-3. The location of the surfaces may be understood from the piece numbering and fracture numbering in Figure 2-1. For more overview photographs of fracture surfaces, cf. Appendix 1.

The epoxy layer is slightly loose at some points and some minor pieces have fallen off (also see Sigurdsson and Hjerne 2014), but the selected surfaces for study seems to be largely intact. However, it is noteworthy that these photos show one of the surfaces and thus the corresponding opposite side may also have an epoxy layer. The darker areas in the fracture surface overview photographs should not necessarily be regarded as non-epoxy covered because the epoxy has in some areas a thin layer of clay materials that make the epoxy surface appear dark in UV-light. This circumstance was observed clearly by studying loose epoxy flakes from both the top and broken side in UV-light.

Similarly, examples of epoxy occurrence in photos from KXTT4 are shown in Figure 2-4, both from the Feature A and from Feature A'. It may be noted that the coverage of epoxy is much less in Feature A'.

It is not possible in this case to determine the smallest fracture the epoxy has penetrated since it depends on the injection pressure, distance from the injection borehole, hardening of the epoxy, connectivity of the fractures and pores.

Inside the borehole, the annular space used for injecting the epoxy has given a thick (1–2 mm) epoxy layer between the white plastic dummy and the borehole wall inside the injection section, which shows up very brightly in the photos.

It may be concluded that the injection of epoxy has been successful and that the epoxy occurs in most of the fractures intersecting the borehole. The amount of epoxy varies, depending on the fracture apertures, but in the major planes of Feature A the extent of epoxy penetration is at least to the perimeter of the drill core. In Feature A' the epoxy has penetrated only a few centimetres along the fracture plane.

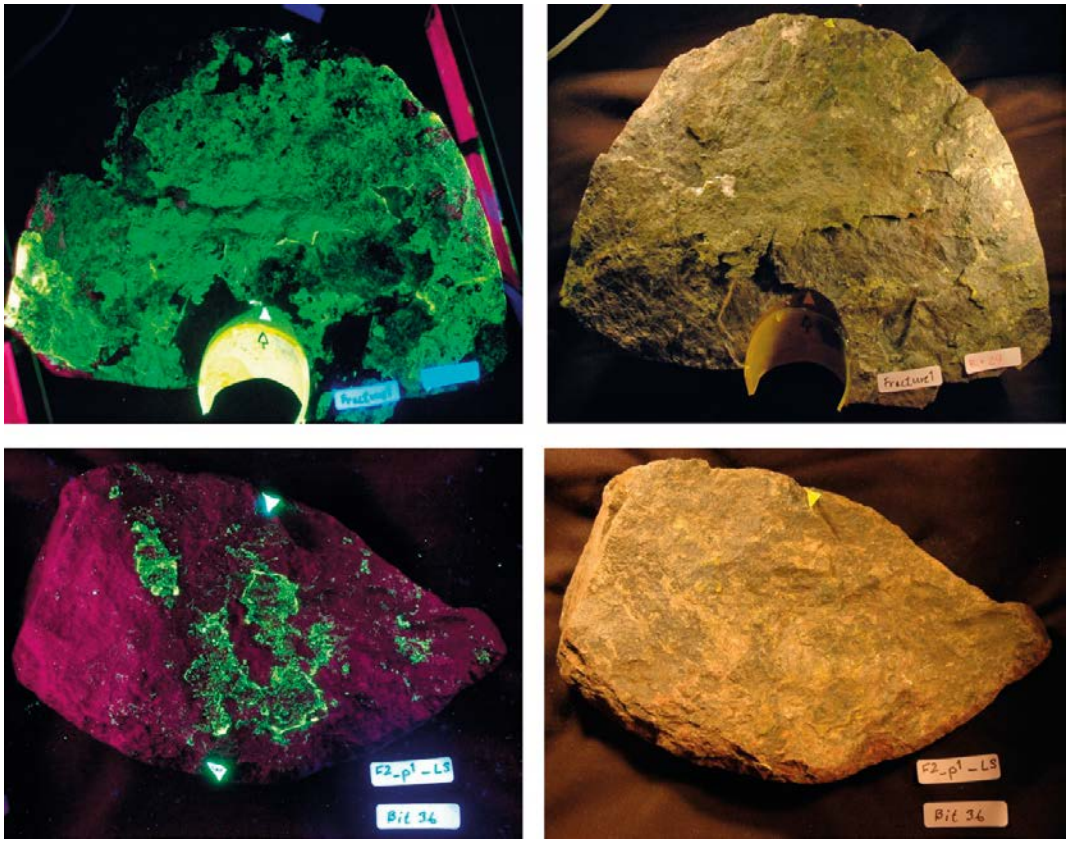

Figure 2-3. *Two example of surfaces on core piece from KXTT3, 29 (Fracture 1) and 36 (Fracture 3). Core piece 29 (upper two images) has a large amount of epoxy and piece 36 (the lower two images) has a varying amount of epoxy. The left images are acquired at UV-light and the ones to the right at ordinary light.*

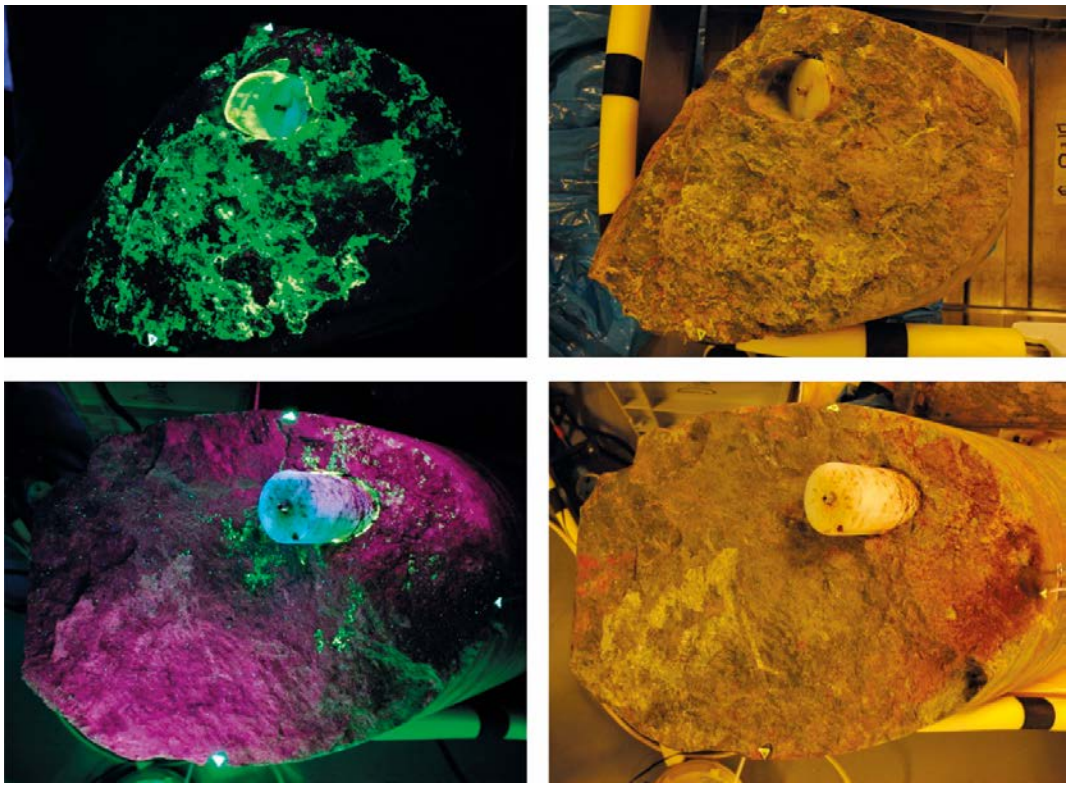

Figure 2-4. *Two example of surfaces on core piece from KXTT4, 3 (Feature A) and 11 (Feature A'). Core piece 3 (upper two images) has a large amount of epoxy and 36 (the lower two images) has a small amount of epoxy. The diameter of the drill cores is 278 mm.*

2.4 Selected fractures for analysis

From the recovered material in KXTT3 and KXTT4 some of the surfaces were selected for further study. Since one of the overall objectives of the studies was to characterise and describe the geometry of the pores that has governed the tracer test results, it was judged reasonable to focus the sampling to the fracture where the largest apertures were to be expected. To be able to analyse and describe spatial correlation of fracture aperture, sampling of continuous data from as large area as possible, was also desirable.

Further it was of special interest to take samples from both boreholes KXTT3 and KXTT4 such that the results could be compared. Finally it was of interest to characterise Feature A', although the apertures seemed clearly smaller, since preliminary overview radiation measurements with a portable contamination monitor indicated high values from this surface. Also the previous conceptual models for the flow in the TRUE-1 area (Winberg et al. 2000) has included the flow path in Feature A' and therefore a characterisation was desired.

Figure 2-5. *Researchers in the stage of selecting samples for study and planning the steps forward.*

After the first analysis of the two opposite (mating) surfaces it was concluded that the epoxy most often seemed to be present on one of the two sides, i.e. the epoxy layer was not split in itself (only sometimes if there was several subparallell epoxy layers). Therefore, it was decided to select the surface where most epoxy was present, and to consider the epoxy layer at a point on this surface as a fair estimate of the total aperture for this particular point of the common plane of the two fracture surfaces. By studying the loose pieces of epoxy with microscope it was realised that epoxy flakes that were almost constant in thickness, observable from the side of the flake, could look partly black in UV light on the surface, if the epoxy was covered by some fine material. Based on these two observations, is was concluded that it was not possible to directly use the *overview* photographs to do any kind of quantitative measurement regarding epoxy occurrence or apertures, although this had originally been planned, and that sectioning through the epoxy layer would be the only way for more detailed study.

3 Cutting of core samples into slices and rods

In order to carry out the analyses planned for the core material, it had to be cut into slices and rods. To be able to cut the core pieces into slices without destroying and dislodging the epoxy layer attached to the fracture surfaces, the surfaces were first reinforced with a layer of strong epoxy. The epoxy used was a two component, fast-gelling room temperature curing epoxy (EPO-TEK 302, Epoxy Technology Inc.) and a dark blue dye was added to ensure that this epoxy would not be mixed-up with the in situ injected fluorescent epoxy in the image analysis to follow. The epoxy layer was applied in a fairly thin (ca 1–5 mm thick) layer by pouring the epoxy onto the surface and when needed using a knife to spread it out over the surface. At surface edges where needed, modelling clay or tape was used to keep the reinforcement epoxy in place while hardening. Figure 3-1 shows an example of a core piece with the fracture surface covered with reinforcing epoxy. On top of this surface reference tapes were added to keep track of the relative coordinates of the slices.

Each sample was cut using a rock cutter into ca 1 cm thick slices, cf. Figure 3-2 and Figure 3-3. The larger cutter was needed to divide the larger pieces and to cut away excessive rock from the rock surfaces. The cut itself is about 5 mm wide when using the larger cutter. For the cutting of the smaller pieces into slices a smaller rock cutter was used. The cut from the blade was in the case about 2 mm wide. Some of the slices were further cut into even smaller pieces, denoted rods.

As expected, it was established after the overcoring that the core from the target section of KXTT4 was showing levels of radioactivity above the natural background due to previously performed tracer tests (Sigurdsson and Hjerne 2014). Hence, cutting (Figure 3-4) and analysis of the drill core sample from borehole KXTT4 was made at the intermediate storage for radioactive waste (CLAB), due to radiation protection measures and regulations. Exactly the same procedures and equipment for cutting and photography was otherwise used for these samples as for samples from KXTT3.

In Appendix 2, overview photographs of all slices are shown as they are put as a stack for each sample. A full overview and understanding of the available material for the following analysis can be obtained from this appendix.

Figure 3-1. *KXTT3, core piece 15 with reinforced surface and measurements tapes were added as reference lines before cutting.*

Figure 3-2. *The cutting of core pieces from KXTT3 into slices and rods.*

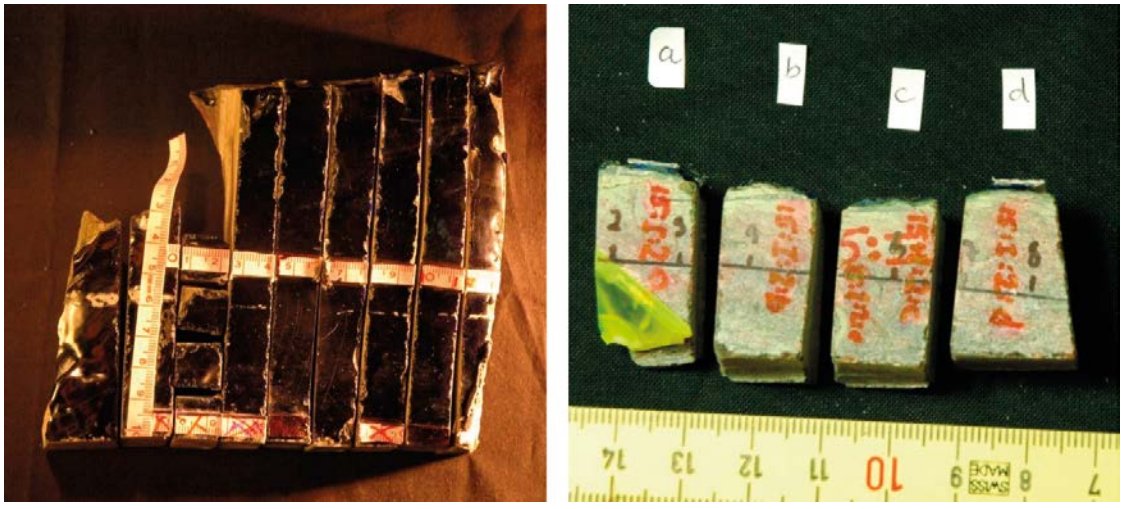

Figure 3-3. *Slices and rods of core piece 15 from KXTT3.*

Figure 3-4. *The cutting of core pieces in KXTT4 into slices and rods. This was made in a controlled area at CLAB (intermediate storage for radioactive waste) since the drill core displayed a radiation level above the criteria for free handling.*

Three different fractures planes have been studied, and each was given a separate orthogonal coordinate system in mm. The coordinate systems for the three fractures are only relative for each respective fracture plane and borehole. Thus the coordinate systems have no connection to the global coordinate system at the Äspö Hard Rock Laboratory, although it is possible to translate the local fracture coordinates to a global coordinates system since the position and direction of Feature A is known. For all fracture planes the origin of coordinates was placed in the centre of the original 76 mm borehole. Positive y-values are towards the top of the core.

In case of Fracture 1 (main fracture plane of Feature A) in KXTT3, sample slices from both the lower and upper surface are available, see Figure 3-5. The coordinate system for upper and lower surfaces is the same and the pictures may be simply combined (on top of each other without one being reversed) to obtain information on slices that are situated opposite each other. Positive values on the x-axis of Fracture 1 in KXTT3 are towards the left side of the core.

The distribution of the slices on the fracture plane of Feature A in drill core KXTT4 is shown in Figure 3-6, and the corresponding diagrams for Feature A' is given in Figure 3-7. Positive values on the x-axis of Feature A and A' in KXTT4 is towards the right side of the core.

The photography has been performed only on one side of the cuts and each such section or profile is given a name. The way of naming the profiles (and the rock slice to which it belongs has the same name) is the following: The first number refers to the original core piece (see Figure 2-1). The second roman number, I–IV, gives the part of the fracture surface (applies to the larger surfaces which were divided into smaller pieces). These different parts were later cut into slices in different directions to enable a study of anisotropic character. The third number indicates the slice and finally, in case of a rod, the order is given with a letter.

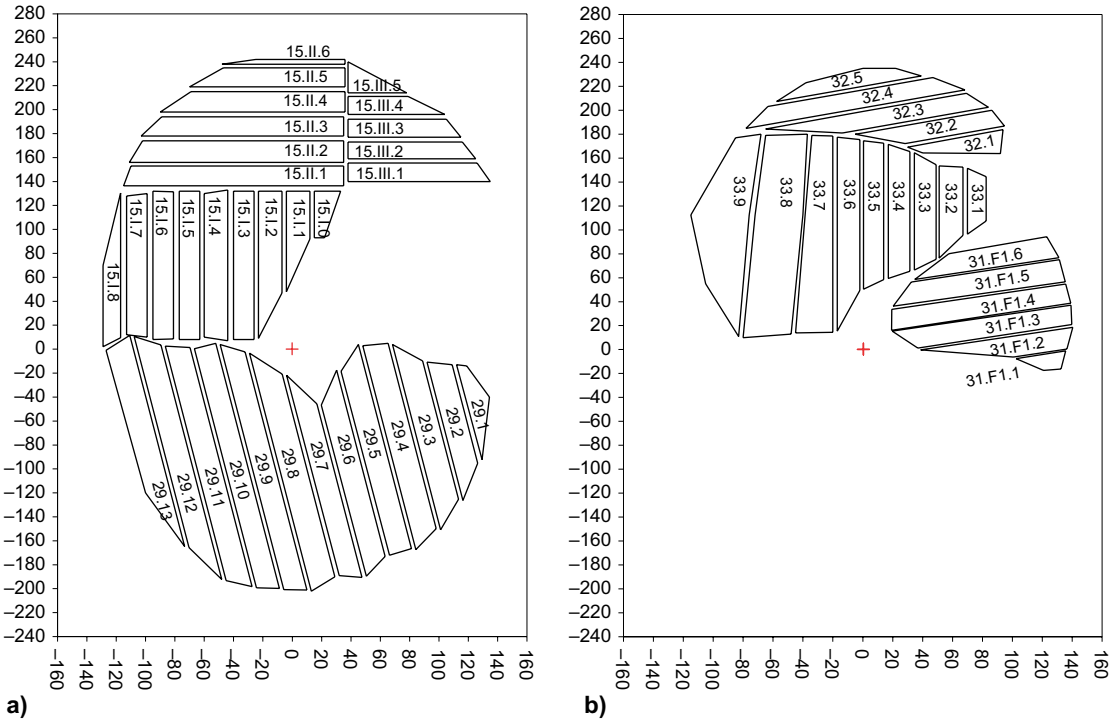

Figure 3-5. *Illustration of slices and fracture specific coordinate system of KXTT3, Fracture 1 a) upper surface b) lower surface. The y-axis is mm positive towards the top of the core. The x-axis is mm positive towards the left side of the core looking into the borehole.*

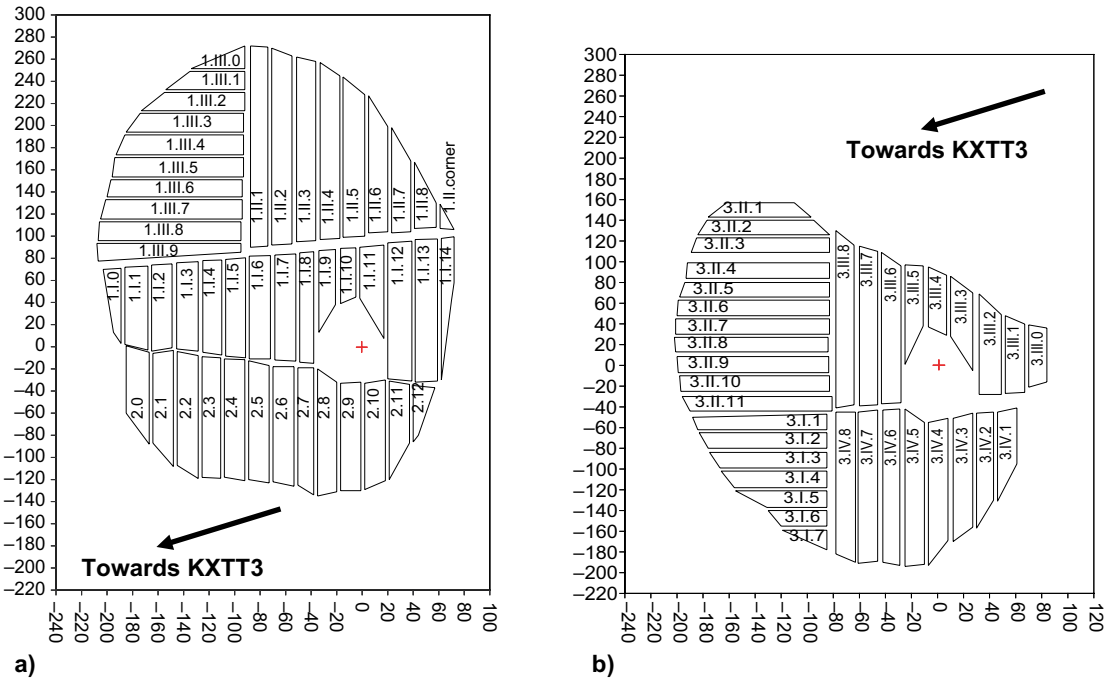

Figure 3-6. *Illustration of slices and fracture specific coordinate system of KXTT4, Feature A a) upper surface b) lower surface. The y-axis is mm positive towards the top of the core. The x-axis is mm positive towards the right side of the core looking into the borehole. The arrow shows the approximate direction from KXTT4 to KXTT3 along Feature A.*

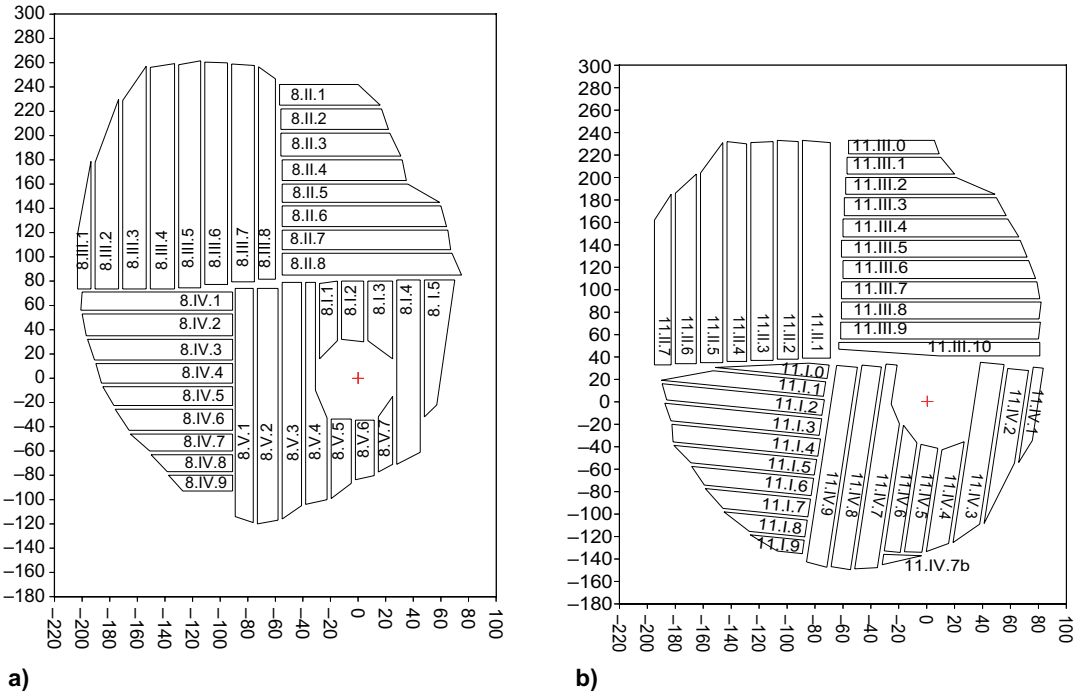

Figure 3-7. *Illustration of slices and fracture specific coordinate system of KXTT4, Feature A' a) upper surface b) lower surface. The y-axis is mm positive towards the top of the core. The x-axis is mm positive towards the right side of the core looking into the borehole.*

4 Close-up imaging of samples slices

A digital camera was used to take overview photographs. The overview photographs of the fracture surfaces are presented in Appendix 1. To take the close-up photographs a microscope (Sagitta stereoscope IS) was used, with a digital eyepiece camera (1.3 Megapixels) attached to it. For ordinary lighting two spotlights were utilised and for the UV-lighting two lamps were used as shown in Figure 4-1. Appendix 3 gives overview images of the whole slices while Appendix 4 presents all close-up images.

Not all available slices were photographed and those profiles that were selected for the close-up images are presented in Table 4-1 for KXTT3, in Table 4-2 for Feature A in KXTT4 and in Table 4-3 for Feature A' in KXTT4. The reason why so few photographs were taken for Feature A' was simply the fact that the amount of epoxy found on this surface was so small.

Examples of how the images look like in sections at different light conditions are illustrated in Figure 4-2 through Figure 4-6.

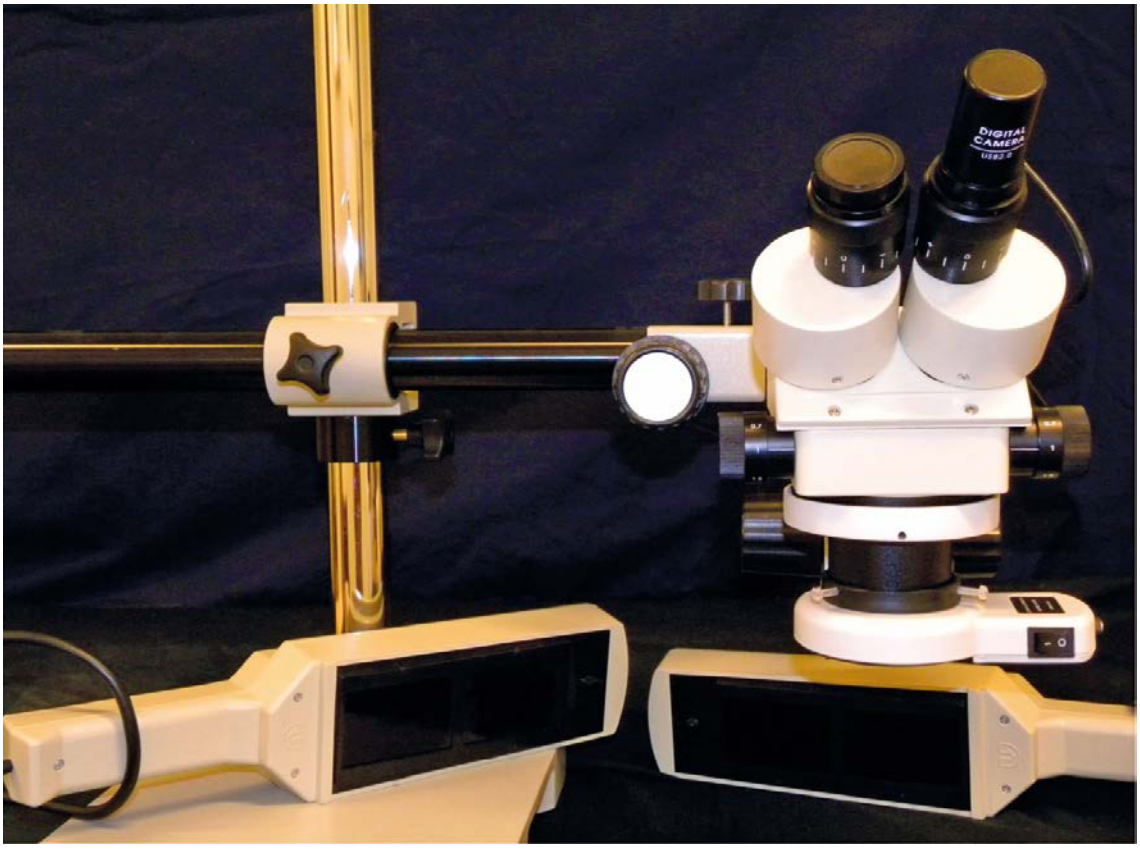

Figure 4-1. *The equipment used for taking close-up images; the microscope on a tripod, two UV lamps, one lamp used for ordinary lighting (together with two spotlights that is not shown in this picture) and the digital camera.*

Table 4-1. 60 of the 76 slices in KXTT3 have been photographed in close-up. A blank row means that the core piece does not have any slice with this name.

Slice no	Core piece [1]									
	15.I	15.II	15.III	21	29	31.F1 [2]	31.F2 [2]	32	33	36
0	N									
1	Y	Y	Y	N	N	N	N	N	Y	N
2	Y	Y	Y	Y	Y	Y	Y	Y	Y	Y
3	Y	Y	Y	Y	Y	Y	Y	Y	Y	Y
4	Y	Y	Y	Y	Y	Y	Y	Y	Y	Y
5	Y	Y	N	Y	Y	Y	Y	N	Y	Y
6	Y	N		Y	Y	N	N		Y	Y
7	Y			N	Y				Y	Y
8	N				Y				Y	Y
9					Y					Y
10					Y					N
11					Y					
12					Y					
13					Y					
14					N					

[1] Y/N = Yes/No to if the slice have been photographed in close-up.
[2] F1 and F2 stands for Fracture 1 and Fracture 2, see Figure 2-2.

Table 4-2. 11 of the 83 slices in KXTT4, Feature A have been photographed in close-up. A blank row means that the core piece does not have any slice with this name.

Slice no	Core piece [1]							
	1.I	1.II	1.III	2	3.I	3.II	3.III	3.IV
0	N		N	N		N	N	
1	N	N	N	N	N	N	N	N
2	N	N	N	N	N	N	N	N
3	N	N	N	N	Y	N	Y	Y
4	N	N	N	N	N	N	N	N
5	N	N	N	N	N	N	N	Y
6	N	Y	N	N	N	N	Y	N
7	N	N	Y	N	N	N	N	Y
8	N	N	N	N		N	N	N
9	N		N	Y		Y		
10	N			N		N		
11	N			N		N		
12	N			N				
13	Y			N				
14	N							

[1] Y/N = Yes/No to if the slice have been photographed in close-up.

Table 4-3. 1 of the 75 slices in KXTT4, feature A' have been photographed in close-up. A blank row means that the core piece does not have any slice with this name.

Slice no	Core piece [1]								
	8.I	8.II	8.III	8.IV	8.V	11.I	11.II	11.III	11.IV
0						N		N	
1	N	N	N	N	N	N	N	N	N
2	N	N	N	N	N	N	N	N	N
3	N	N	N	N	N	N	N	N	N
4	N	N	N	N	N	N	N	N	N
5	N	N	N	N	N	N	N	N	N
6		N	N	N	N	N	N	N	N
7		N	N	N	N	N	N	N	N
8		N	N	N		N		N	Y
9				N		N		N	N
10						N		N	

[1] Y/N = Yes/No to if the slice have been photographed in close-up.

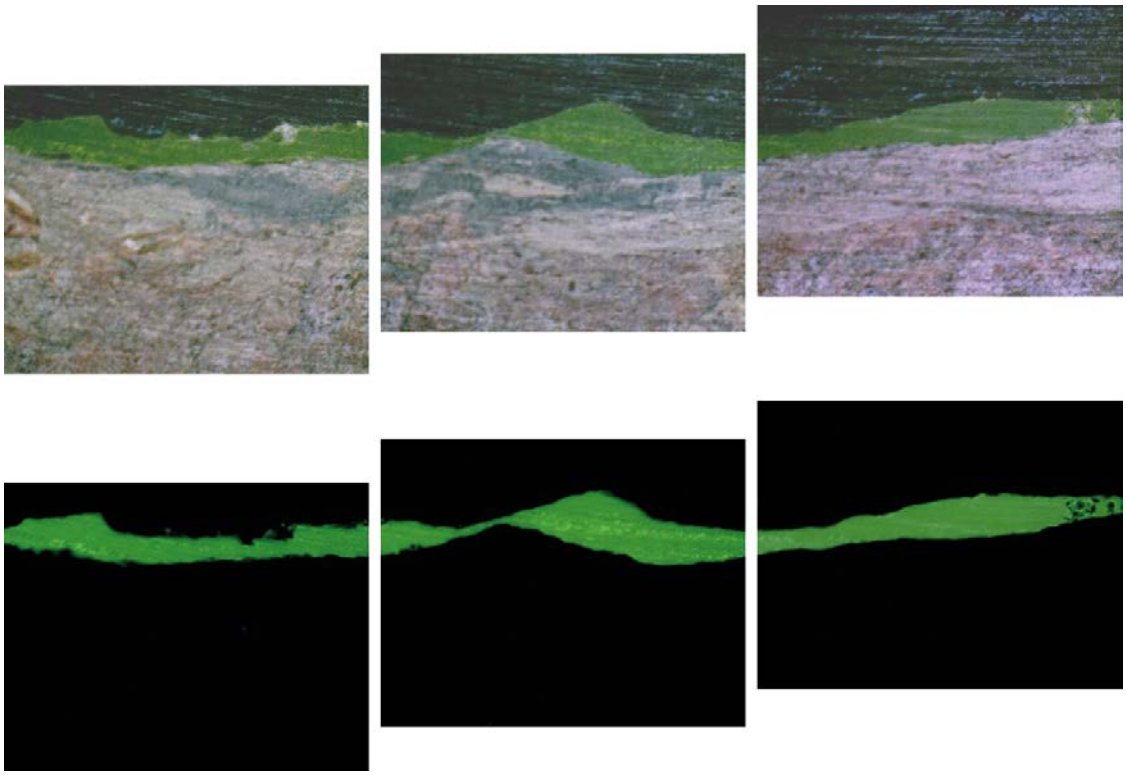

Figure 4-2. *Three close-up images (at both ordinary and UV ligh) for slice 9 of core piece 29 (photographs 29.9.14–29.9.16). The frame size is 12.8×10.3 mm (width × height).*

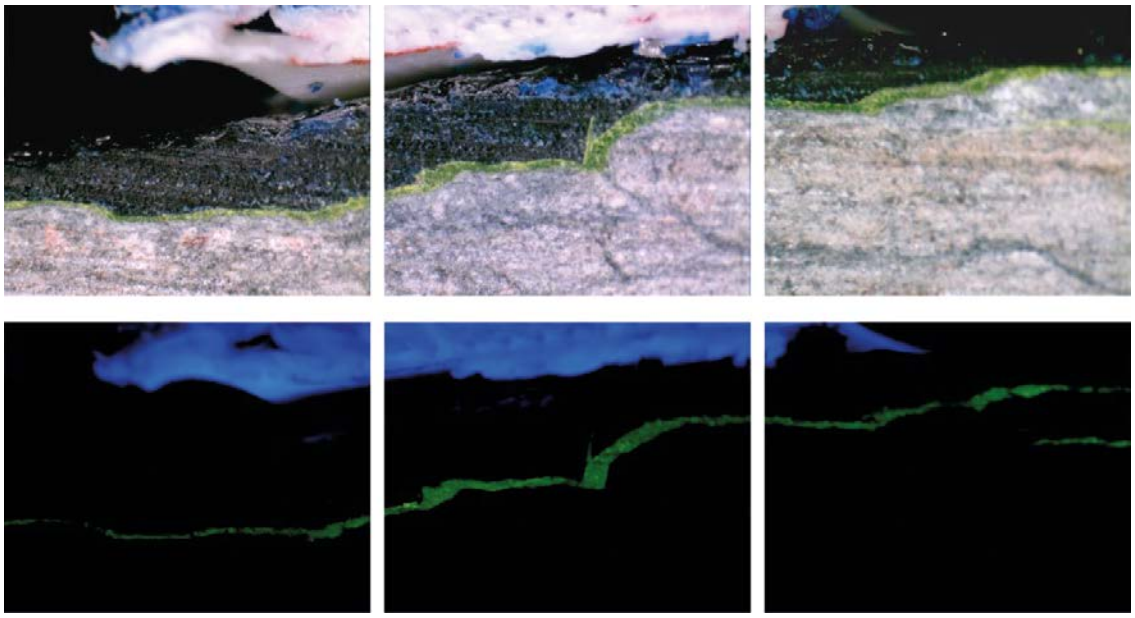

Figure 4-3. *Three close-up images (at both ordinary and UV light) for slice 2 of core piece 15.III (photographs 15.III.2.2–15.III.2.4). The frame size is 5.4×4.3 mm (width × height). This profile has a horizontal direction (cf. Figure 3-5) and the shear displacement of the fracture (in this plane) that can be inferred from the middle image corresponds to a sinistral strike-slip movement on Feature A. In most close-up images it is not possible to see any clear match between opposing surfaces and to infer any shear movement direction. The white in the photographs (blue in UV light) is a part of a measuring tape glued on top of the reinforced fracture surface.*

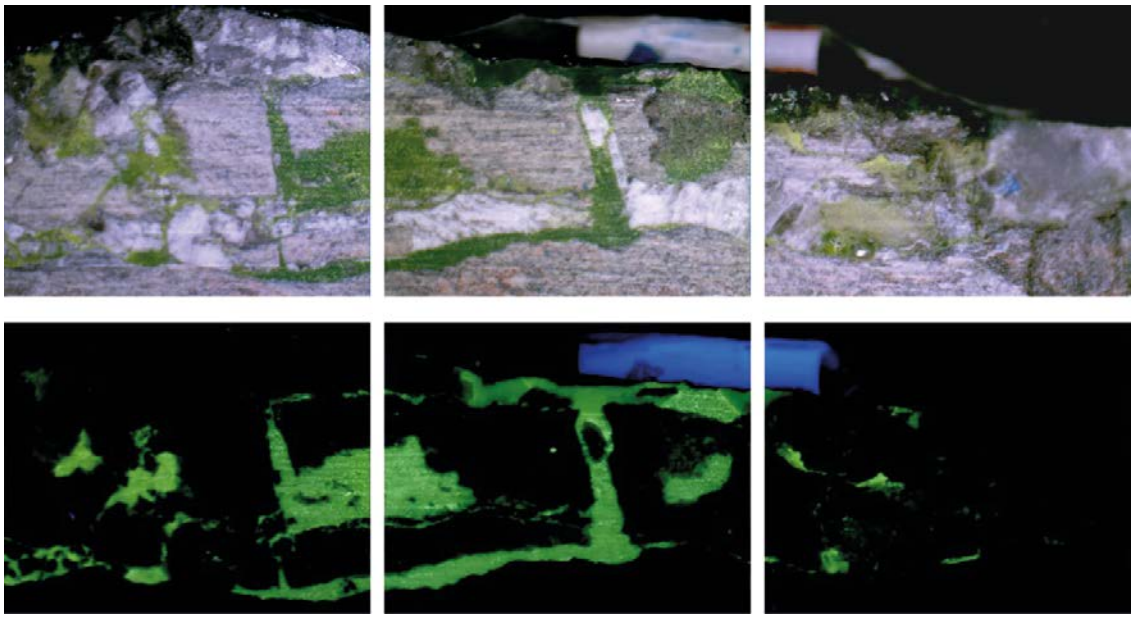

Figure 4-4. *Three close-up images (at both ordinary and UV light) for slice 2 of core piece 33 (photographs 33.2.3–33.2.5). The frame size is 12.1×9.6 mm (width × height). The white in the photographs (blue in UV light) is a part of a measuring tape glued on top of the reinforced fracture surface.*

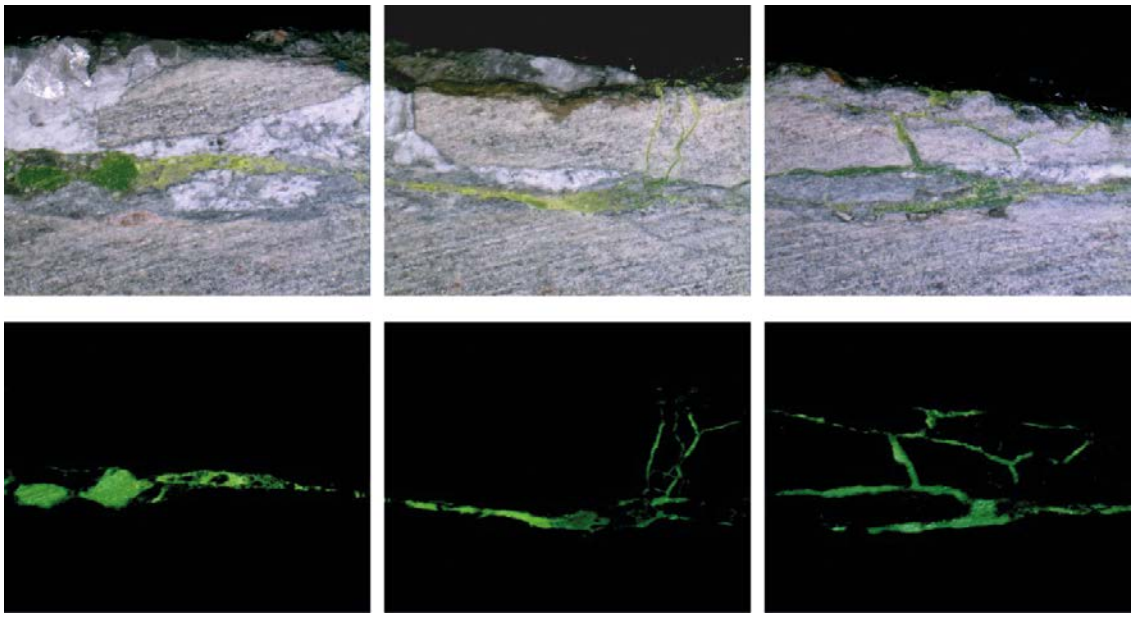

Figure 4-5. *Three close-up images (a both ordinary and UV light) for slice 6 of core piece 33 (photographs 33.6.3–33.6.5). The frame size is 9.6×7.7 mm (width × height).*

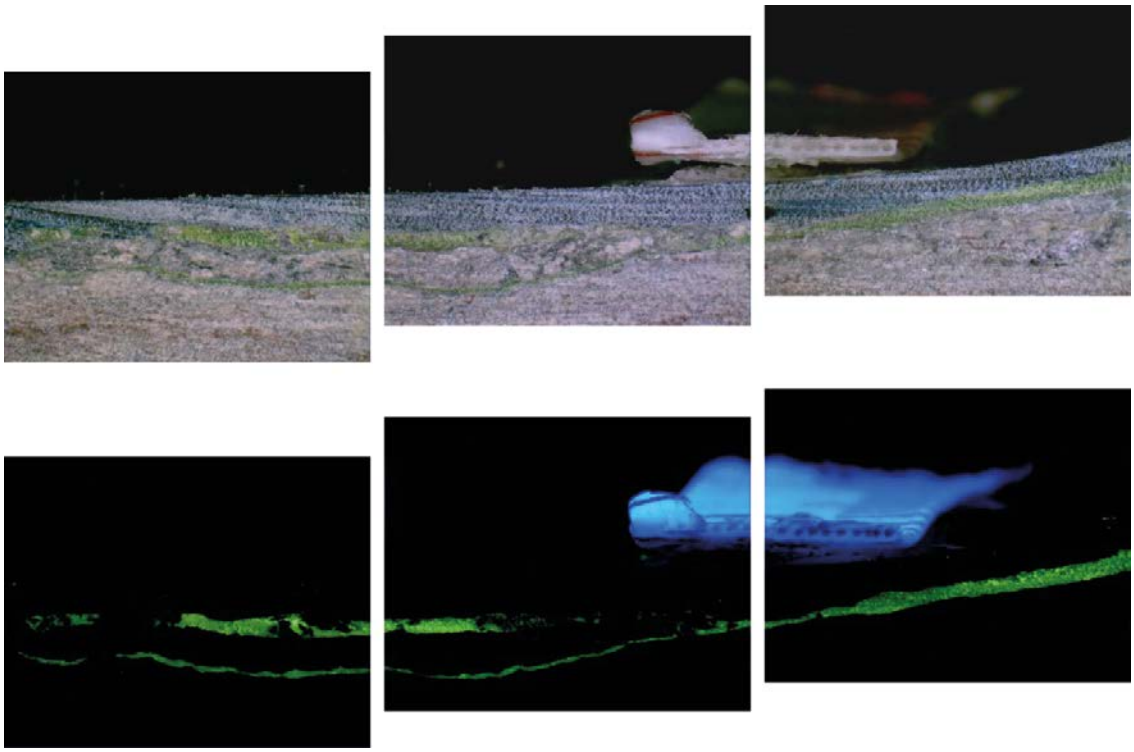

Figure 4-6. *Three close-up images (at both ordinary and UV ligh) for slice 2 of core piece 29 (photographs 29.2.3–29.2.5). The frame size is 10.9×8.7 mm (width × height). The white in the photographs (blue in UV light) is a part of a measuring tape glued on top of the reinforced fracture surface.*

5 Analysis of fracture pore volume

5.1 Methodology for pore volume analysis

5.1.1 Image pre processing

Each image, acquired as a colour image, will consist of one red, one green and one blue image (RGB). In this case we used the green image because the fluorescence has a yellow-green colour and this pre-processing had been successfully tested in a previous similar study (Hakami and Wang 2005). Using the intensity of this green image a threshold value was chosen to convert the image into a binary image (i.e. an image which consists of only black or white pixels). The binarisation was made using the computer program RockImage developed within the TRUE-project. The thresholding algorithm used was the BCV (between class variance), see further Hakami and Wang (2005). No other pre-processing procedures were applied in this study.

5.1.2 Categorisation of the pore volume geometry

To enable some quantitative characterisation of the variation of character over the fracture surface, the images were classified depending on the pattern of the epoxy in each image (Figure 5-1). As is illustrated in this figure the images sometimes show only one single open fracture plane and in other images the white pattern of the epoxy has a much more complex geometry due to fracture branches and rock fragments embedded in the fracture pore space.

For each image the number of subparallel fractures (or layers) may be estimated and this number is denoted N in Figure 5-1. Furthermore, an estimation of the total number of particles (fragments) surrounded by epoxy in the image may be made. This number is denoted P in Figure 5-1. The estimation of N and P was only used to help find the limits between the classes and to obtain some non-subjective description of the classes.

Apart from the classification (classes A–F) described above regarding the geometrical *character* of the actual fracture pore space, classification of the judged *quality* (intactness) of the fracture sample was made according to the following:

I No epoxy in the photograph (these images are not included in the statistics).

J Broken epoxy layer, looks like a piece have been lost (the mean cumulative apertures calculated are corrected for the missing part).

K Part of the epoxy layer is loose, some may have been lost.

L End pieces of a slice. Some epoxy may be lost at the end (the mean cumulative apertures calculated are corrected for the missing part).

M There is epoxy in the photograph, but not on the top surface. Epoxy might be stuck on the opposite fracture surface (i.e. stuck on another not analysed core piece), have been lost or never been there. These images are not included in the statistics.

N The epoxy layer is intact (this is the best quality class).

X Uncertain (not included in statistics).

5.1.3 Determination of mean aperture from close-up images

In each binary close-up image along the fracture profile the amount of epoxy can be calculated by counting the number of white pixels in the frame. The number of epoxy pixels multiplied with the pixel area divided by the width (in the picture frame) of the fracture covered by the image gives the average epoxy thickness over this distance. Each image is about 10 mm wide (the scale may be slightly different but the scale is known for each images). This average epoxy "thickness" is here used as the definition of the *mean cumulative aperture* parameter value, b_m, determined for each image, even in the case when the pore geometry is complex and actually consists of several epoxy layers. It is noteworthy here that the mean *cumulative* aperture, b_m, is thus not the same as the commonly used point aperture, which has also been measured along two shorter profiles as described in the next section. However, in a single fracture plane case the true mean of the point wise aperture in an image will be equal to the mean *cumulative* aperture b_m as defined here for the whole image.

Class A – Single plain fracture

N<1.2
Pd1

Picture to the right shows an example of classification J (broken epoxy layer)

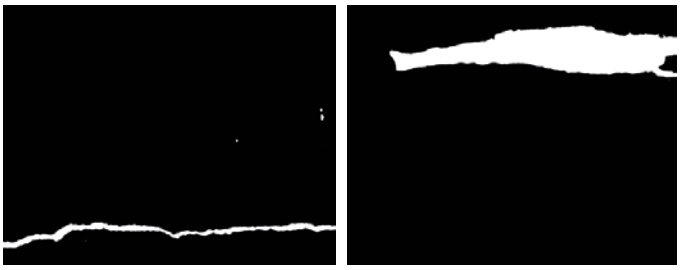

Class B – Single slightly complex fracture

1.2<N<2
1<P<3

Picture also show classification N (intact epoxy layer)

Class C – Two fractures without connection

N=2
Pd1

Class D – Thin fault with plenty of fragments and particles

2<N<3
3<P<10

Picture to the right shows an example of classification L (end of profile piece)

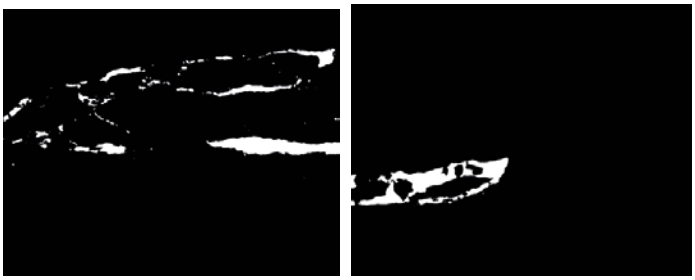

Class E – Fault zone; complex geometry

N>3
P>10

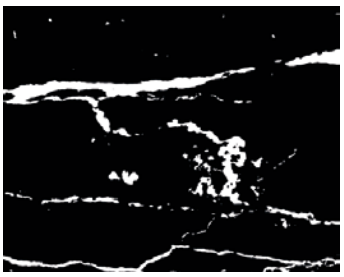

Class F – There is no epoxy

Figure 5-1. *All images were classified into different classes A–F depending on the complexity of the epoxy (white) pattern in the image. N is the estimated average number of sub parallel fractures (or layers) in the image. P is the estimated total number of particles (fragments) surrounded by epoxy in the image. Image width ca 11 mm.*

5.1.4 Detailed aperture measurements along selected profiles

In previous section it is described how the aperture was measured as a mean value over the whole width of the image. This means that the aperture variation and correlation for a smaller scale than the image size cannot be captured. Therefore we also selected a few short profiles where the aperture was measured as point values along the profile.

Figure 5-2, Figure 5-3, Figure 5-5 and, Figure 5-6 describe how this parameter is defined. The length of the lines at a constant distance in a direction perpendicular to the overall fracture plane (not the point wise shortest distance) is used to give the point wise aperture value. The aperture values measured along the profiles are presented as curves in Figure 5-4 and Figure 5-7, respectively.

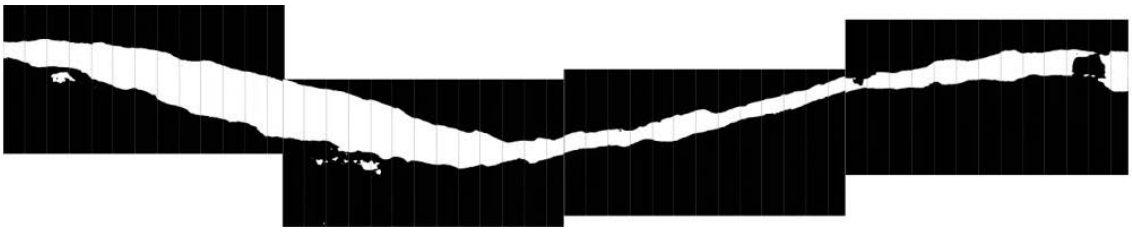

Figure 5-2. *Binary images of photographs 29.7.5 to 29.7.9 (belongs to Feature A in KXTT3). For a closer look (of the first image) see Figure 5-3. Each image is about 12 mm.*

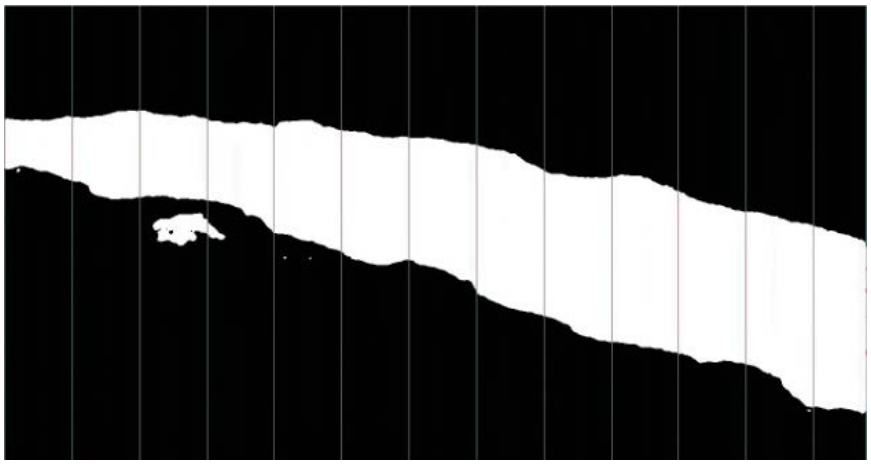

Figure 5-3. *Binary image of photograph 29.7.5 (see also Figure 5-2). The lines are one pixel thick and are placed approximately 100 pixels from each other (the last one is placed c. 80 pixels from the right side of the image). Where there is more than one line at the same x-distance their lengths are added, to represent the cumulative aperture of this point.*

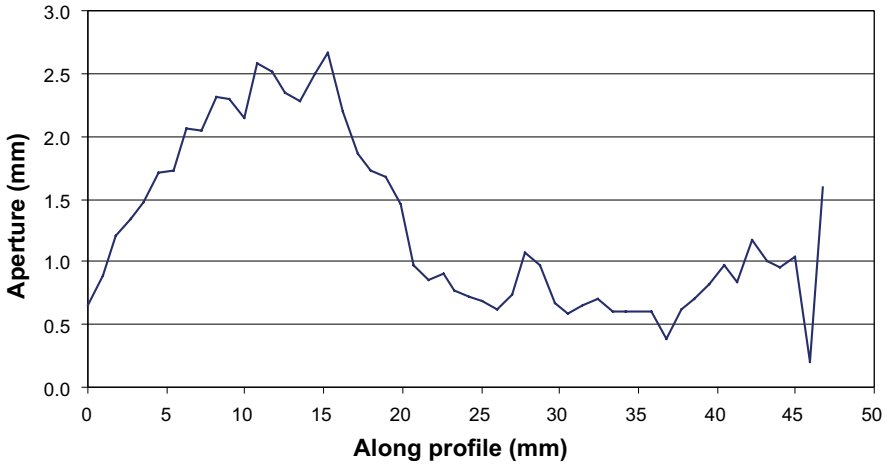

Figure 5-4. *Measured aperture values along part of profile on slice 29.7 (images 29.7.5 to 29.7.9), see images in Figure 5-2*

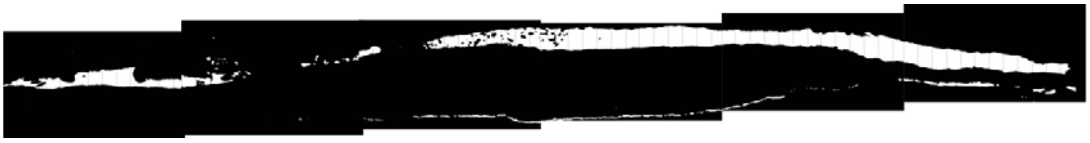

Figure 5-5. *Binary images of photograph s 3.IV.3.7 to 3.IV.3.12 (belongs to Feature A in KXTT4). For a closer look (of image 3.IV.3.10) see Figure 5-6.*

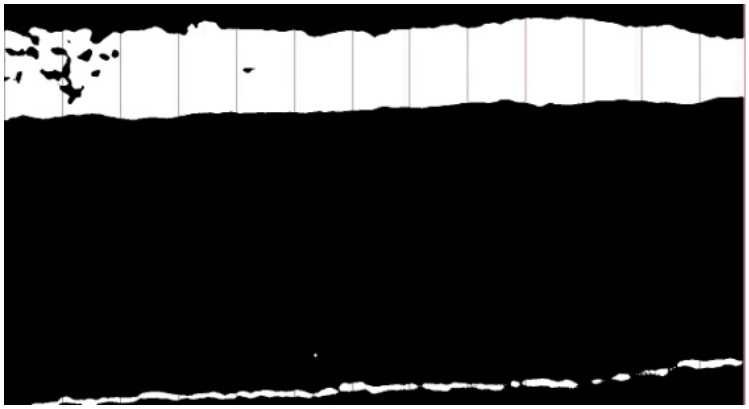

Figure 5-6. *Binary image of photograph 3.IV.3.10 (see also Figure 5-5). The lines are one pixel thick and are placed approximately 100 pixels from each other (the last one is placed c. 80 pixels from the right side of the image). The vertical length of the lines are used to calculate the aperture in each point.*

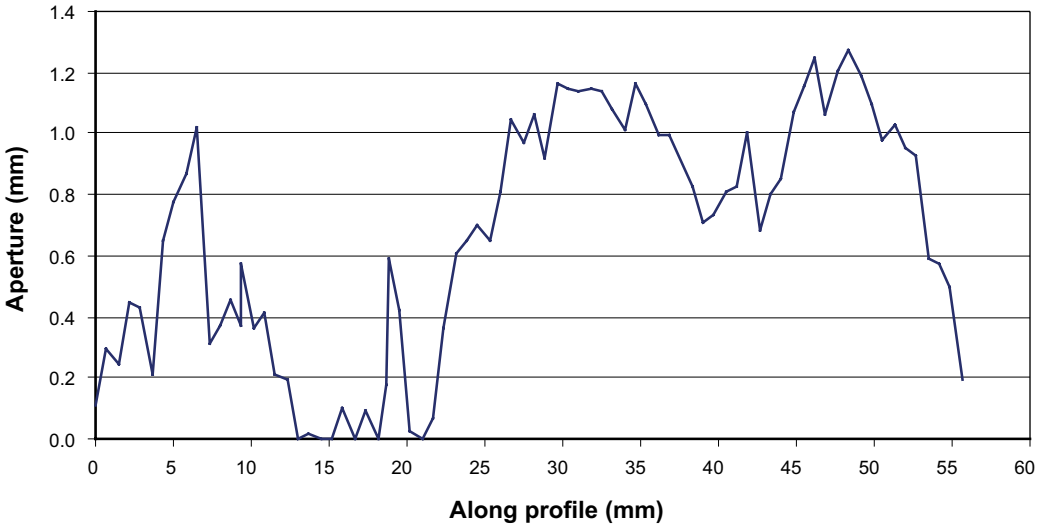

Figure 5-7. *Cumulated aperture(i.e. the sum of several apertures in the cases where there are several parallel fracture branches) along profile on slice 3.IV.3 (images 3.IV.3.7 to 3.IV.3.12), see images in Figure 5-5.*

5.2 Results of fracture pore volume analysis

5.2.1 Pore geometry classes

In Table 5-1 the results from classification of images are given for all analysed samples in terms of the number of images falling into each class. The percentage of images for each class is given in Table 5-2. It may be noted that three classes are almost equally frequent in the case of Feature A; the class with one single fracture plane, the single slightly complex fracture and the class denoted *thin fault with plenty of fragments and particles*. A variation in character is seen for all studied fracture samples. Particularly noteworthy is that the percentage number for Feature A at the borehole KXTT3 intersection is quite similar to the percentages for Feature A intersection at borehole KXTT4. If the division of classes is simplified by combining B and C, D and E, respectively, it is noted that Feature A has about one third in each category, A, BC, and DE.

The actual location of the images in the different classes may be understood from the diagrams in Figure 5-8 and Figure 5-9 for KXTT3 and KXTT4, respectively. The class F is the images which does not include any epoxy, and it may be noted that there is a tendency that such images are located in the outer part of the studied area, but not only in the outer parts. The class F images also tend to be located next to each other. This means, as already observed to some extent from the overall photographs of the fracture surfaces, that the epoxy layer did not cover the whole area. But we do not interpret this as true contact areas since it is also known that epoxy was stuck also to the opposite side of the fracture and that epoxy pieces have been lost from the samples.

Table 5-1. Total number of close-up images that has been classified into the different fracture classes (Figure 5-1).

	Fracture 1 KXTT3	Fracture 2 KXTT3	Feature A KXTT4	Feature A' KXTT4
A – Single fracture plane	122	4	31	0
B – Single slightly complex fracture	95	3	32	4
C – Two fractures without connection	8	0	7	0
D – Thin fault with plenty of fragments and particles	96	5	26	2
E – Fault zone; complex geometry	7	0	3	0
F – There is no epoxy	184	1	50	11
No of slices	43	1	11	1
No of photos	512	13	149	17

Table 5-2. Percentage of close-up images that has been classified into the fracture classes A–E (Class F not included in this calculation). The different classes are described in Section 5.1.2 and Figure 5-1.

	Fracture 1 KXTT3	Fracture 2 KXTT3	Feature A KXTT4	Feature A' KXTT4
A – Single plain fracture	37%	33%	31%	–
B – Single slightly complex fracture	29%	25%	32%	67%
C – Two fractures without connection	2%	–	7%	–
D – Thin fault with plenty of fragments and particles	29%	42%	26%	33%
E – Fault zone; complex geometry	2%	–	3%	–
No of slices	*41*	*1*	*11*	*1*
No of images in Class A–E	328	12	99	6

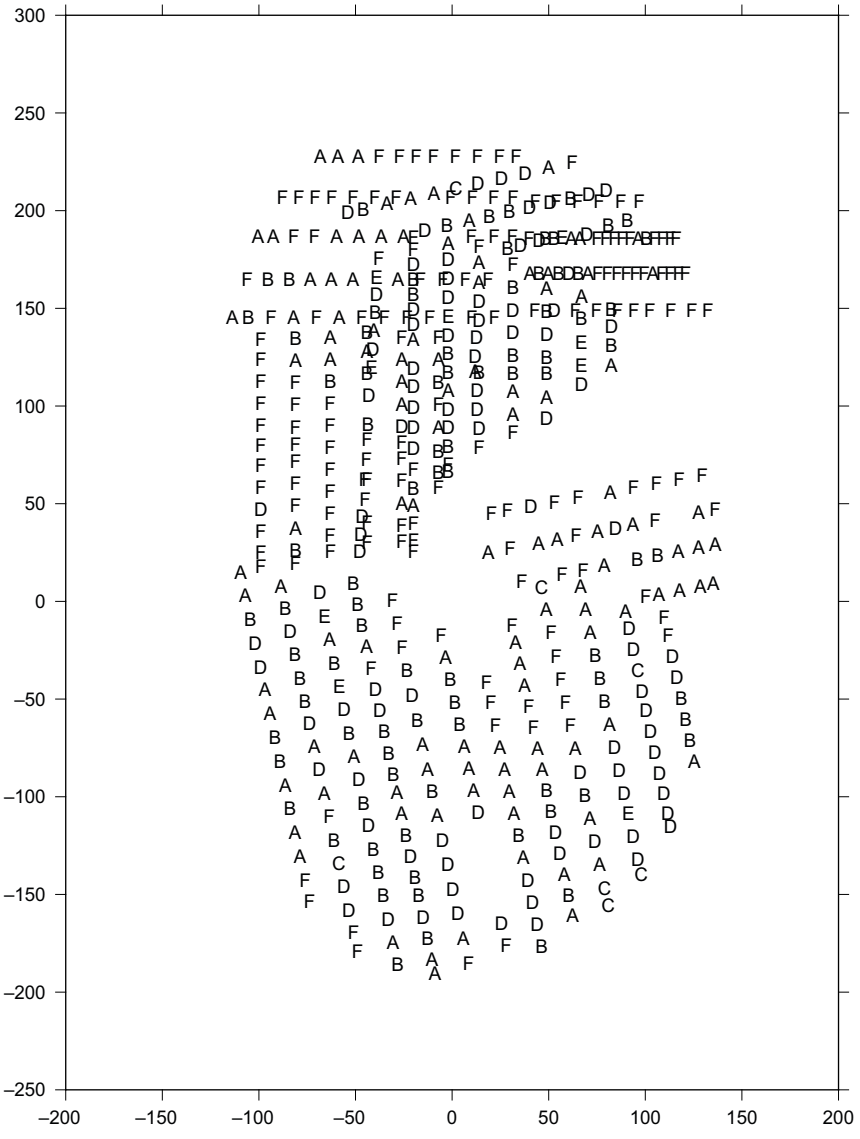

Figure 5-8. *A map showing fracture classification for KXTT3 Fracture 1. Results from both sides of the fracture shown on the same plane (x- and y-axes in mm).*

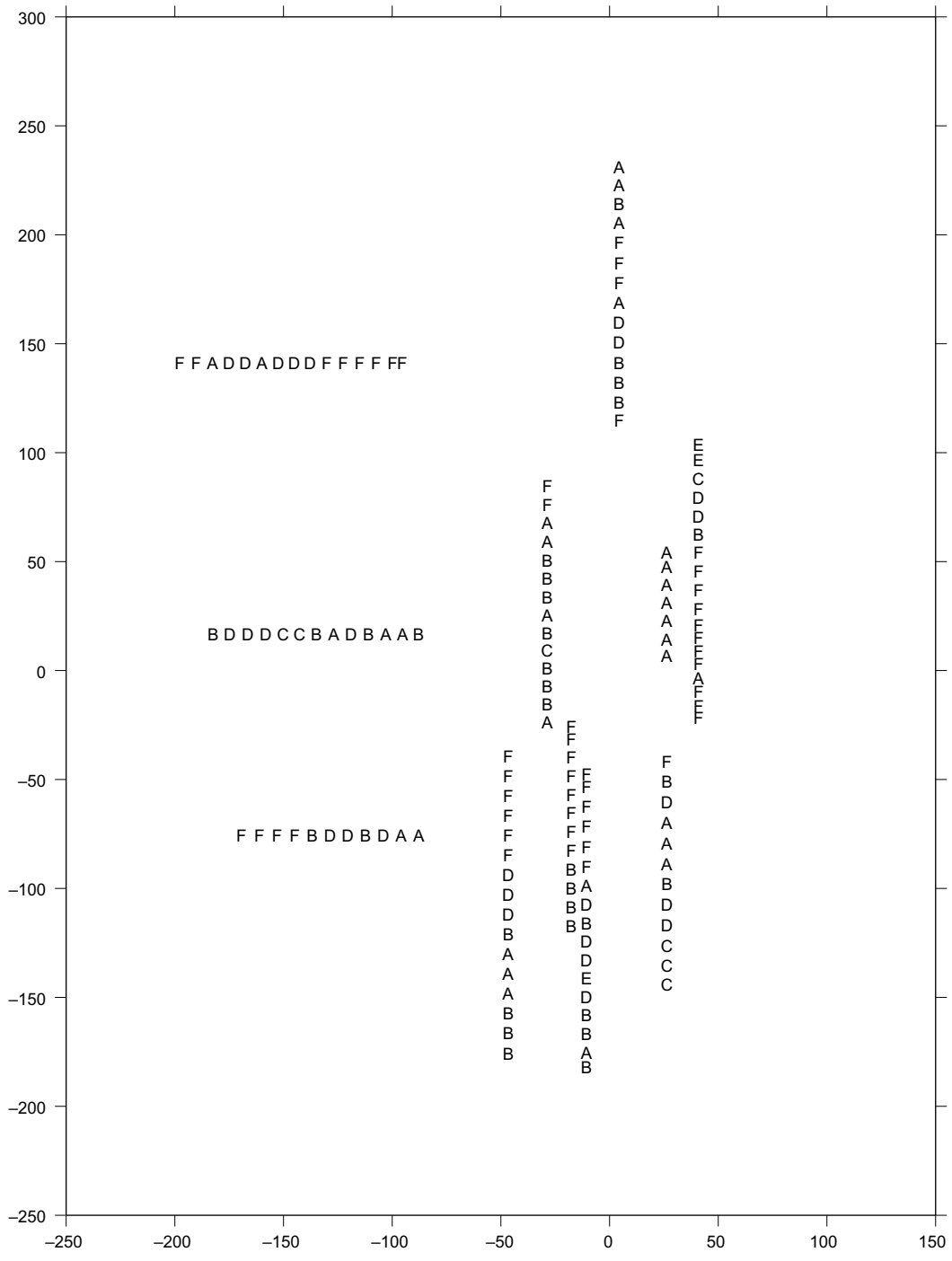

Figure 5-9. *A map showing fracture classification for KXTT4 Feature A (x- and y-axes in mm).*

Obviously, as can be noted from Figure 5-9, the spatial coverage of the close-up image data is much less for Feature A in KXTT4 compared to KXTT3. However the general appearance of the results seems similar. Also for KXTT4 there are areas where epoxy is missing but as for KXTT3 this not interpreted as contact areas (zero aperture) for the fracture. No clear correlation between image character class and the location (e.g.left/right/upper lower side) on the sample surface may be noted for any of the two samples.

As described in Section 5.1.2 the images were classified in terms of image quality. The results from this classifications indicate that quite many images (43 out of 661 from Fracture 1 of Feature A in KXTT3 and KXTT4) has an epoxy layer that is interpreted as being broken, i.e. abruptly cut. This is taken as a sign that it is correct to consider the epoxy layer originally having been almost continuously covering the surface (over the amples area), but with a varying geometrical character and aperture.

5.2.2 Aperture measurements

The mean *cumulative* aperture value was calculated for each close-up image, as described in Section 5.1.3. The results from the measurements are summarised in Table 5-3. From the aperture measurements it may be noted that the mean values are on the same order of magnitude for all classes of images for Feature A, in the span 0.25–0.80 mm. It should be remembered that since there is a complexity in the geometry the aperture entity is not possible to simply translate into the aperture of a single conductive plane. However, it is reasonable to expect that the sum of apertures is at least in the same order of magnitude at different points of the surface plane, because the overall separation of the two rock surfaces on each side of the movement plane is the same, when the rock blocks is sheared with respect to each other. At some points the shear plane may be divided into several and at some point it consists of a single plane. But extensive thick fracture infillings will naturally be a factor increasing the complexity and variability of the pore space.

Histograms for the mean apertures are presented inFigure 5-10 and Figure 5-11, respectively, for KXTT3 and KXTT4. (The Class F images are not included in the histograms, because they are judged to generally be places for "missing" epoxy, and not places for zero aperture, see Section 2.3.) Both histograms illustrates the typical logarithmic distribution for fracture apertures, with a long tail towards the upper values.

The spatial distribution of the measured mean cumulative apertures is illustrated by plotting a symbol of different size in the fracture coordinate system, see Figure 5-12 and Figure 5-13. It is noticeable that there is a clear spatial correlation in the aperture, with areas of larger apertures being concentrated. Obviously this impression may be slightly influenced by the distribution of the data collection points itself. A more objective and quantitative estimation of the spatial correlation may be obtained by calculating the variogram of the aperture data. This is performed in the next section.

Table 5-3. Average values of the measured mean cumulative apertures of the images. The images that did not include any epoxy at all, or had a broken epoxy layer (classes I and J for image quality) are not included in the calculation of average values. (cf. Figure 5-1 for examples of the different classes).

	Fracture 1 KXTT3	**Fracture 2 KXTT3**	**Feature A KXTT4**	**Feature A' KXTT4**
Class (see Section 5.1.2)	**Mean cumulative aperture, b_m (mm)**	**Mean cumulative aperture, b_m (mm)**	**Mean cumulative aperture, b_m (mm)**	**Mean cumulative aperture, b_m (mm)**
A – Single plain fracture	0.35	0.63	0.25	–
B – Single slightly complex fracture	0.46	0.41	0.55	0.02
C – Two fractures without connection	0.50	–	0.78	–
D – Thin fault with plenty of fragments and particles	0.45	0.52	0.51	0.08
E – Fault zone; complex geometry	0.80	–	0.67	–
Average (Class A–E)	0.42	0.52	0.48	0.04
No of slices	24	1	11	1
No of photos	296	11	91	6

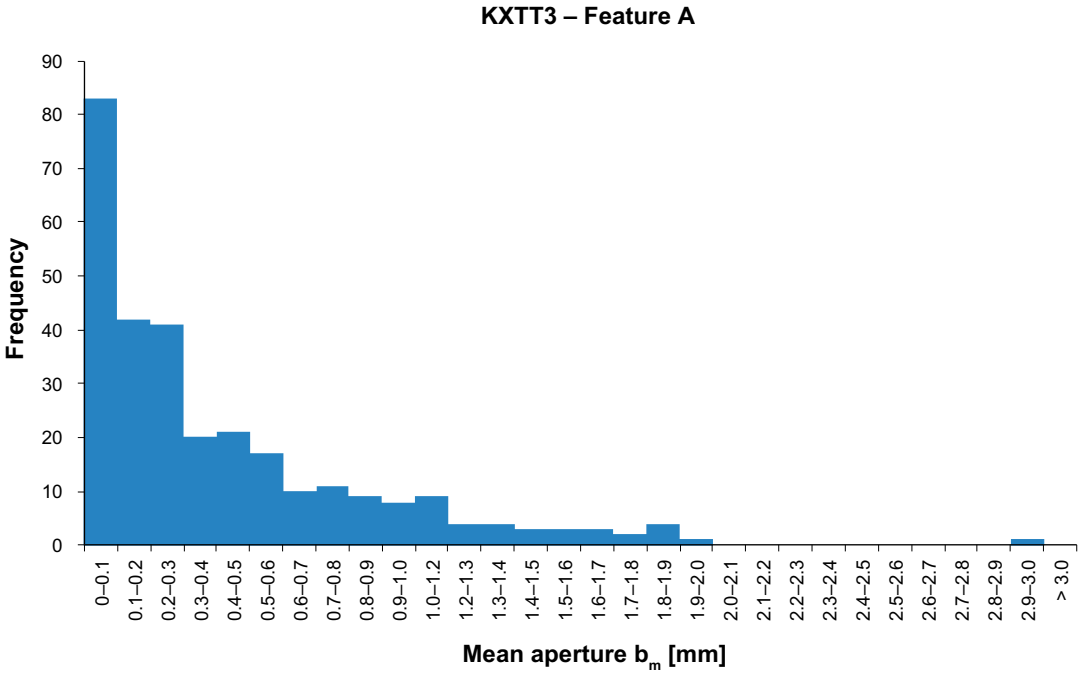

Figure 5-10. *Histogram of the mean apertures, bm, measured from KXTT3, Feature A. The class F (no epozy in the whole image) are not included.*

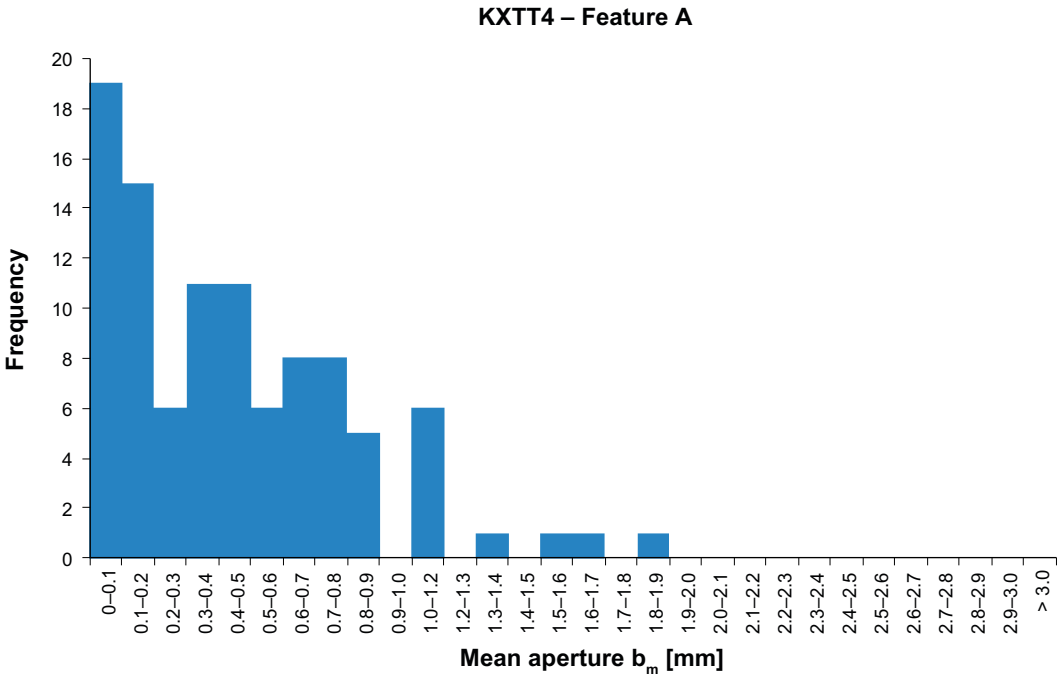

Figure 5-11. *Histogram of the mean apertures, bm, measured from KXTT3, Feature A. The class F (no epozy in the whole image) are not included.*

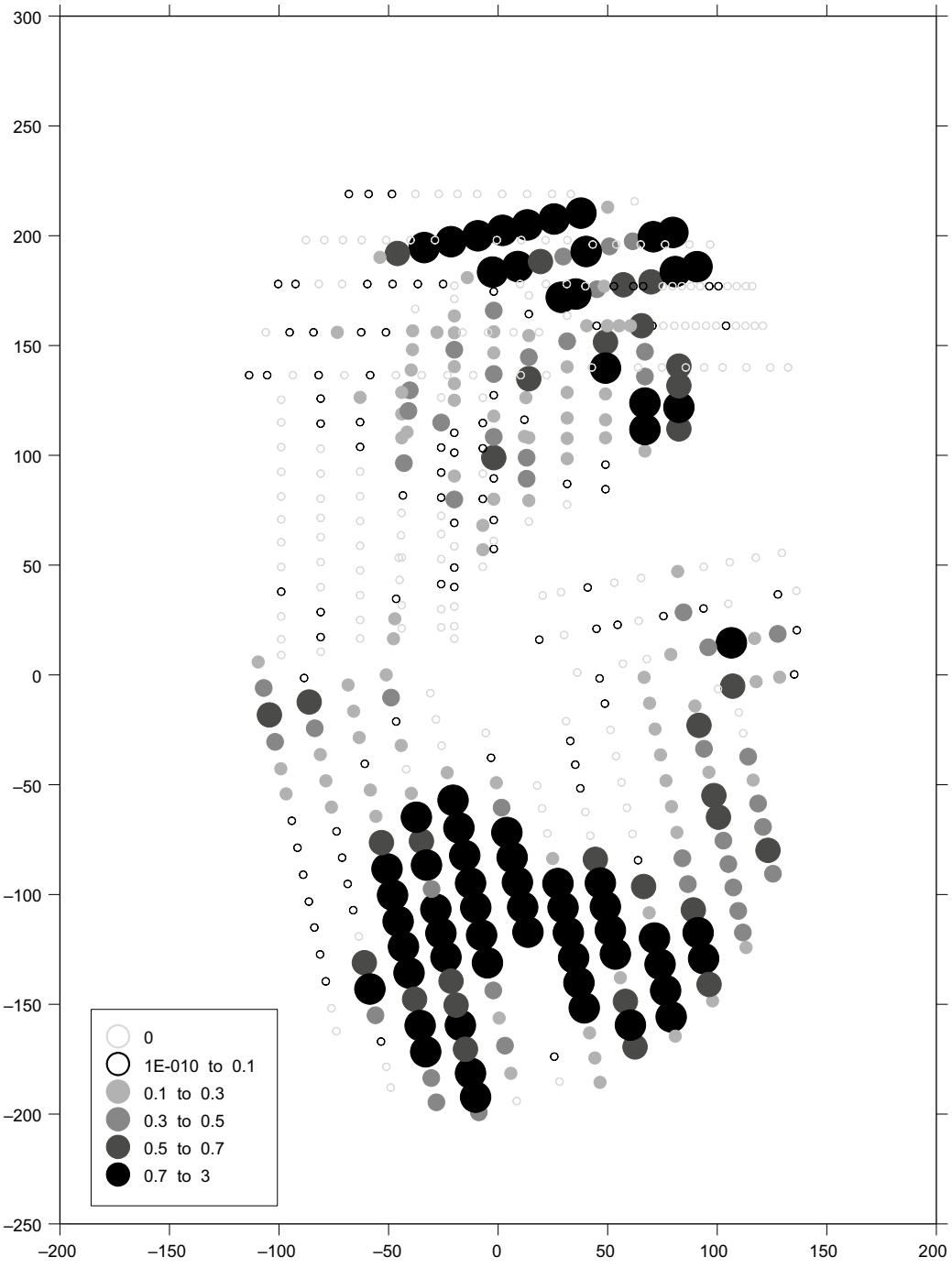

Figure 5-12. *A map showing mean cumulative aperture, b_m in mm, for all of the photographs (both upper and lower surfaces) taken for KXTT3 Fracture 1 (x- and y-axes in mm). If an upper surface photo is exactly opposite one from the lower surface, their b_m-values are added together.*

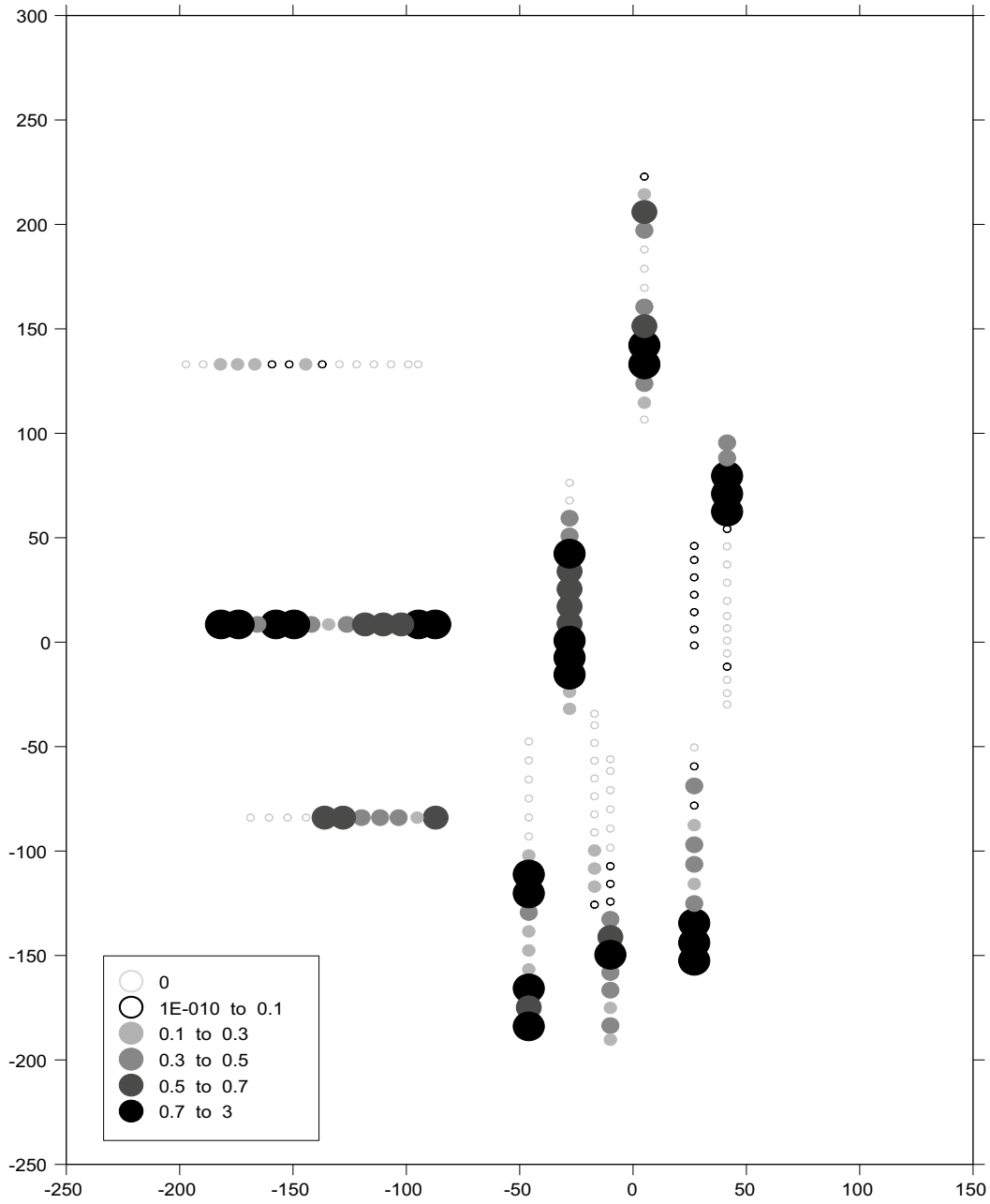

Figure 5-13. *A map showing mean cumulative aperture, b_m in mm, for all of the photographs (both upper and lower surfaces) taken for KXTT4 Feature A (x- and y-axes in mm).*

5.2.3 Spatial correlation of fracture aperture

The best way of accurately calculating the spatial correlation would be to have access of dense point wise data on a regular grid from as large a continuous surface area as possible. In this particular case only point wise measurements for short distance of two short examples (Section 5.1.4) were made available. On the other hand, based on the maps of mean cumulative aperture data from the close-up images previously shown in Figure 5-12 and Figure 5-13, we expect the spatial correlation of the apertures to be clearly longer than 10 mm. If the correlation distance is clearly longer than the size of the close-up images, this means that the variogram from the mean cumulative apertures from these images can still be used to estimate the correlation distance for the apertures.

Figure 5-14 gives the resulting aperture variogram from the two short profiles from KXTT3 and KXTT4 with point wise data. However, the sample behind these curves is too small, i.e. only single profiles and also too few profiles, too enable any firm conclusion regarding the actual spatial correlation. Nevertheless, both variograms show increasing values for at least 30 mm lag distances, which supports the use of the mean cumulative aperture data for further analysis of the spatial correlation.

Figure 5-15 gives the two variograms from mean cumulative apertures on the main fracture in Feature A where it intersects borehole KXTT3 and KXTT4, respectively. It can be concluded from these two variograms that the practical range (correlation distance) is in the same order for both samples. Also, the overall variation in the aperture data (the sill level) is of the same order (0.18–0.22 mm^2) for both samples.

A practical range around 75 mm for Feature A apertures is in agreement with the results from previous studies concerning aperture distributions (Hakami 1995), in which the spatial correlation distance is seen to be correlated to the mean cumulative aperture and in particular to the coefficient of variation.

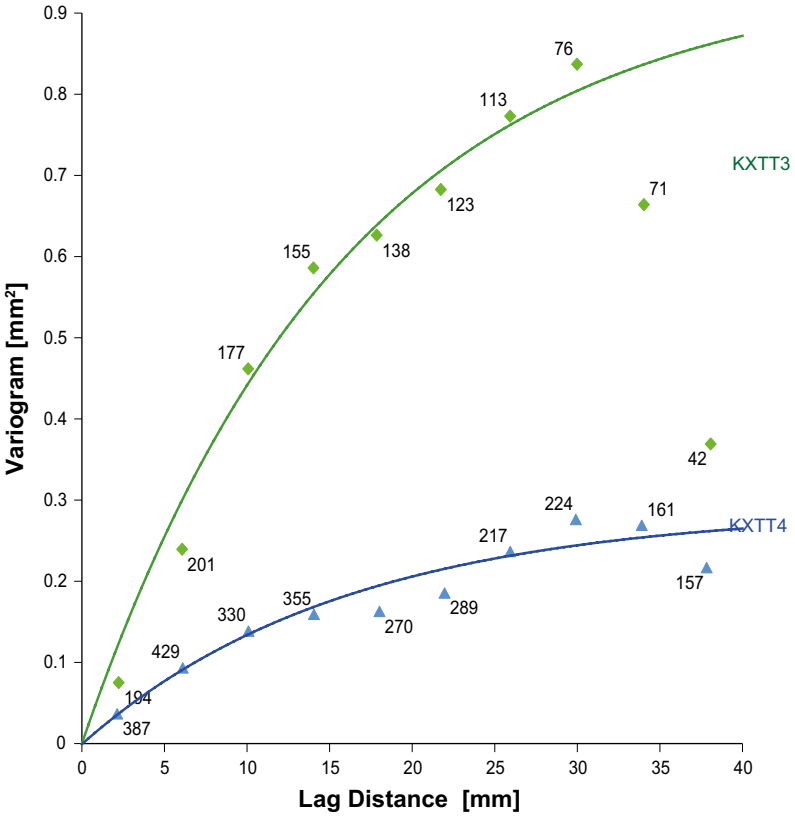

Figure 5-14. *Variogram results from the two short profiles in KXTT3 and KXTT4 where the apertures were measured in more detail. The Y-axis shows variance of the difference between field values of b at two locations at a certain distance (lag) and the X-axis shows the lag distances. The curves are exponential variogram models, both having practical range of 48 mm and a sill level of 0.95 and 0.29, respectively.*

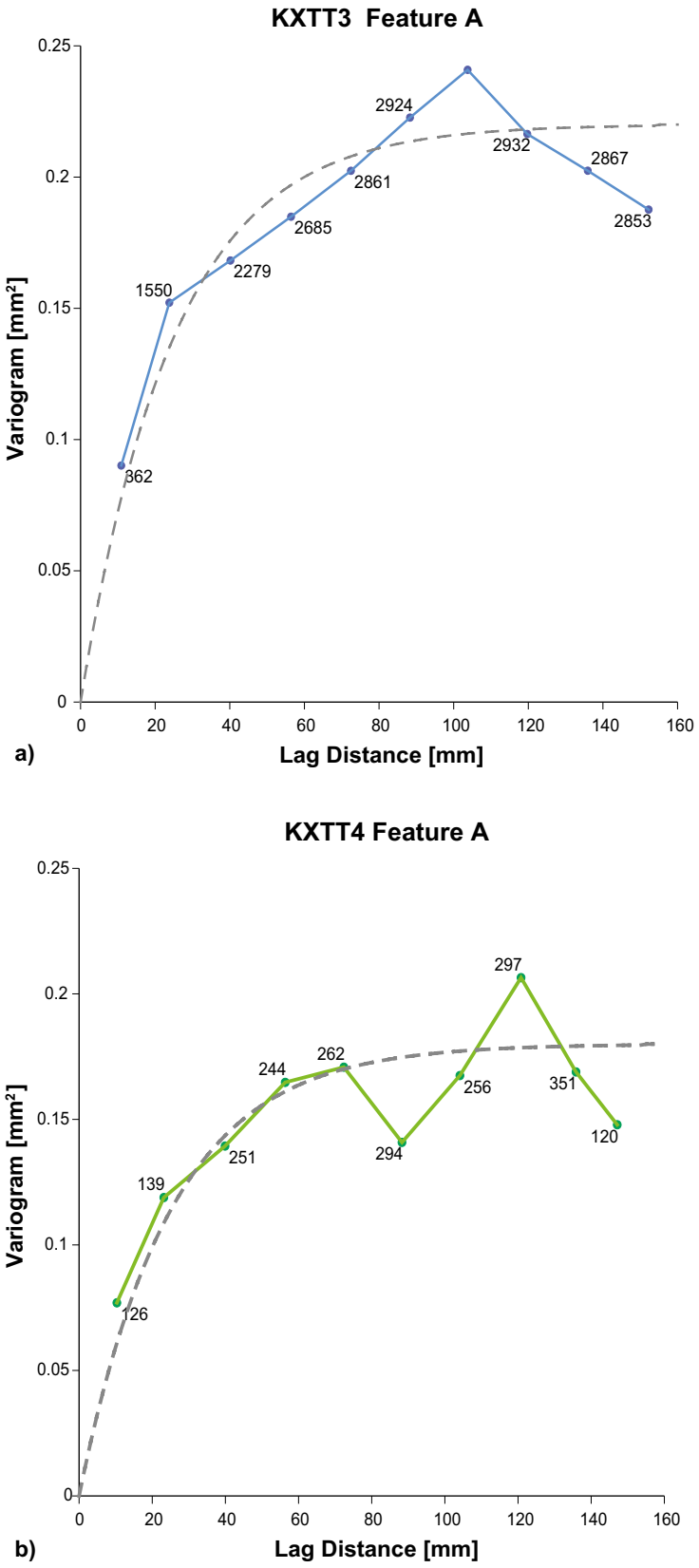

Figure 5-15. *Variogram of measured mean cumulative aperture, b_m, a) KXTT3 Feature A, and b) KXTT4 Feature A. Class F excluded. The Y-axis shows the variance of the difference between field values at a certain distance (lag) and the X-axis shows the lag. Labels are the number of pairs behind each value. The dashed line is an exponential variogram model, having a practical range (i.e. lag when curve reaches 95% of sill) of 75 mm (both cases) and a sill (levelling-off) level of a) 0.22 and b) 0.18, respectively.*

6 Mineralogical investigations

6.1 Introduction to mineralogical investigations

Detailed investigations have been carried out on fracture coatings from Feature A, from drill cores KXTT3 (which has been used as a pumping section in earlier performed tracer tests) and KXTT4 (used for injection of tracer) (Winberg et al. 2000). Earlier investigations of fracture surfaces of Feature A zone have not been able to detect any clay minerals on the fracture surfaces (Winberg et al. 2000), mainly due to conventional (double barrel) drilling, in which soft or loose material is easily flushed away. However, clay minerals have been interpreted to be present on the fracture coatings, based on retention results and modelling (Winberg et al. 2000). Therefore it was of special importance in the current study to try to detect and characterise potential clay mineral occurrences (as well as other soft or brittle phases). There is a higher potential to find preserved clay minerals than in the studies of Winberg et al. (2000), mainly due to that the fracture zone was impregnated with epoxy prior to overcoring, which has enabled preservation of the soft clay minerals. Another reason is that the core diameter is larger which has enabled sampling of larger samples.

Methods used include scanning electron microscope investigation (SEM-EDS) of fracture coatings/fillings and the wall rock, as well as X-ray diffractometry (XRD) of fracture coating material. The objective and scope was to characterise the fracture coatings in order to add to the understanding of the tracer test results. Especially mineralogy, crystal morphology, the thickness and roughness of the coating and the morphology of the fracture surfaces have been studied. Furthermore, detailed investigation of the fracture coatings and fillings in the different samples, which generally contain several fracture filling generations, gives information of the geological history of Feature A. Where present, epoxy intrusion into fracture coatings and into the wall rock was also investigated. As mentioned in Chapter 3, the core from KXTT4 had to be handled inside CLAB due to increased levels of radioactivity. However, some samples of KXTT4 displayed so low levels of radioactivity that it was possible to carry out mineralogical investigations outside CLAB. The samples used are interpreted to be representative for the whole of Feature A, since the variation within the samples generally is larger than the variation between them, as shown in the sample descriptions below.

6.2 Methods for mineralogical investigations

6.2.1 X-ray diffraction

The XRD analyses were carried out by the Swedish Geological Survey, Uppsala. In addition to analysis of a whole rock sample (WR), a fine-grained fraction (FG < 2 μm) was analysed for clay mineral identification. The whole rock sample was ground in an agate mortar in acetone and the powder was randomly orientated in the sample holder. The fine-grained fraction was dispersed in distilled water, treated in ultrasound in order to disperse clay particles and was in addition treated in sodium-hexametaphosphate solution. The samples were then filtered and oriented according to Drever (1973). Measurements were carried out in three steps; 1) dried sample 2) after being saturated with ethyleneglycol for two hours and 3) after heating to 400°C for two hours. A Siemens D5000 theta-theta-diffractometer with Cu-radiation (CuK_{α}) and graphite monochromator at 40 kV and 40 mA was used. Whole rock sample scans were run from 2° to 65° (2-theta) without using orientation of the samples. Fine fraction scans were run from 2° to 35° (2-theta) with step size 0.02° (2-theta) and counting time 1 s/step. The analyses were performed with a fixed 1° divergence slit, a 2-mm antiscatter slit and a 0.1-mm receiving slit. Bruker AXS DIFFRAC^{PLUS} 2.2 and EVA software were used for raw data evaluation. The minerals were identified using the Powder Diffraction File (PDF database version 1994) and clay mineral data from Brindley and Brown (1984) and Jasmund and Lagaly (1993).

6.2.2 SEM-EDS

Fracture surface samples and polished thin sections were investigated using a Hitachi S-3400N scanning electron microscope equipped with an Oxford Instruments energy dispersive system

(SEM-EDS), at the Department of Earth Sciences, University of Gothenburg. The acceleration voltage was 20 kV and the specimen current was about 1nA. X-ray spectrometric corrections were made using an on-line Oxford INCA software. Quantitative chemical analyses were not achieved for fracture surface samples due to the uneven surface of the samples. Minerals from these samples were identified by visual inspection and interpretation of X-ray spectra or qualitative normalized EDS analyses. Thin sections were carbon-coated for electron conductivity. Low-vacuum mode was used when analysing the fracture surface samples (no carbon-coating needed, and no loss of natural contrast caused by the coating, but it is unable to achieve the resolution attainable by conventional coated samples, which often have better signal/noise ratio for the samples), in order to avoid the use of any irreversible coating, which is used for electron conductivity under higher vacuum conditions.

6.3 Results of mineralogical investigations of KXTT3

6.3.1 Sample 25

Sample 25 includes the surface of Fracture 1 of Feature A (Figure 6-1) and the thin section has been prepared so that it includes the wall rock and the fracture coating facing Fracture 1 (Figure 6-2). The sample is made up of wall rock, mylonite and calcite-filled fractures, with abundant epoxy penetration.

The wall rock is highly altered (Figure 6-3, alteration increases towards the fracture). Primary minerals are fragmented and deformed (e.g. quartz, plagioclase and K-feldspar). Re-crystallised quartz and newly formed epidote occupies the space between the primary minerals and the distance between the fragments (mainly 1–2 mm grains, defined as *fault breccia fragments* in Andersson et al. (2002a)) increase towards the fracture and the size of the fragments decrease towards the fracture.

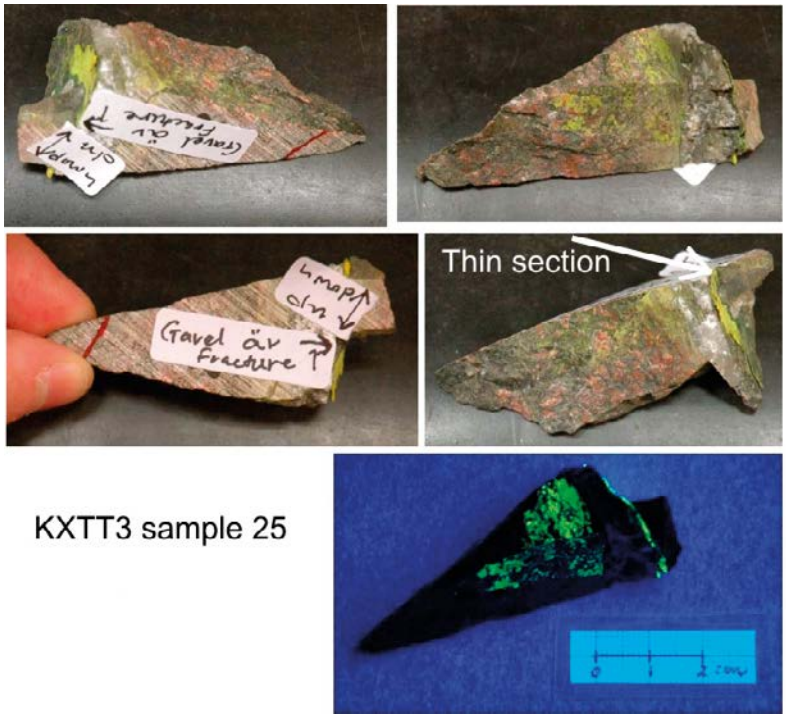

Figure 6-1. *Photographs of sample 25, KXTT3.*

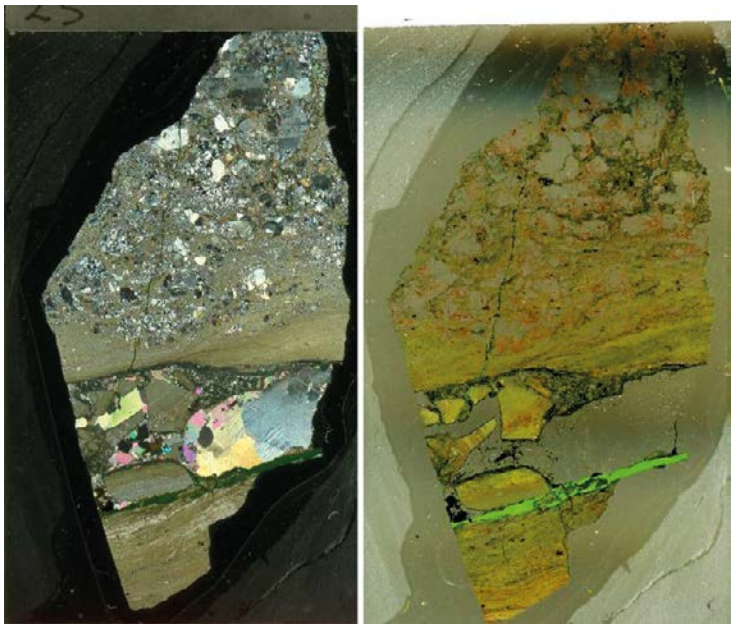

Figure 6-2. *Scanned thin section from sample 25, KXTT3 (left: crossed polars; right: plane polarised light). Epoxy (green-yellow) is preferentially found in a fracture in the bottom part of the thin section, but also in a thin fracture cutting into the wall rock. Width of each image is ~2 cm.*

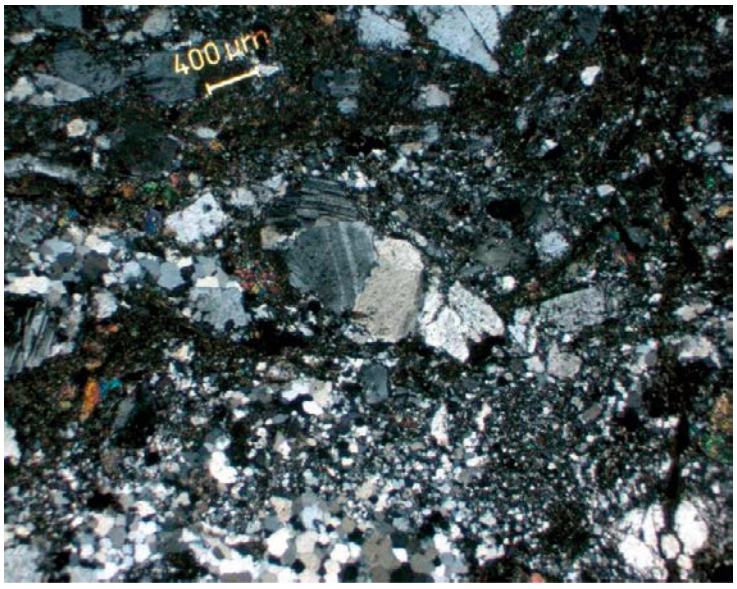

Figure 6-3. *Photomicrograph of the altered wall rock in sample 25, KXTT3.*

Fracture filling consists of the following fracture filling generations (oldest to youngest):

1. Mylonite: Epidote and quartz-rich, with ductile flow textures (Figure 6-4). The thickness is 2–5 mm. Is also found as fragments in younger fillings and in the epoxy.
2. Quartz-K-feldspar filled fractures (Figure 6-5). The thickness of these fracture fillings are 0.2–0.6 mm.
3. Calcite filled fracture with angular mylonite fragments (Figure 6-6). The thickness of this fracture filling is 5 mm.
4. Barite (euhedral) is present on the rim of the calcite-filled fracture (Figure 6-7). Chlorite/clay minerals coat the rim of the epoxy-filled fractures.

Epoxy (thickness 200–700 µm, average 400 µm) fills an undulating fracture, in the border between mylonite (generation 1) and calcite (generation 3) (Figure 6-4 and Figure 6-7). Epoxy is also found in a more narrow fracture (< 100 µm) that runs perpendicular to the fracture into the wall rock through the whole thin section (Figure 6-5).

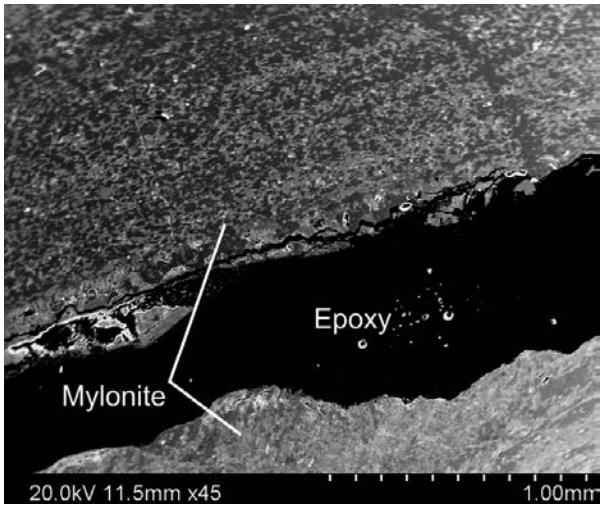

Figure 6-4. *Back-scattered SEM-image from sample 25 (KXTT3) of epoxy in a fracture cutting through mylonite. Total length of the scale bar is 1mm (distance between each tic is 0.1 mm).*

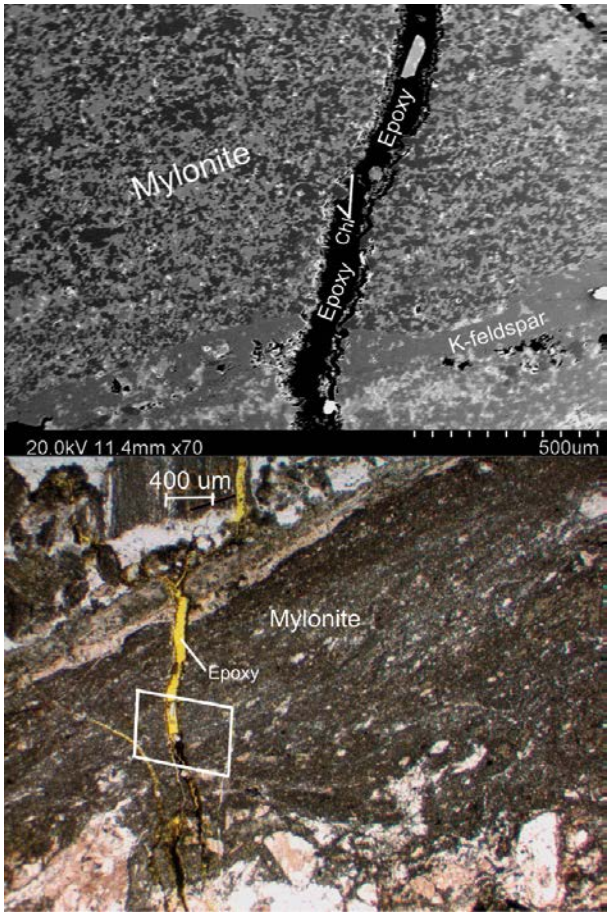

Figure 6-5. *Upper image: Back-scattered SEM-image from sample 25 (KXTT3) of epoxy in a fracture cutting through mylonite and a K-feldspar-quartz filling. Bottom image: photomicrograph of the same feature as in the upper image (position of the upper image is indicated by a white rectangle).*

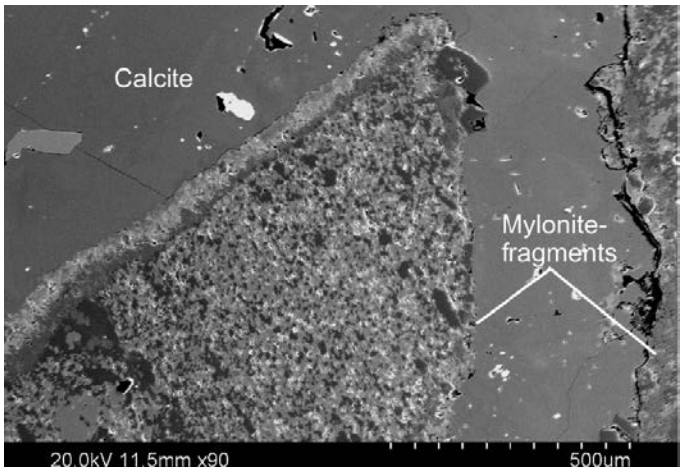

Figure 6-6. *Back-scattered SEM-image from sample 25 (KXTT3) of a calcite-filling containing older mylonite fragments.*

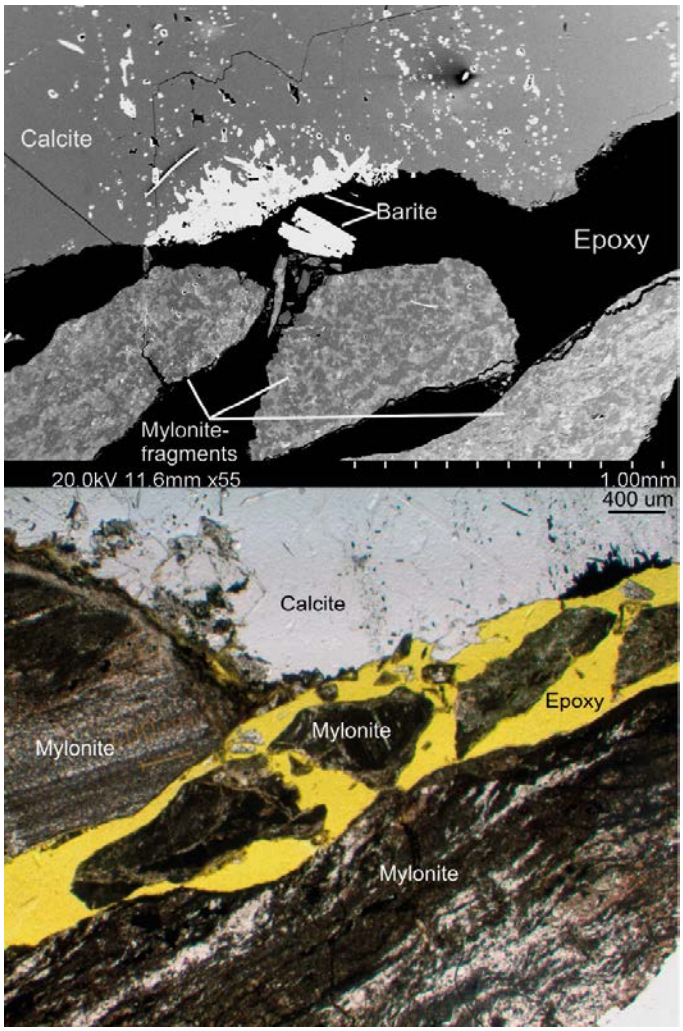

Figure 6-7. *Upper image: Back-scattered SEM-image from sample 25 (KXTT3) of epoxy in a fracture in the border zone between a calcite-filling (coated by younger barite) and older mylonite (now present as fragments in the epoxy). Bottom image: microphotograph of the same feature as in the upper image (the upper image corresponds roughly to the upper right part of the bottom image, although the whole area shown in the upper image is not included in the bottom image).*

6.3.2 Sample 26

Sample 26 includes the surface of Fracture 1 of Feature A (Figure 6-8) and the thin section has been prepared so that it covers this surface (Figure 6-9). The sample is made up of wall rock and fracture filling/coating facing Fracture 1 of Feature A. A fracture cutting through the fracture filling is filled with epoxy.

Figure 6-8. *Photographs of the sample.*

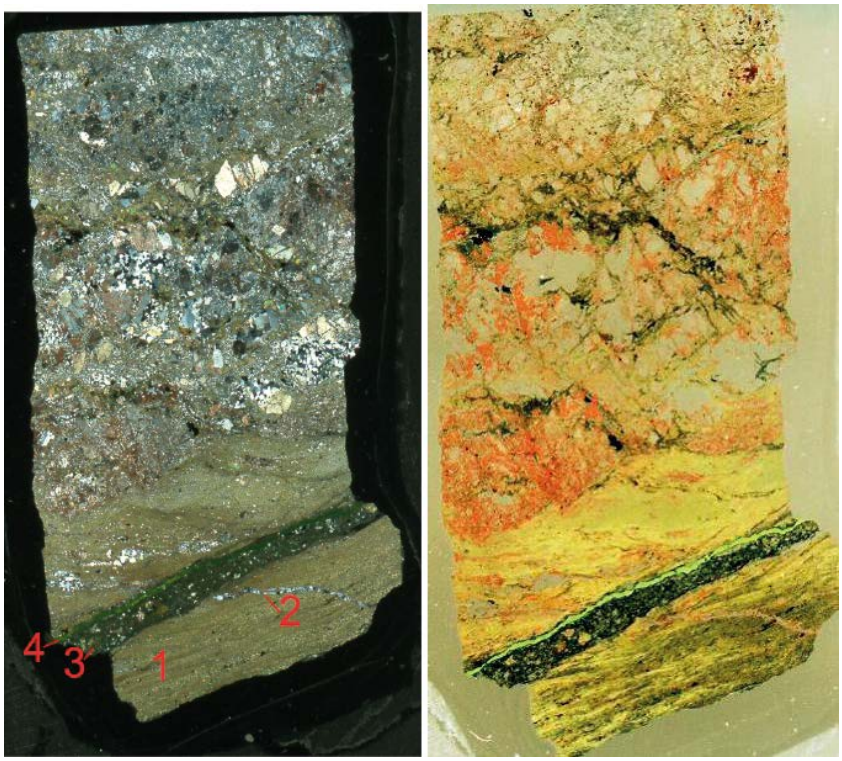

Figure 6-9. *Scanned thin section from sample 26, KXTT3 (left: crossed polars; right: plane polarised light). Epoxy (green-yellow) is preferentially found in a fracture in the bottom part of the thin section. Numbers refer to the order of formation (see list below) Width of each image is ~2 cm.*

The wall rock is highly altered, red-stained, and foliated (Figure 6-10). It has a large proportion of re-crystallised quartz and fragmented primary crystals of plagioclase, microcline etc. It is occasionally cataclastic.

Fracture filling consists of the following generations (oldest to youngest):

1. Mylonite (~1 cm thick); epidote-rich and quartz-rich with ductile-flow textures (Figure 6-11).
2. Brittle veins (~100–200 µm thick) filled with prehnite, quartz, K-feldspar, chlorite, cuts through generation 1 (Figure 6-11).
3. Chlorite- and illite-rich cataclasite bordered by K-feldspar rich/fluorite filling. Cuts through generations 1 and 2 (Figure 6-12).
4. Chlorite/clay minerals (Figure 6-13).

Epoxy (~200 µm thick) fills an undulating fracture inside the fracture mineral generation 3. The rim of the fracture filled with epoxy is partly coated with chlorite or chlorite/clay minerals (see Figure 6-13).

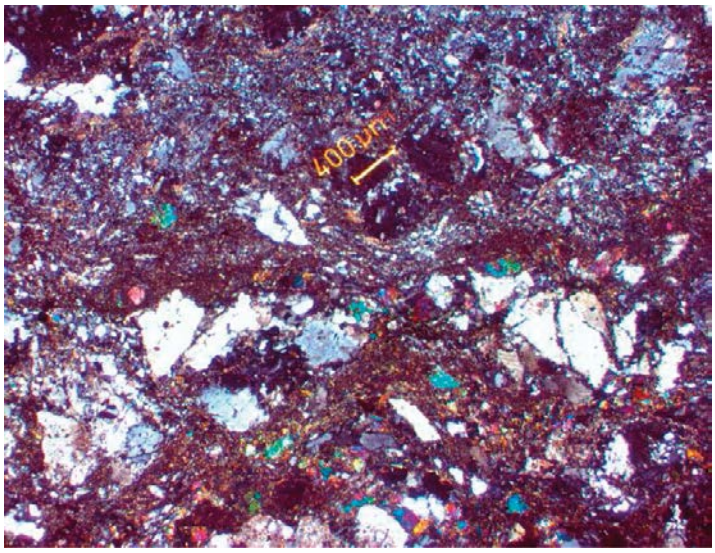

Figure 6-10. *Photomicrograph of the altered wall rock in sample 26, KXTT3.*

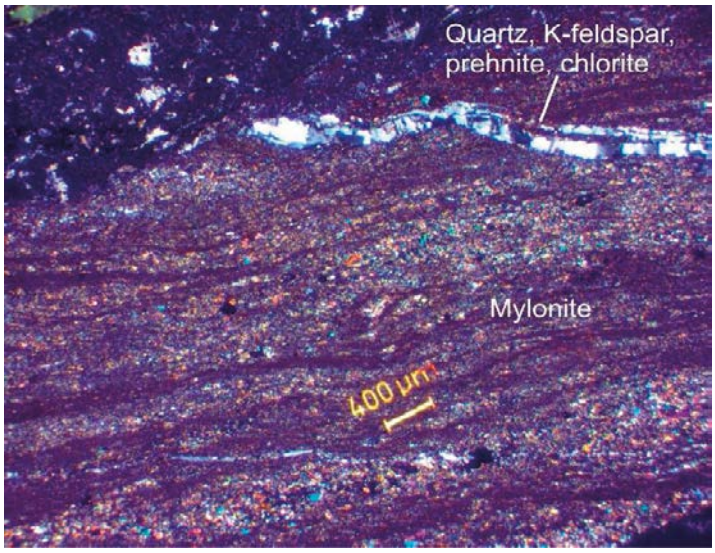

Figure 6-11. *Photomicrograph from sample 26 (KXTT3) of the mylonite and a younger fracture filled with quartz, K-feldspar, prehnite and chlorite.*

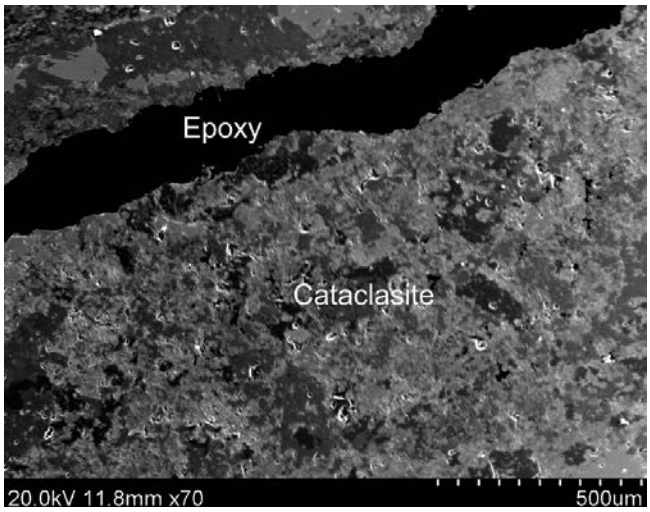

Figure 6-12. *Back-scattered SEM-image from sample 26 (KXTT3) of epoxy in a fracture cutting through cataclasite.*

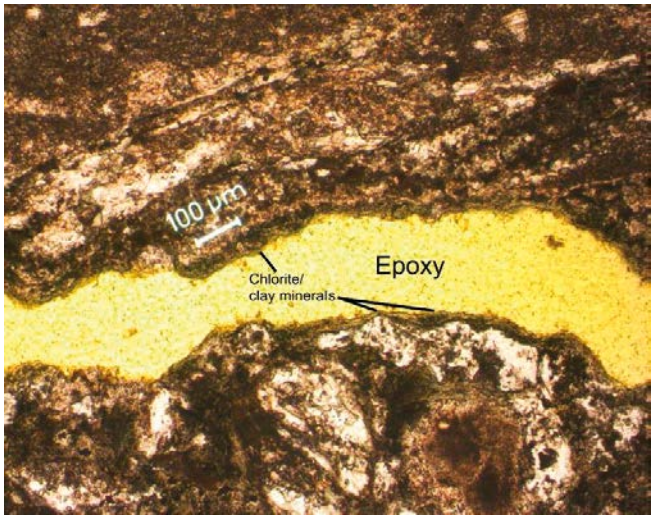

Figure 6-13. *Photomicrograph from sample 26 (KXTT3) of epoxy in a fracture coated by chlorite/clay minerals.*

X-ray diffraction analysis of the fracture minerals present on the fracture surface (Figure 6-14) shows that the whole rock sample is rich in chlorite and quartz. In addition, it includes K-feldspar and plagioclase. The fine-grained fraction is dominated by chlorite (Figure 6-15). There is possibly also a small component of a mixed-layer clay together with chlorite. A small expansion of the chlorite peaks is visible after heating, especially at about ca. 4.7 Å, which might indicate a collapse (during heating of the sample) of a chlorite/smectite-phase. A modest intensity increase around 18 Å in the dry sample can not be tied with confidence to any mineral, but may indicate the presence of a mixed-layer mineral.

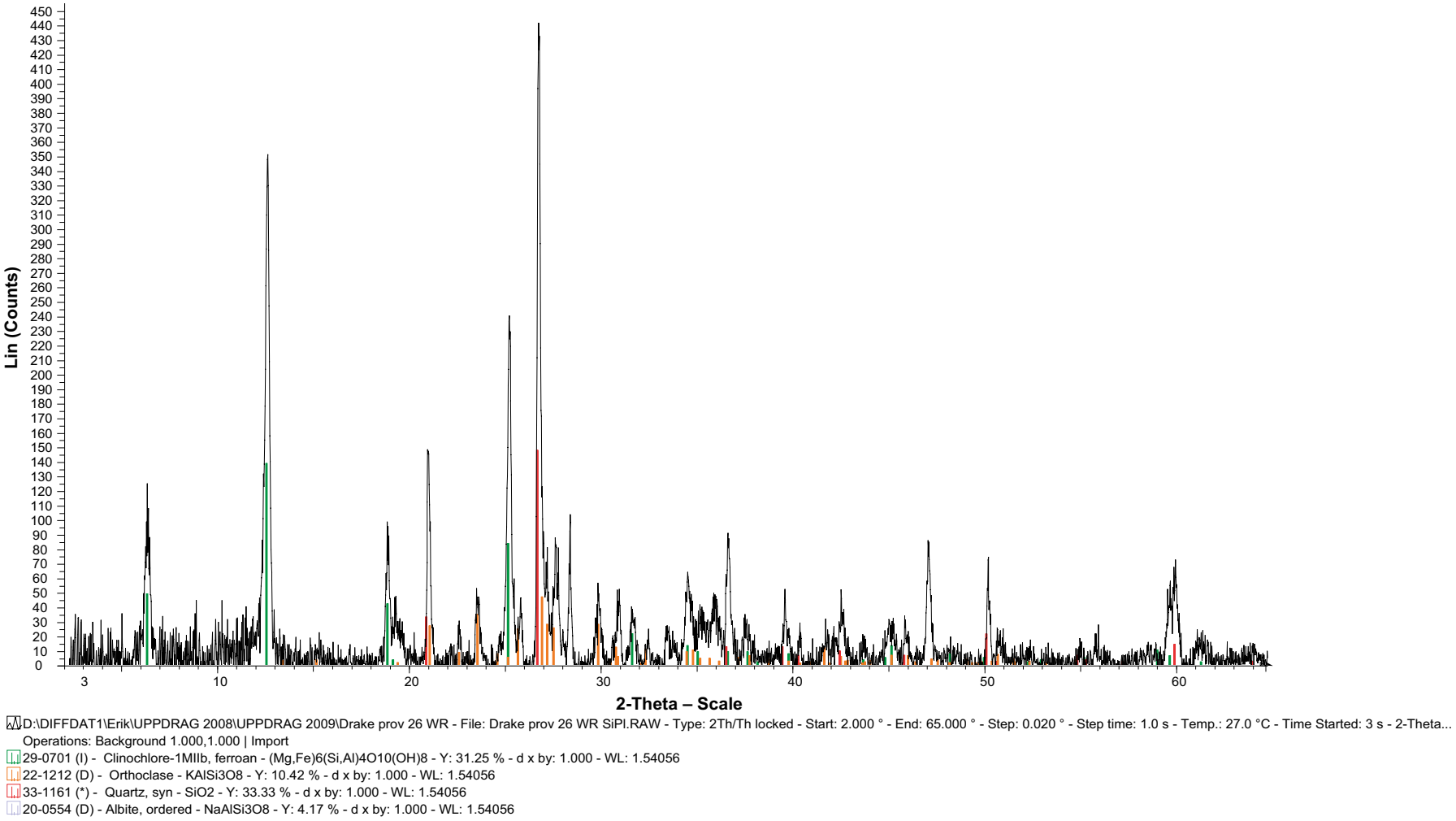

Figure 6-14. *XRD spectrum for whole rock fraction of sample 26, KXTT3.*

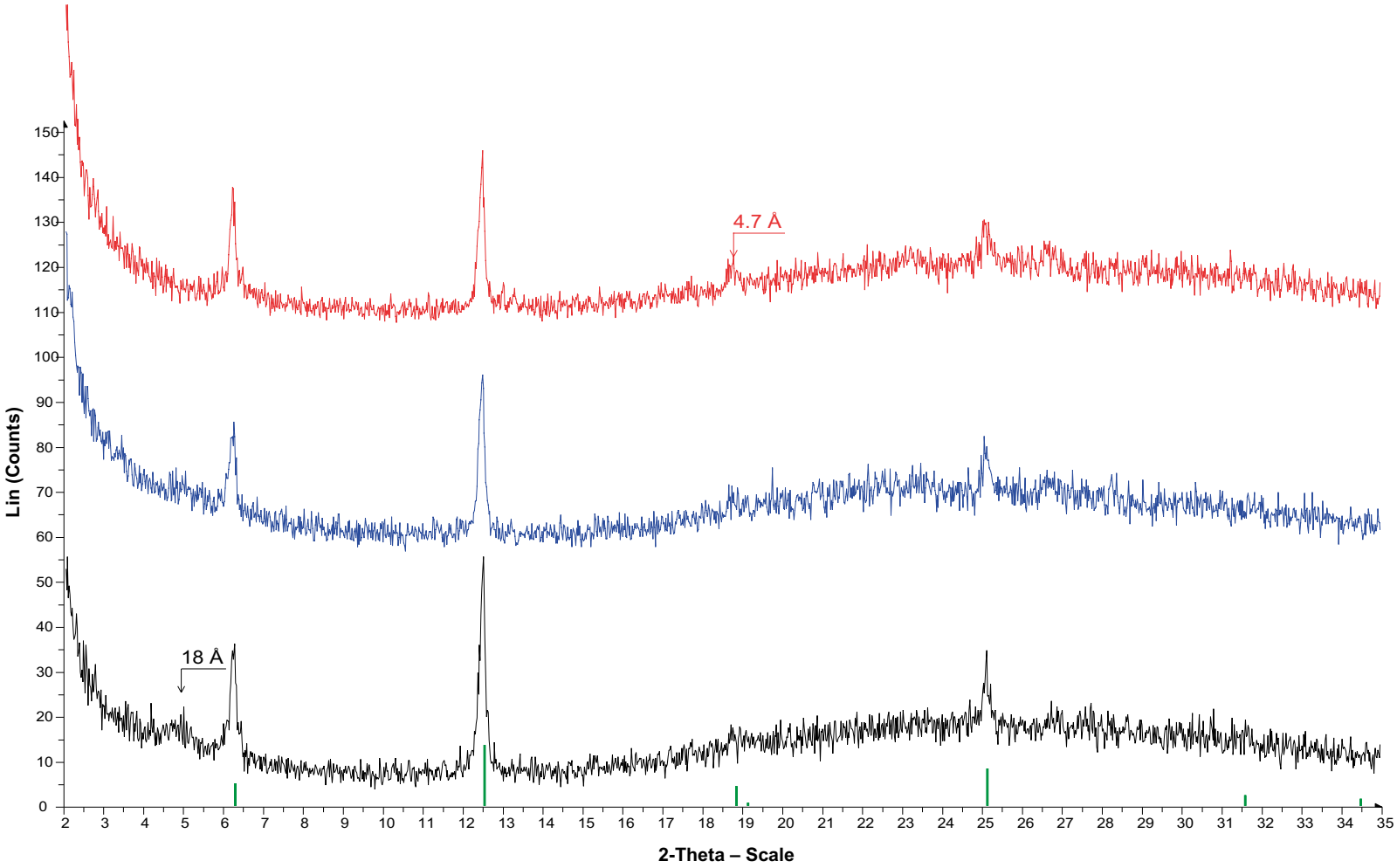

Figure 6-15. *XRD spectrum for fine-grained fraction of sample 26, KXTT3. Black curve is for dry sample, blue for EG (ethylene-glycol)-saturated sample and red for heated sample.*

6.3.3 Sample 31 (part of)

The sample is a part of piece 31 and features fracture surfaces associated with Fracture 1 and Fracture 2 of Feature A. The surfaces of both fractures have been investigated using SEM and scraped-off material from both fractures has been analysed with XRD. A thin section has been prepared from Fracture 2.

Fracture 1

Fracture minerals on epoxy-layer are mainly chlorite/clay minerals and some Fe-oxide crystals (Figure 6-17).

Figure 6-16. *Scan of fracture surface of Fracture 1, part of piece 31, KXTT3.*

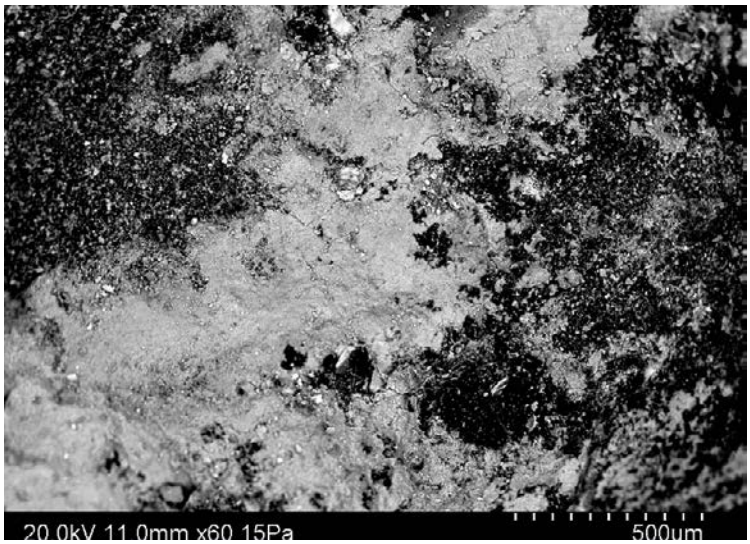

Figure 6-17. *Back-scattered SEM-image from sample 31-fracture 1 (KXTT3) of chlorite/clay mineral (bright) on epoxy (dark).*

The fracture surface below the epoxy cover is mainly (> 60%) made up of a commonly very smooth and thin cover of chlorite and clay minerals (Figure 6-18, occasionally striated, Figure 6-19). EDS-analyses indicate the presence of both pure chlorite and a mineral resembling chlorite but with additional Ca, and is probably mainly corrensite, which is a mixed-layer clay mineral made up of chlorite/smectite-vermiculite. Individual crystals of clay minerals sometimes (< 20% of the surface area) make the surface more rough occasionally (Figure 6-20). Small amounts of other minerals (< 20% of the surface area), e.g. REE-carbonate (Figure 6-21), pyrite (Figure 6-22), calcite (Figure 6-23), and fluorite are present as well. Clusters of wall rock fragments are also found on the fracture surface (< 5% of the surface area, Figure 6-24, e.g. biotite, quartz, K-feldspar and Fe-oxides).

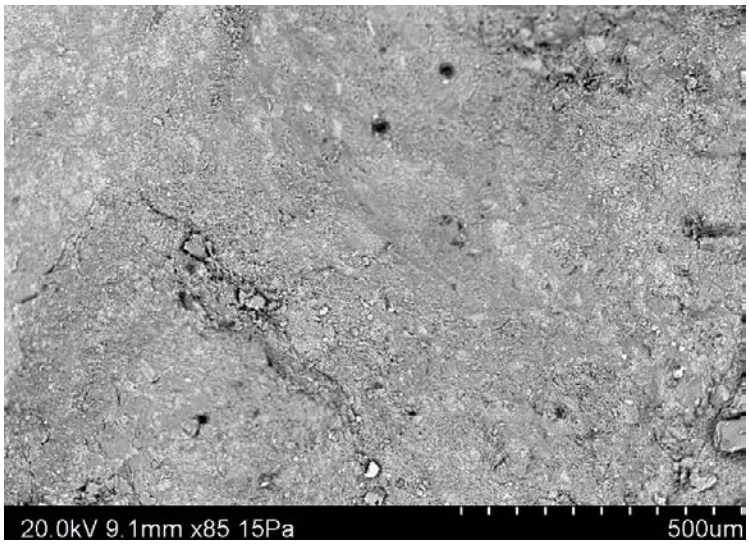

Figure 6-18. *Back-scattered SEM-image from sample 31-fracture 1 (KXTT3) of chlorite/clay mineral dominated fracture surface.*

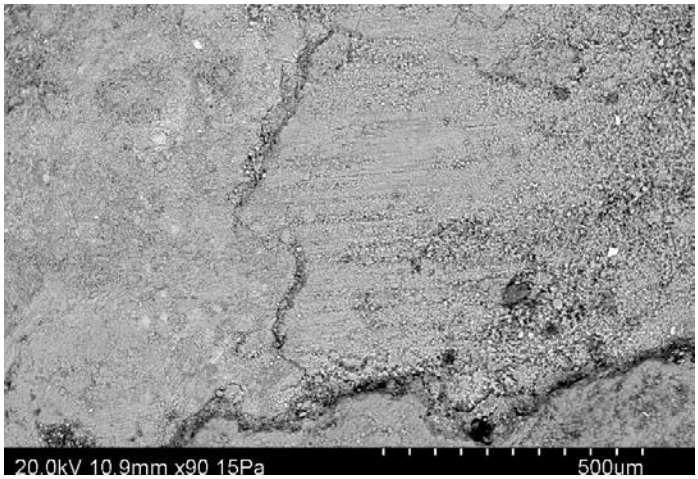

Figure 6-19. *Back-scattered SEM-image from sample 31-fracture 1 (KXTT3) of chlorite/clay dominated fracture surface with striation.*

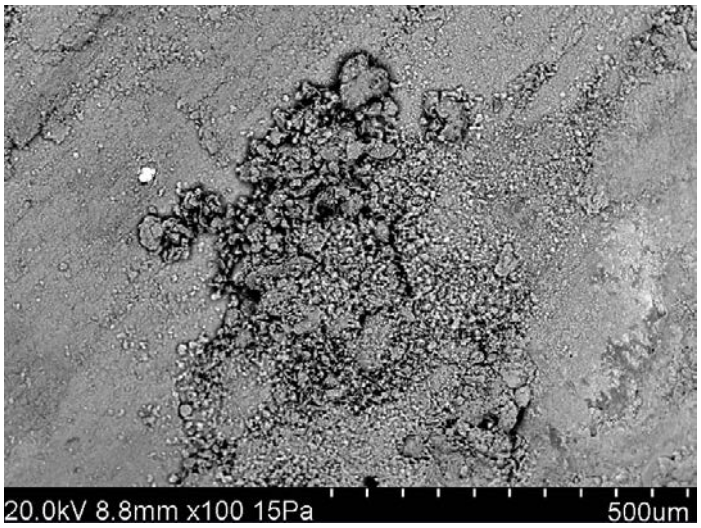

Figure 6-20. *Image from sample 31-fracture 1 (KXTT3) of a locally slightly more rough part of the chlorite/clay mineral coating.*

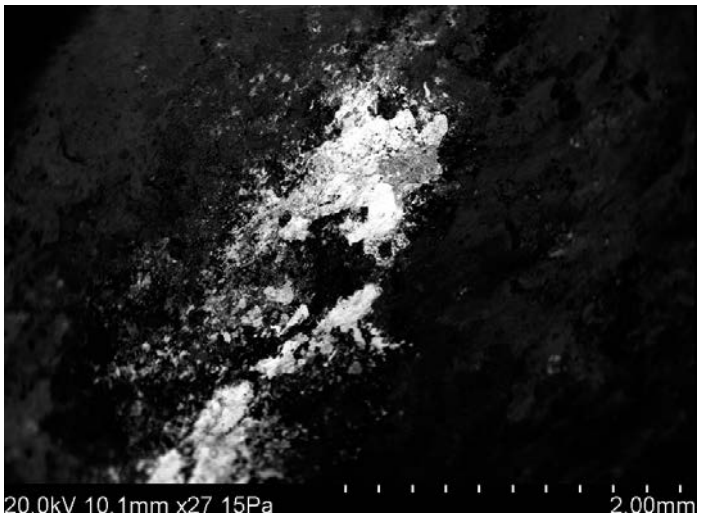

Figure 6-21. *REE-carbonate (bright), and chlorite/clay minerals (dark) in sample 31-fracture 1 (KXTT3).*

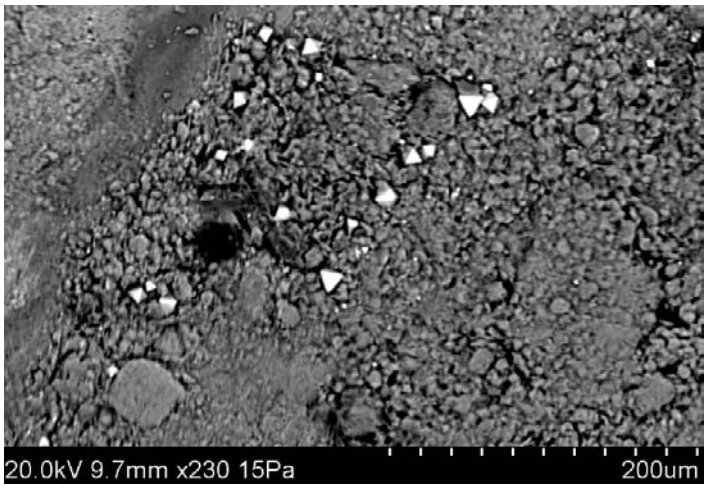

Figure 6-22. *Back-scattered SEM-image from sample 31-fracture 1 (KXTT3) of euhedral pyrite (bright) on chlorite/clay minerals.*

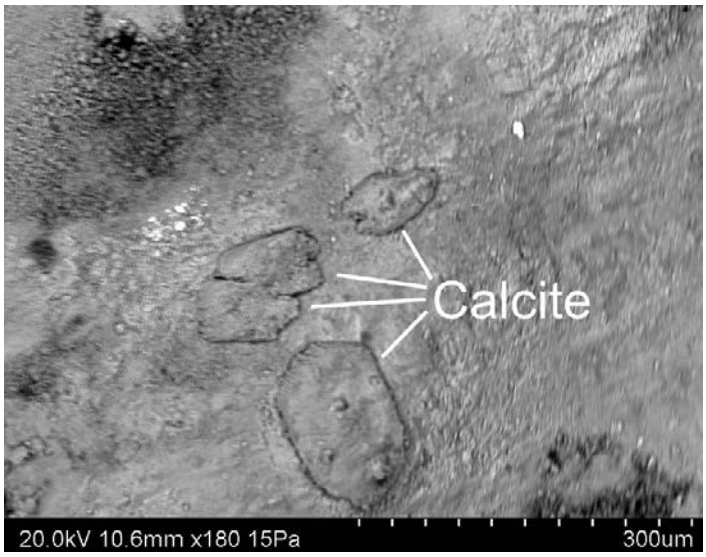

Figure 6-23. *Back-scattered SEM-image from sample 31-fracture 1 (KXTT3) of calcite.*

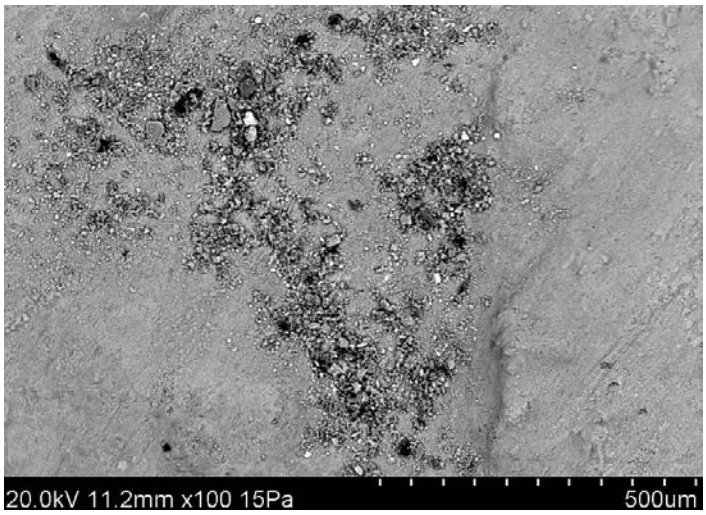

Figure 6-24. *Back-scattered SEM-image from sample 31-fracture 1 (KXTT3) of clusters of wall rock fragments, which are scattered across the fracture surface.*

X-ray diffraction analysis of the fracture minerals present on the fracture surface shows that the whole rock sample is very rich in chlorite. Other minerals are epidote, quartz, K-feldspar and some plagioclase (Figure 6-25).

The fine-grained fraction is dominated by chlorite (Figure 6-26). A diffuse peak at about 16.5 Å in the EG-saturated sample indicates the presence of small amounts of a swelling clay mineral, probably a poorly ordered mixed-layer clay of smectite/chlorite type.

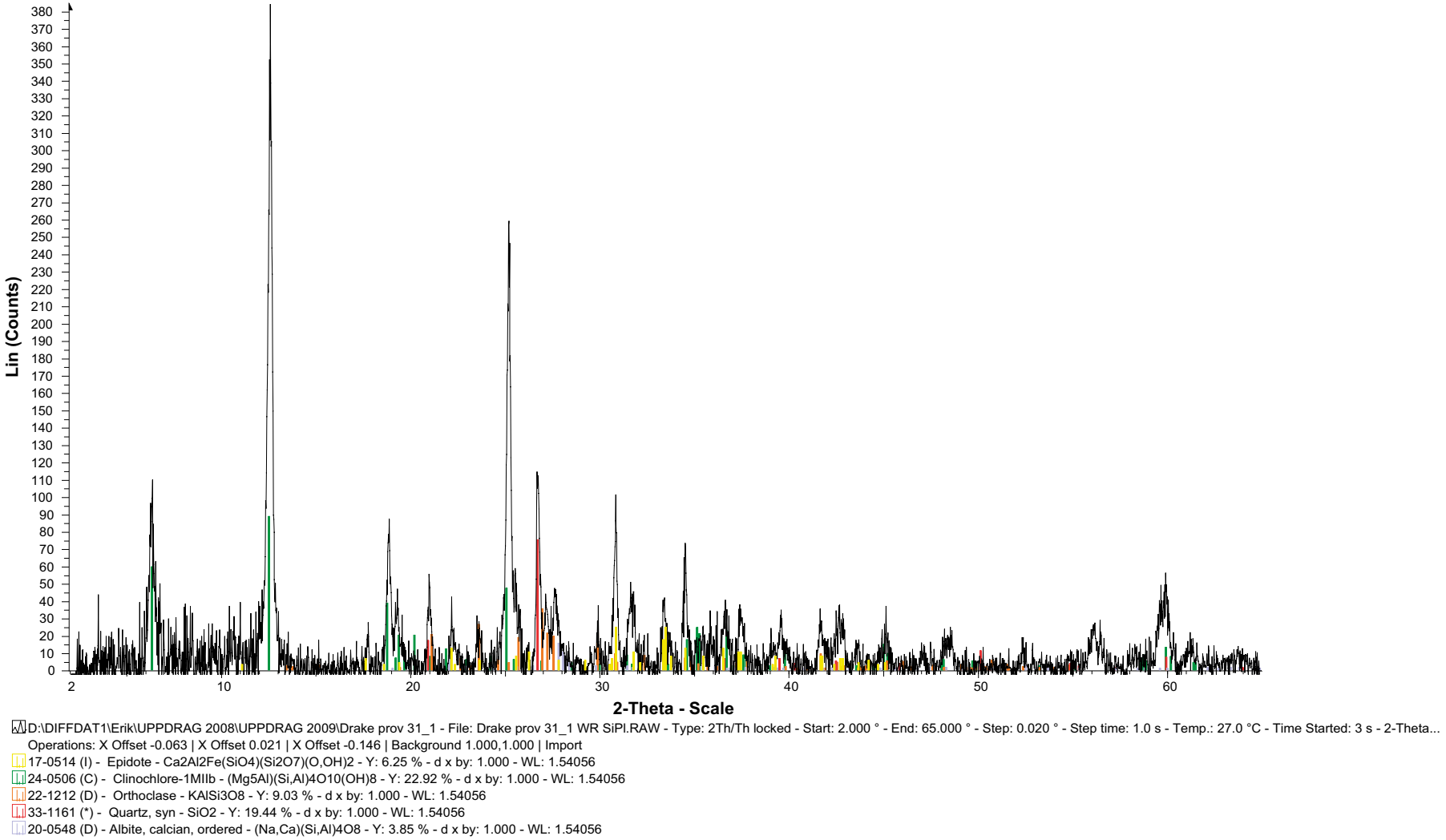

Figure 6-25. *XRD spectrum for whole rock fraction of sample 31-fracture 1, KXTT3.*

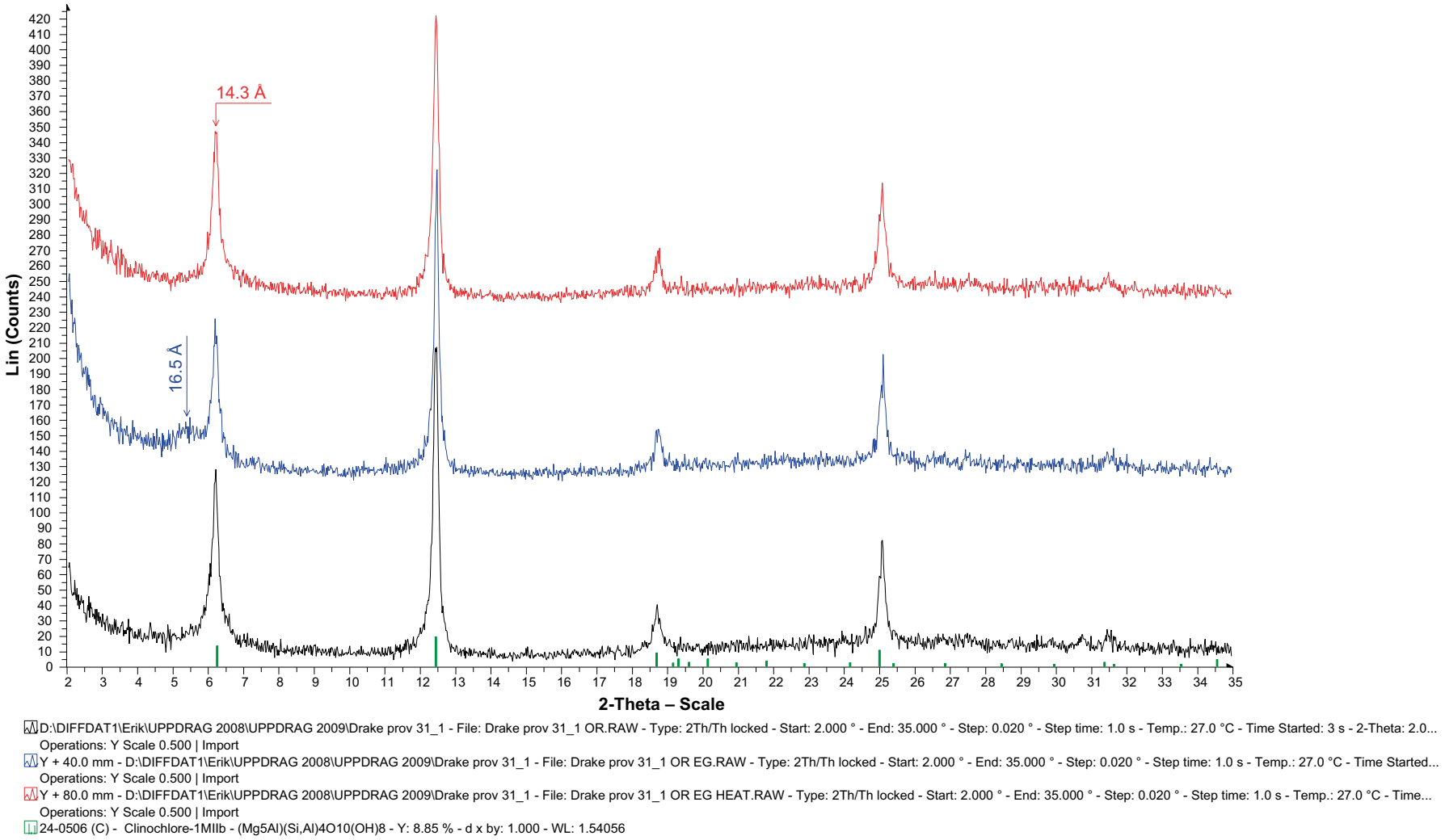

Figure 6-26. *XRD spectrum for fine-grained fraction of sample 31-fracture 1, KXTT3. Black curve is for dry sample, blue for EG (ethylene-glycol)-saturated sample and red for heated sample.*

Fracture 2

Fracture minerals on the epoxy-layer (Figure 6-27) are mainly chlorite/clay minerals and some Fe-oxide crystals (Figure 6-28).

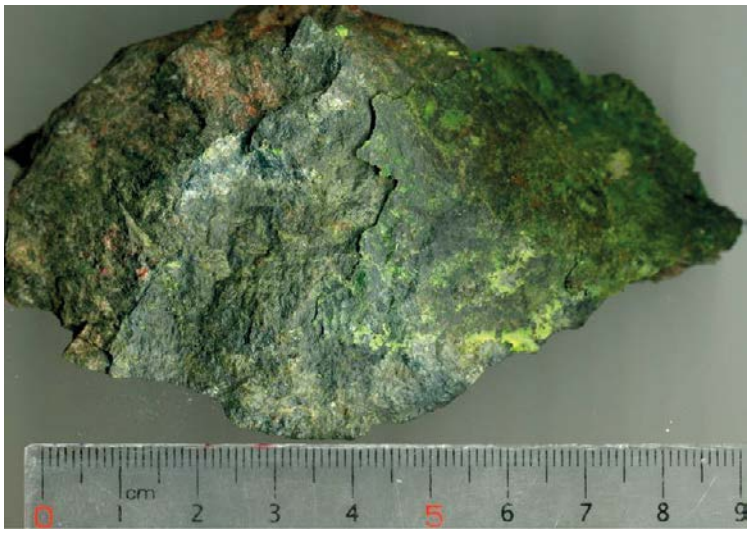

Figure 6-27. *Scan of fracture surface of sample 31-fracture 2, KXTT3.*

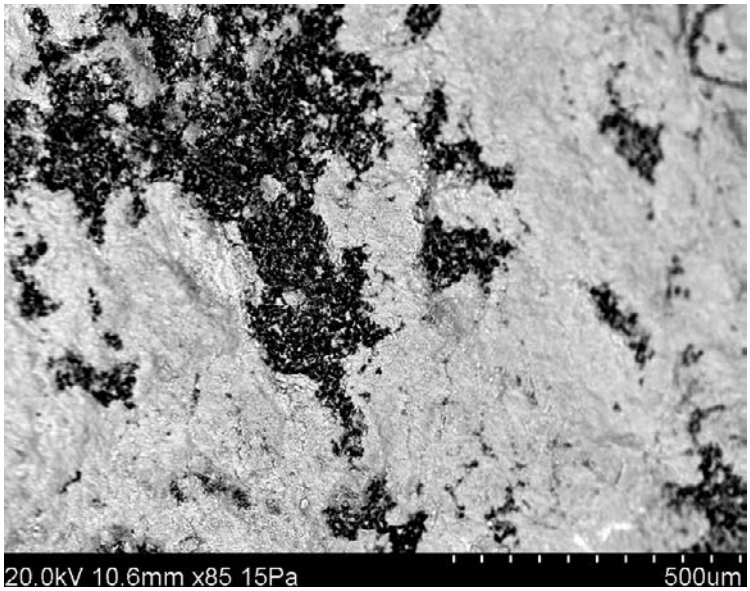

Figure 6-28. *Back-scattered SEM-image from sample 31-fracture 2 (KXTT3) of chlorite/clay mineral (bright) on epoxy (dark).*

The fracture surface below the epoxy cover is mainly made up of a thin cover of chlorite and clay minerals (Figure 6-29, occasionally smooth and striated). EDS-analyses indicate the presence of both pure chlorite and a mineral resembling chlorite but with additional Ca, and is probably mainly corrensite, which is a mixed-layer clay mineral made up of chlorite/smectite-vermiculite. Illite is also very abundant, as well as epidote and K-feldspar (Figure 6-30). Individual crystals of clay minerals sometimes make the surface rougher. Small amounts of other minerals (< 10% of the surface area), e.g. calcite, sphalerite, quartz (Figure 6-31) and some galena, are also present. Clusters of wall rock fragments are also present on the fracture surface (< 5% of the surface area, Figure 6-32, e.g. biotite, quartz, K-feldspar and Fe-oxides).

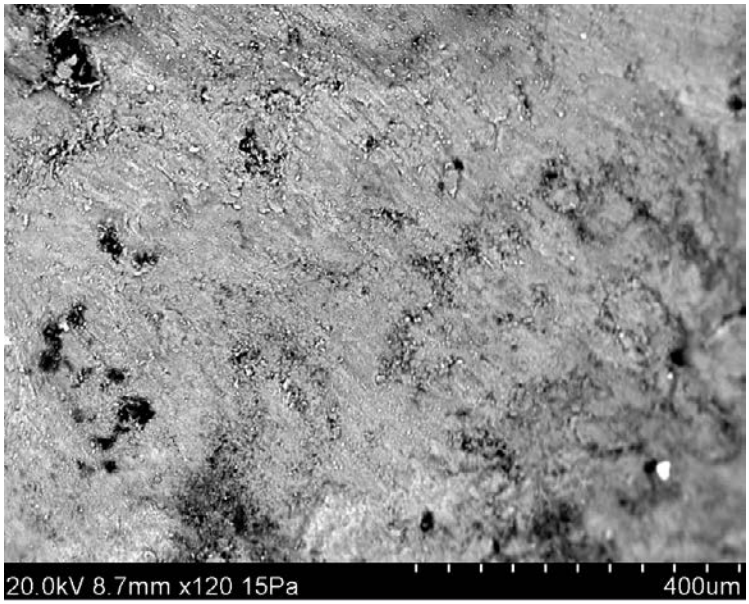

Figure 6-29. *Back-scattered SEM-image from sample 31-fracture 2 (KXTT3) of chlorite/clay mineral dominated fracture surface.*

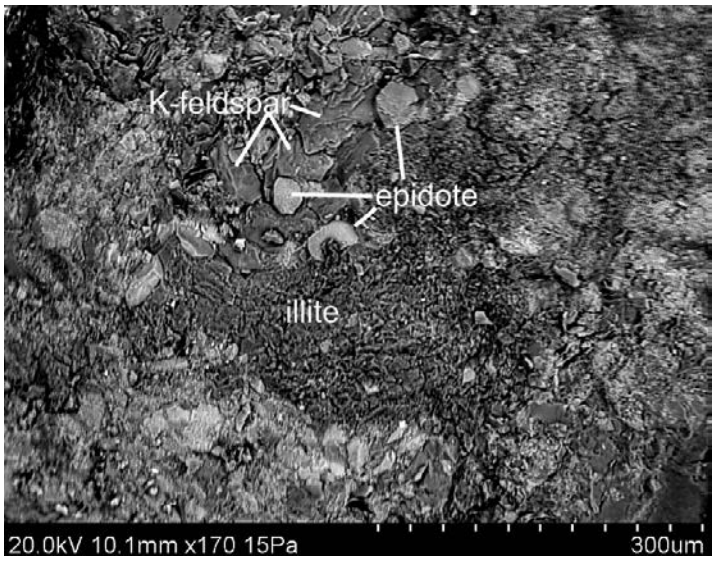

Figure 6-30. *Back-scattered SEM-image from sample 31-fracture 2 (KXTT3) of epidote, illite and K-feldspar.*

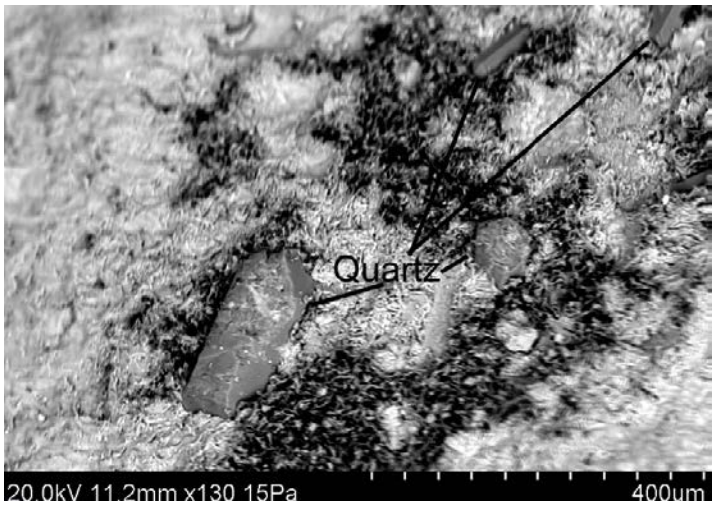

Figure 6-31. *Back-scattered SEM-image from sample 31-fracture 2 (KXTT3) of chlorite/clay mineral and euhedral quartz crystals.*

Figure 6-32. *Back-scattered SEM-image from sample 31-fracture 2 (KXTT3) of wall rock fragments in the fracture coating.*

X-ray diffraction analysis of the fracture minerals present on the fracture surface shows that the whole rock sample is chlorite- and quartz-rich (Figure 6-33). Apart from these minerals the sample also includes K-feldspar and plagioclase. Some weak peaks match clinozoisite (an almost iron-free epidote), but this identification is very uncertain.

The fine-grained fraction is dominated by chlorite (Figure 6-34). The ratio between the peaks at 14.4 and 7.1 Å suggests that it is relatively Fe-rich. A diffuse peak at about 16.3 Å in the EG-saturated sample indicates the presence of small amounts of a swelling clay mineral, probably poorly ordered mixed-layer clay of smectite/chlorite type.

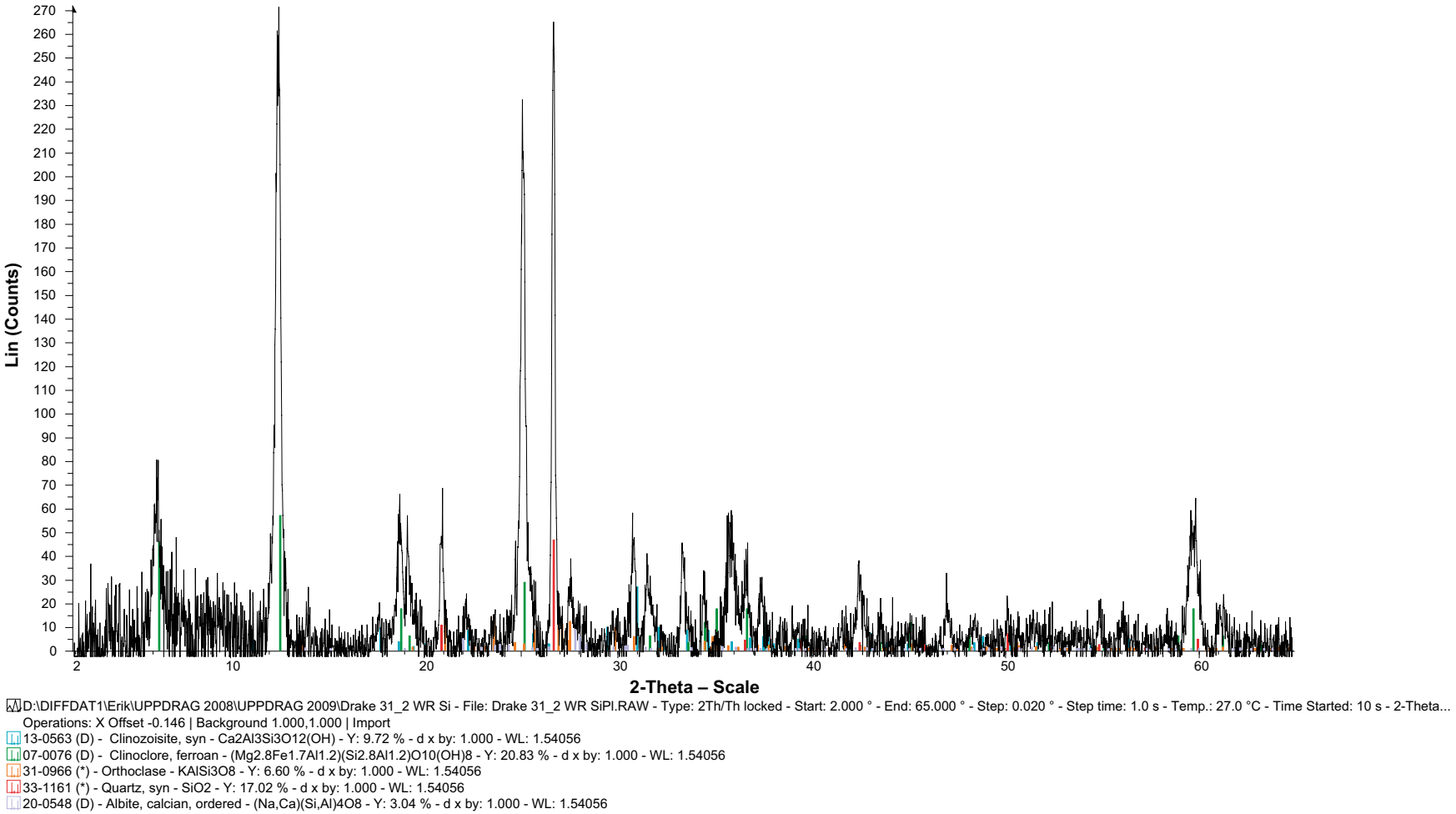

Figure 6-33. *XRD spectrum for whole rock fraction of sample 31-fracture 2, KXTT3.*

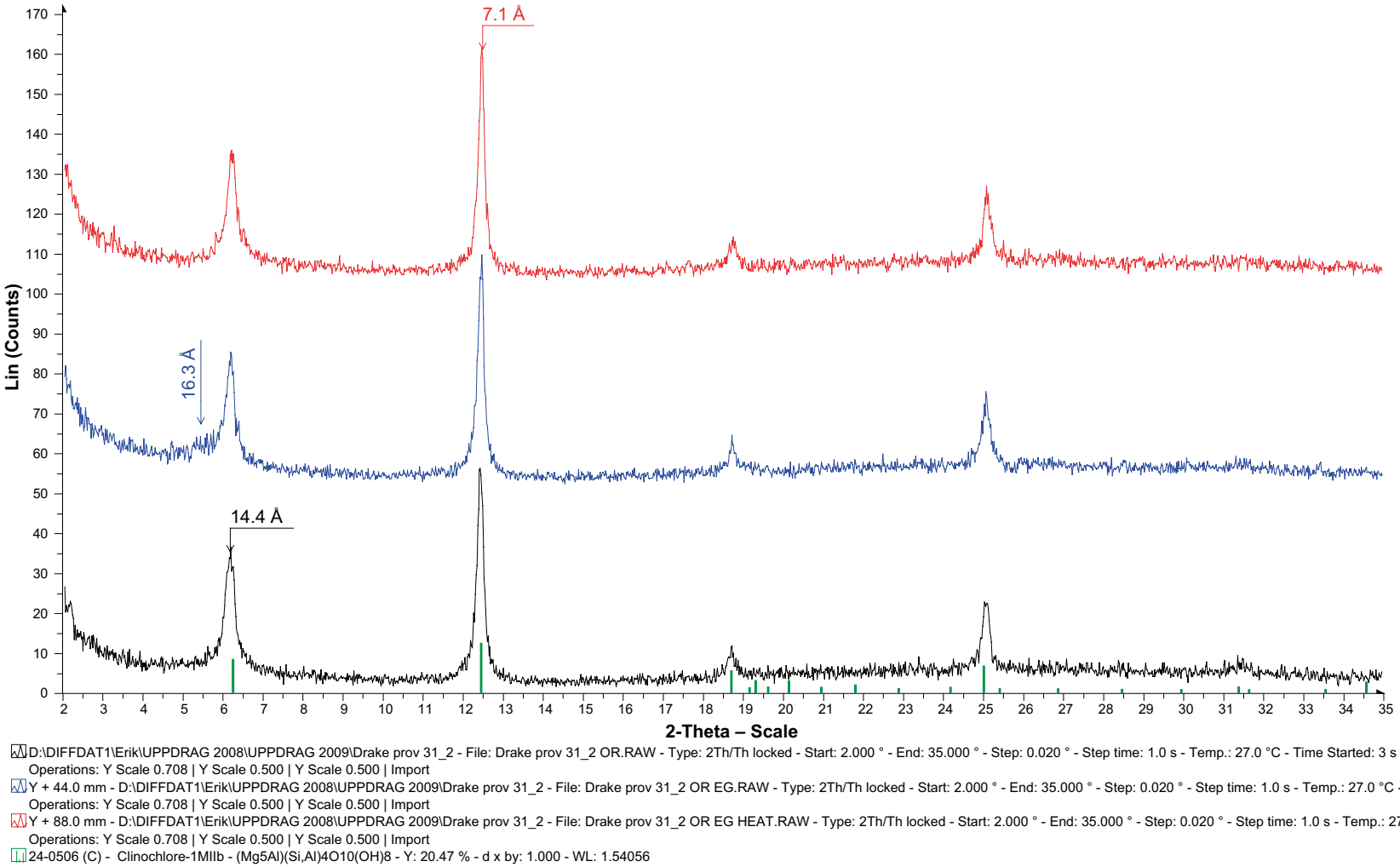

Figure 6-34. *XRD spectrum for fine-grained fraction of sample 31-fracture 2, KXTT3. Black curve is for dry sample, blue for EG (ethylene-glycol)-saturated sample and red for heated sample.*

The thin section is made up of wall rock, a fracture filling/coating facing Fracture 2 and epoxy as an outermost layer facing Fracture 2 (Figure 6-35).

The wall rock contains several bands of mylonite with only a few fragments of the primary wall rock crystals. Quartz has been re-crystallised and epidote has formed.

The fracture filling consists of the following generations (oldest to youngest):

1. Epidote-rich mylonite with no remaining wall rock fragments (Figure 6-36). The mylonite is ~1–2 mm thick.
2. Cataclasite (hematite-bearing) cutting through the wall rock and the mylonite in 0.1–0.5 mm thick veins (Figure 6-37).
3. Fractures coated and/or completely filled with euhedral K-feldspar (hematite-stained), chlorite and prehnite (possibly also laumontite). This filling/coating is in places coated by epoxy, but is mostly coated by younger fracture coatings (Generation 4 in this sample) (Figure 6-38 and Figure 6-39).
4. Chlorite-/clay mineral-rich filling borders to epoxy (Figure 6-38, Figure 6-39 and Figure 6-40) and is found in between generation 3 minerals and the epoxy (also on opposite side of epoxy). The thickness is 100–500 µm.

The thickness of epoxy in the main fracture is 100–800 µm (See further about the results from epoxy measurements in Section 5.2). Epoxy has also intruded the fracture filling through a couple of micro-fractures (Figure 6-40).

Figure 6-35. *Scanned thin section from sample 31-fracture 2, KXTT3 (left: crossed polars; right: plane polarised light). Epoxy (green-yellow) is preferentially found as an outermost layer on the fracture surface in the upper part of the thin section. Width of each image is ~2 cm.*

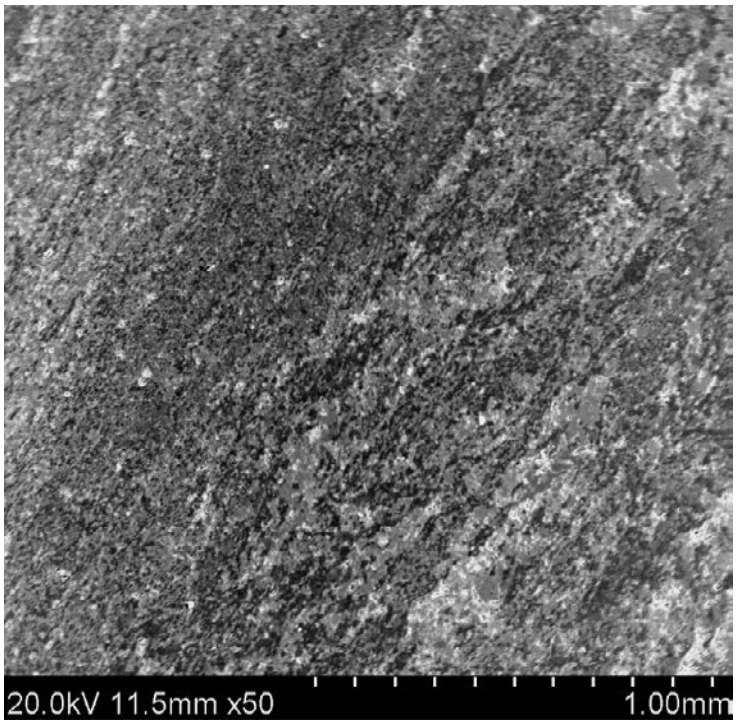

Figure 6-36. *Back-scattered SEM-image from sample 31-fracture 2 (KXTT3) of mylonite.*

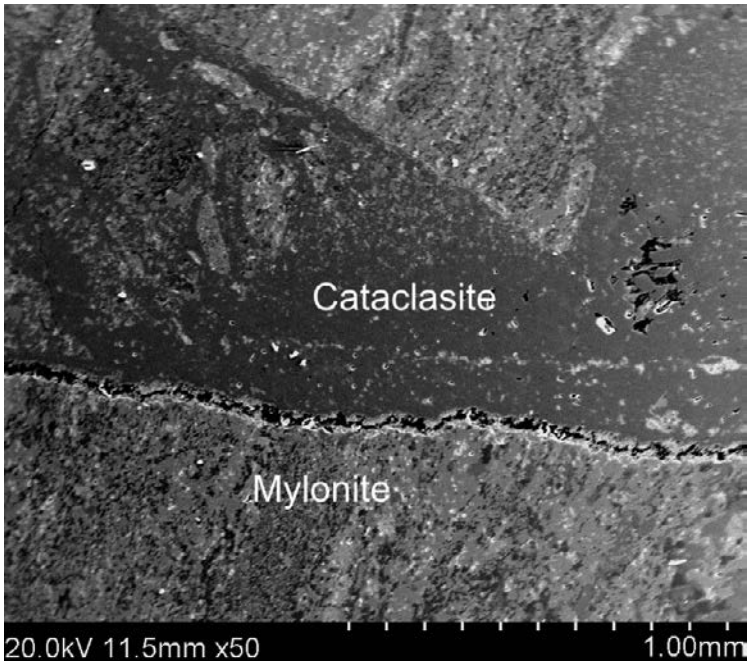

Figure 6-37. *Back-scattered SEM-image from sample 31-fracture 2 (KXTT3) of cataclasite cutting through mylonite.*

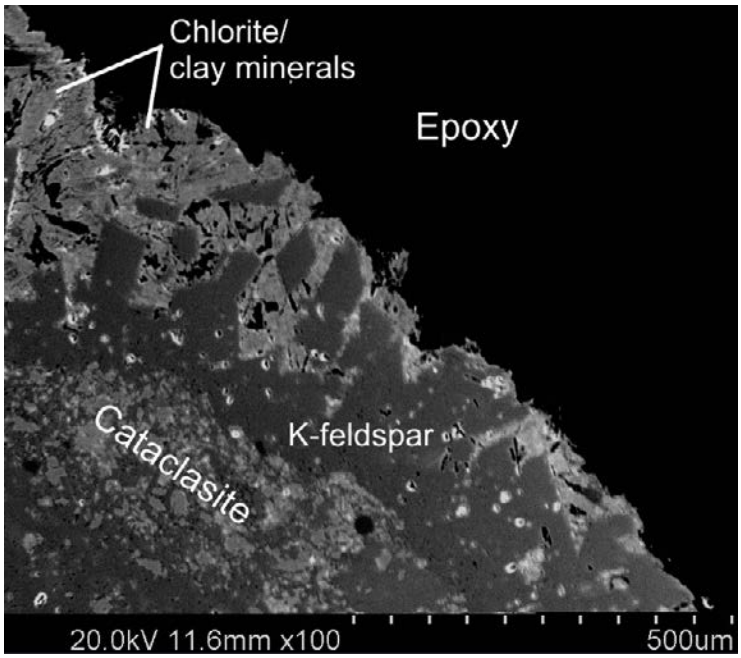

Figure 6-38. *Back-scattered SEM-image from sample 31-fracture 2 (KXTT3) of epoxy outside three generations of fracture filling/coating, in chronological order: cataclasite, K-feldspar and chlorite/clay minerals (youngest).*

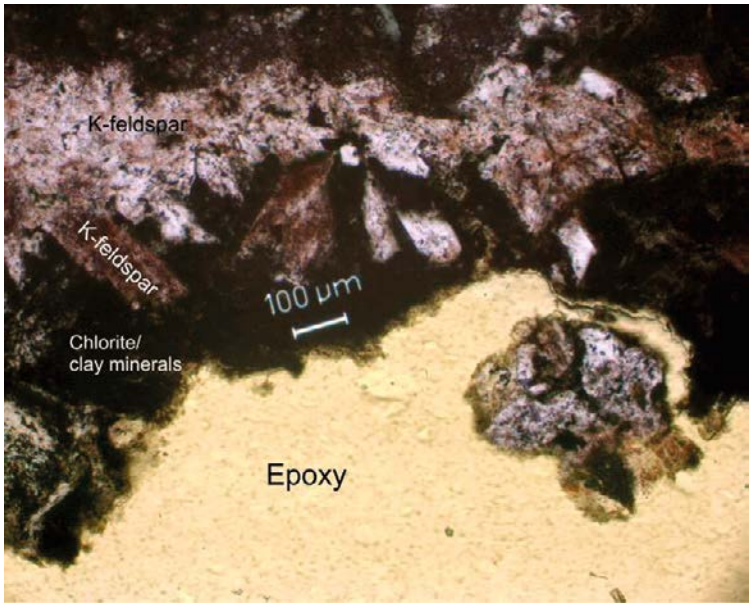

Figure 6-39. *Microphotograph from sample 31-fracture 2 (KXTT3) of epoxy coating two generations of fracture filling/coating, in chronological order: K-feldspar and chlorite/clay minerals (youngest).*

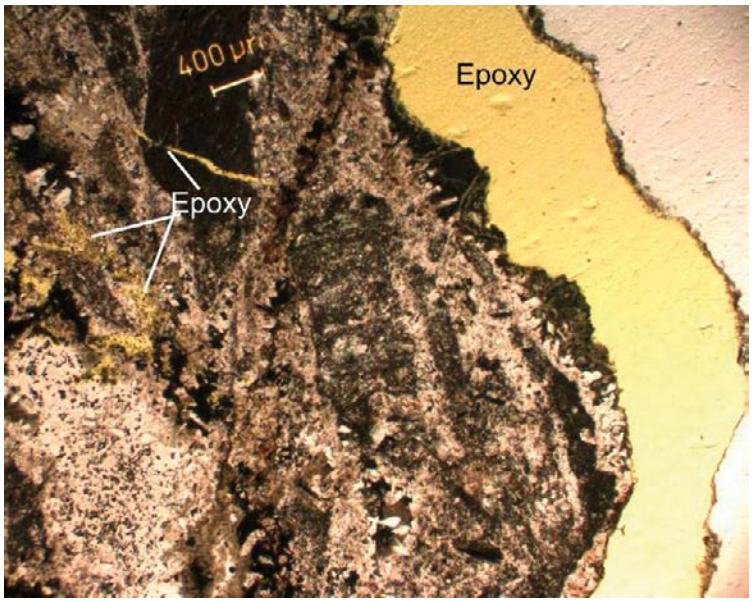

Figure 6-40. *Microphotograph from sample 31-fracture 2 (KXTT3) of epoxy, both on the surface of the fracture and in micro-fractures within the fracture filling.*

6.3.4 Summary of KXTT3 sample characteristics

All of the KXTT3 samples have several generations of fracture fillings/coatings, which shows that Feature A has been reactivated at several events and that it has been water-conducting for a very long time, although the detailed flow path configuration has probably varied.

The oldest secondary mineral assemblage is included in numerous sub-parallel mylonite bands, which are characteristic for Feature A, and are found in most of the samples. Younger cataclasite is also present in some of the samples. More coarse-grained fracture fillings of prehnite, quartz and K-feldspar are younger than the cataclasite, and border the fractures in some of the samples. The next generation consists dominantly of calcite, but also fluorite, pyrite, barite, quartz and clay minerals and some accessory minerals, e.g. some sulphide phases. The outermost coatings are often dominated completely by chlorite and clay minerals, with some additional wall rock fragments, and calcite with related minerals. The fracture surfaces are not always covered by fracture minerals. Instead, the wall rock (or mylonite) is exposed. The clay mineral-chlorite fracture coatings are often very smooth, but may be rougher when euhedral minerals, such as spherulitic corrensite, cubic fluorite and pyrite, or wall rock fragments are abundant. Clay minerals are mainly of mixed-layer type, dominantly of chlorite/smectite type (corrensite), as indicated in the XRD analyses.

6.4 Results of mineralogical investigations of KXTT4

6.4.1 Sample 1-I-0 (Feature A)

This sample consists of a highly altered granitic rock with mylonite bands (Figure 6-41). The two most distinct mylonite bands are about 5 mm thick and are sub-parallel and are both slightly undulating. One of them borders to the open fracture (Feature A), which is associated with the reactivated mylonite. Adularia-filled micro-fractures cut through more intact wall rock sections. The mylonites appear to be located in parts of the rock once dominated by Fe-Mg-rich minerals, whereas feldspar-dominated parts are more intact, although the feldspars are micro-fractured and pseudomorphically replaced by secondary feldspars.

Figure 6-41. *Photograph of 1:I:0 (KXTT4), with the open fracture (Feature A) in the upper part of the sample.*

SEM-investigations of the fracture surface shows that the minerals present are:

- Clay minerals are the dominant minerals along with chlorite (mixed layer-clay, see spectra in Figure 6-42, and SEM-image in Figure 6-43). Grain size maximum of individual crystals is about 40 µm, but the grain size is mainly below 5 µm.
- Chlorite (Fe-rich).
- Quartz (mostly covered by clay minerals, one euhedral ~150 µm big crystal is identified).
- Epidote.
- Fe-oxide.
- Sphalerite (a single 500 µm sized, flat, crystal).
- Pyrite (anhedral, up to 50 µm sized crystals).
- Galena (small crystals, ~20 µm, associated with sphalerite).

At least ~70% of the surface is covered by clay minerals and chlorite. About 15–20% of the fracture surface is not covered by fracture minerals, mainly in a few relatively large uncovered areas. Instead, the wall rock, with mainly K-feldspar, quartz and Fe-oxide, is exposed.

The fracture surface is undulating but quite smooth, occasionally striated in clay mineral-rich parts, and mostly lacks euhedral single crystals or crystal aggregates. If fine-grained crystal aggregates are present, the individual clay mineral crystals are commonly < 10 µm.

6.4.2 Sample 1-III-6 (Feature A)

This sample consists of a highly altered granitic rock with several sub-parallel mylonite bands (Figure 6-44). The two major mylonite bands are about 5 mm thick and are slightly undulating. One of them borders to the open fracture (Feature A), which has reactivated the mylonite. Adularia-filled micro-fractures also exist and are cutting through the more intact wall rock parts. Feldspar-dominated parts of the wall rock are micro-fractured and pseudomorphically replaced by secondary feldspars.

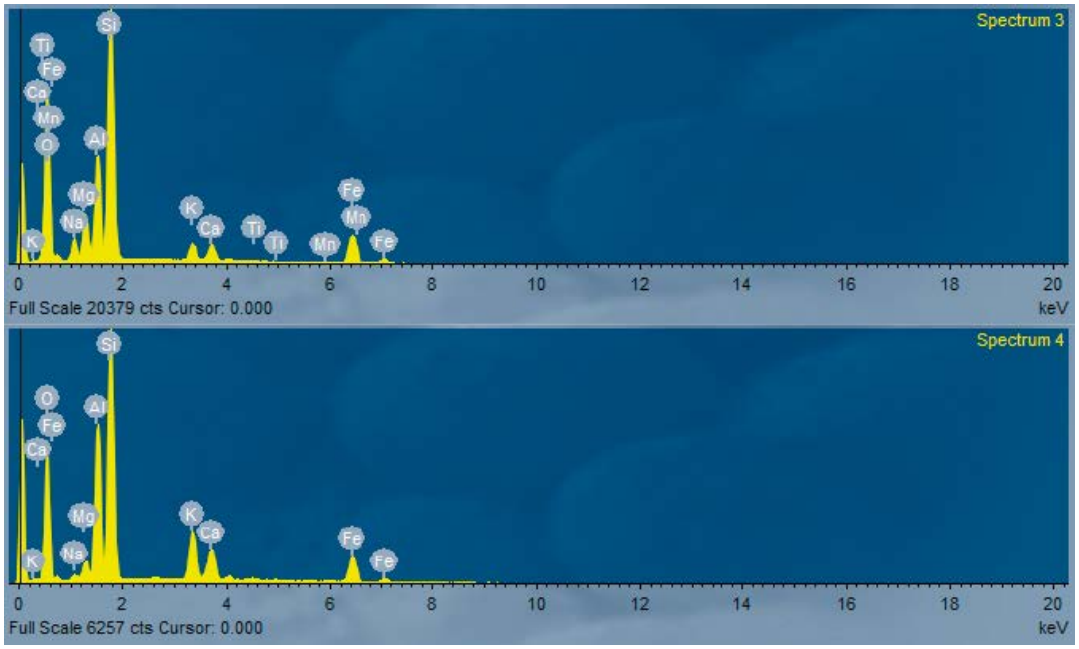

Figure 6-42. *EDS spectra from sample 1-I-0, KXTT4.*

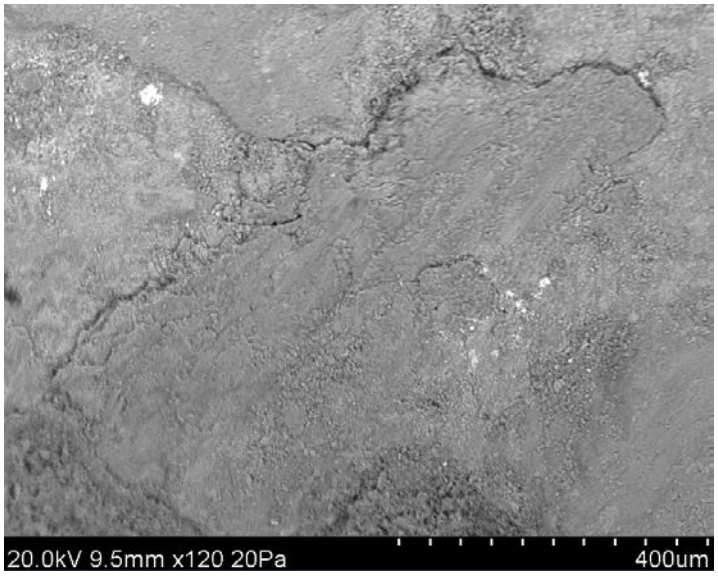

Figure 6-43. *Back-scattered SEM-image from sample 1-I-0 (KXTT4) of smooth layers of clay minerals and chlorite with striations.*

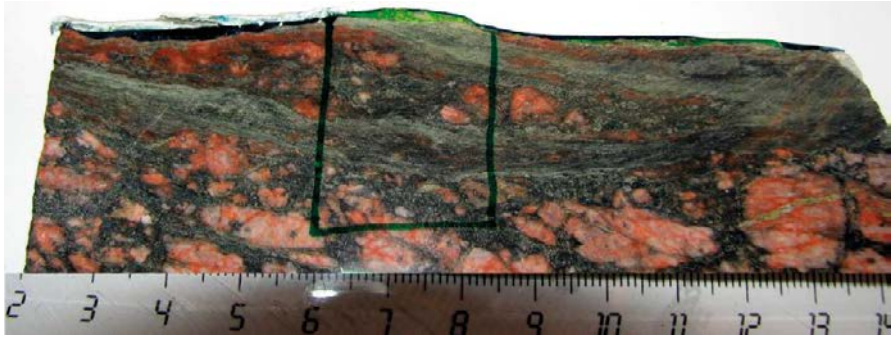

Figure 6-44. *Photograph of 1:III:6 (KXTT4), with the open fracture (Feature A) in the upper part of the sample. The location of the thin section is indicated by the markings.*

This thin section includes about 1 cm of altered wall rock, and closer to the fracture, about two centimetres of mylonite (Figure 6-45 and Figure 6-46), and at the fracture rim, sub-parallel to the mylonite foliation, there is a ~1.5 mm thick fracture coating/filling of euhedral quartz, fluorite, barite, illite, hematite, chlorite and K-feldspar. The latter has been intruded by epoxy, which has entered and fragmented the filling completely, resembling a breccia with an epoxy matrix (Figure 6-47). However, the epoxy has not entered further into the rock than ~1.5 mm, along micro-fractures.

The wall rock is highly altered and is made up of more or less altered primary plagioclase and K-feldspar surrounded by fine-grained bands of mainly re-crystallised quartz and chlorite. The latter have formed from altered biotite and other Fe-Mg minerals. Magnetite is often euhedral and largely unaltered.

The mylonite is made up of alternating bands of grey and greenish grey colour, dominated by fine-grained quartz and epidote+chlorite, respectively. The amount of wall rock fragments varies widely.

6.4.3 Sample 2:5 (Feature A)

This sample consists of a highly altered rock dominated by Fe-Mg-rich minerals and slightly fragmented K-feldspar phenocrysts (cut through by adularia-filled micro-fractures). The presently open fracture (Feature A) has reactivated an epidote-quartz-dominated, mylonite, which now exists as a 5–8 mm thick, quite homogeneous and slightly undulating mylonite, at the fracture rim (Figure 6-48). Thinner mylonite bands, of less than < 1 mm thickness, also exist within the rock, preferentially located to Fe-Mg-mineral-rich parts of the rock.

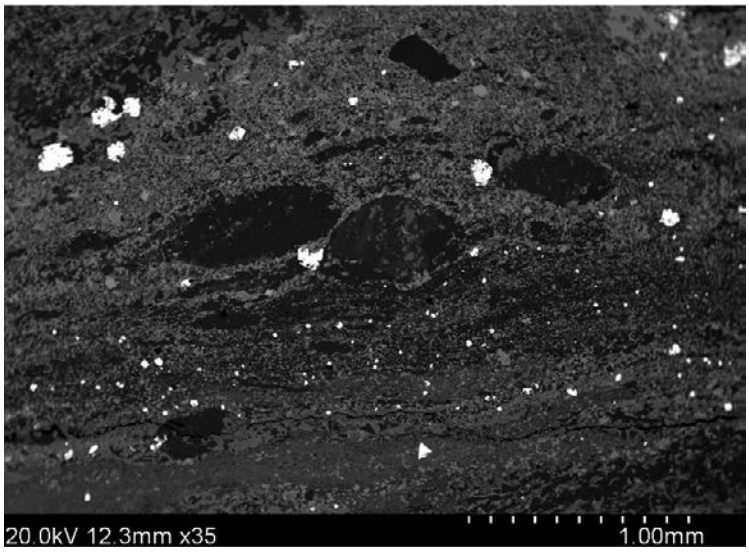

Figure 6-45. *Back-scattered SEM-image from sample 1-III-6 (KXTT4) of mylonite.*

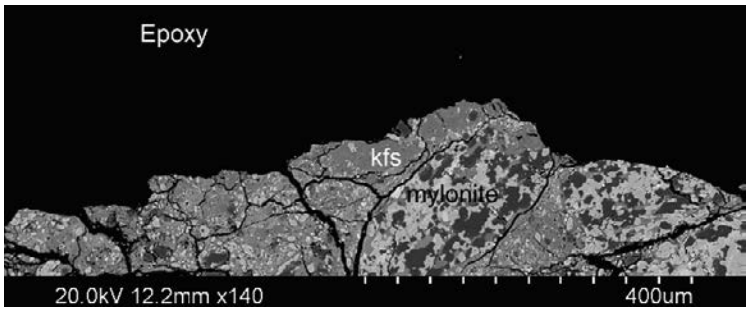

Figure 6-46. *Back-scattered SEM-image from sample 1-III-6 (KXTT4) of mylonite at the fracture rim. K-feldspar crystals (kfs) are present at the fracture rim as well.*

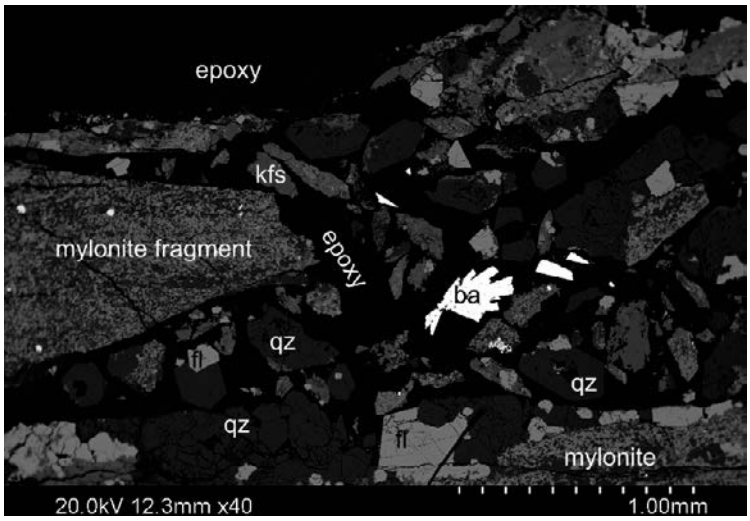

Figure 6-47. *Back-scattered SEM-image from sample 1-III-6 (KXTT4) of the fracture rim next to the main fracture (upper part of image). Epoxy from the fracture has intruded into, and fragmented a fracture coating/ filling of quartz (qz), fluorite (fl), K-feldspar (kfs) and barite (ba), present on top of older mylonite.*

Figure 6-48. *Photograph of 2:5 (KXTT4), with the open fracture (Feature A) in the upper part of the sample. The location of the thin section is indicated by the markings.*

Microscopic investigation of the thin section shows that the wall rock is highly altered in parts. Primary plagioclase and K-feldspar remain but are fractured and partly replaced by secondary minerals. Quartz is re-crystallised. Biotite is altered to chlorite, and subordinate titanite. The magnetite is euhedral and shows only limited alteration to hematite. Some fine-grained pyrite is also present. Primary titanite remains but is sometimes fractured and fragmented. Fe-Mg-rich minerals (mostly fine-grained chlorite and epidote but also euhedral magnetite) form dark bands of semi-ductile character in between the primary feldspars. These bands are particularly noticeable in a couple of very pronounced and undulating bands, with a total thickness of some millimetres. Brighter bands are made up by crypto-crystalline quartz.

The mylonite next to the fracture is mainly made up of epidote and quartz (Figure 6-49). These minerals dominate in different mylonitic bands (up to fourteen individual bands are identified) and their colour depends on the dominating mineral (epidote: green; quartz: grey). Some of the darker bands also feature chlorite and magnetite. K-feldspar (adularia), with reddish colour is also present.

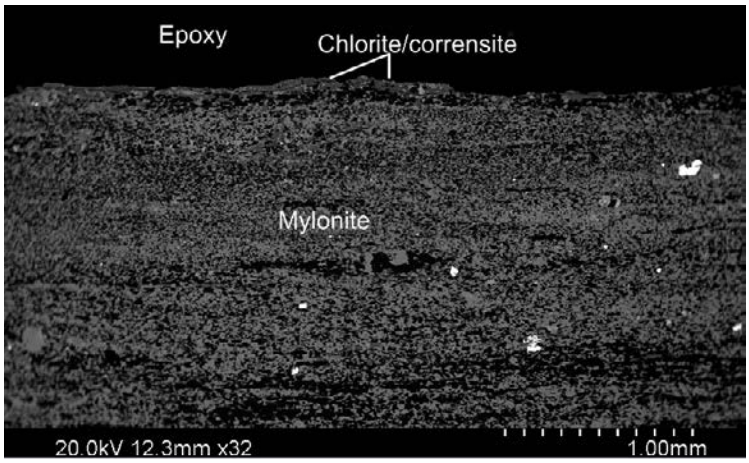

Figure 6-49. *Back-scattered SEM-image from sample 2:5 (KXTT4) of mylonite and the contact between the mylonite and the epoxy-coated fracture, which is sometimes also coated by a thin coating of chlorite/ corrensite. The epoxy was added after drilling (reinforcement of fracture surface).*

The outermost part of the mylonite, next to the epoxy-coated fracture, has a calcite coating, but only a very limited part of the fracture is coated (only ~5% in the thin section, Figure 6-50). The coating is about 40 µm thick. Mylonite borders the rest of the fracture, and is rich in epidote, quartz, K-feldspar, and chlorite. Additionally, some K-feldspar and corrensite/chlorite have grown on the fracture edge and are also younger than the mylonite (Figure 6-49).

Two micro-fractures run at a low angle from the fracture into the mylonite (a barren one is shown in Figure 6-50). One of them is filled with chlorite and corrensite, but none of them contains any epoxy.

6.4.4 Sample 3:II:8 (Feature A)

This sample consists of a highly altered granitic rock with abundant mylonite bands located both along the open fracture (Feature A), as well as within the wall rock (Figure 6-51). Most of the mylonite bands are undulating and sub-parallel to Feature A. At least one fracture within the rock is penetrated by epoxy (along one of the mylonite bands). The outermost part of the sample facing Feature A is partly coated by a couple of millimetres thick fracture filling mainly consisting of calcite, which shows that the fracture/fracture zone has been reactivated at several events (both ductile and brittle).

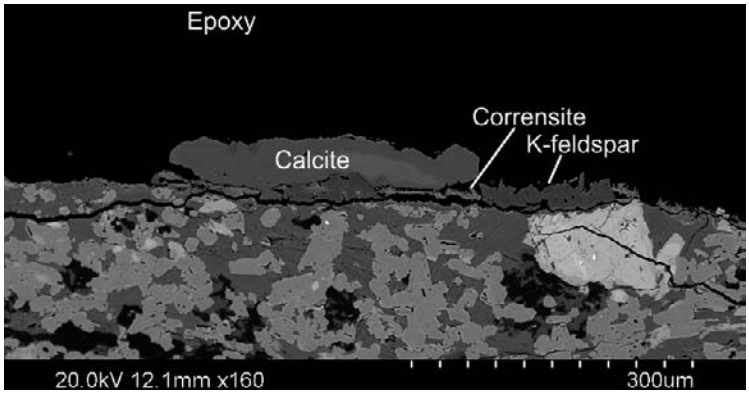

Figure 6-50. *Back-scattered SEM-image from sample 2:5 (KXTT4) of the fracture edge. K-feldspar, corrensite and calcite are the outermost minerals in contact with the epoxy. Mylonite is present beneath the thin fracture coating and one micro-fracture cuts into the mylonite (at a low angle to the fracture). The epoxy was added after drilling (reinforcement of fracture surface).*

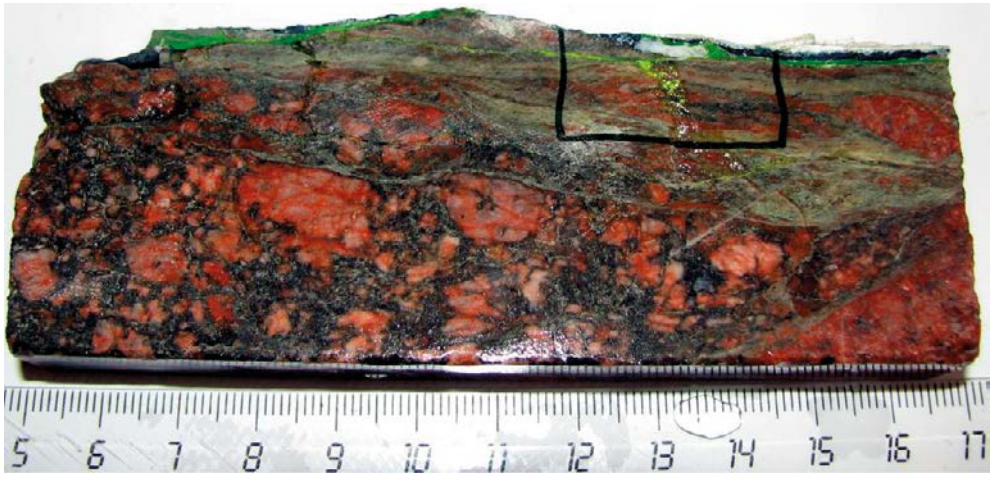

Figure 6-51. *Photograph of 3:II:8 (KXTT4), with the open fracture (Feature A) in the upper part of the sample. The location of the thin section is indicated by the markings. Bright yellow parts are epoxy impregnated fractures.*

Almost the entire thin section is made up of mylonite, which is dominantly fine-grained, greyish and quartz-dominated. Greenish-grey varieties, dominated by epidote and chlorite also exist. Wall rock minerals can be seen as fragments of variable size (mainly 1–5 mm, i.e. fault breccia pieces and fault breccia fragments according to the definition in Andersson et al. (2002a)) in the mylonite, e.g. feldspars and magnetite, which are both partly replaced by secondary minerals e.g. albite and hematite, respectively.

The outermost coating/filling next to the main open fracture is an about 5 mm thick coating of hydrothermal calcite, with associated euhedral quartz, barite, pyrite and fluorite (Figure 6-52). This fracture coating has been quite porous and the voids have been filled up with epoxy (of mm thickness). The epoxy reaches about 5 mm into the wall rock. Between the mylonite and the epoxy (or calcite filling) is a thin coating of K-feldspar (Figure 6-53).

Two micro-fractures cut into the wall rock at low angle to the main fracture and are partly filled with epoxy and calcite. These fractures reach about 1–2 cm into the wall rock/mylonite.

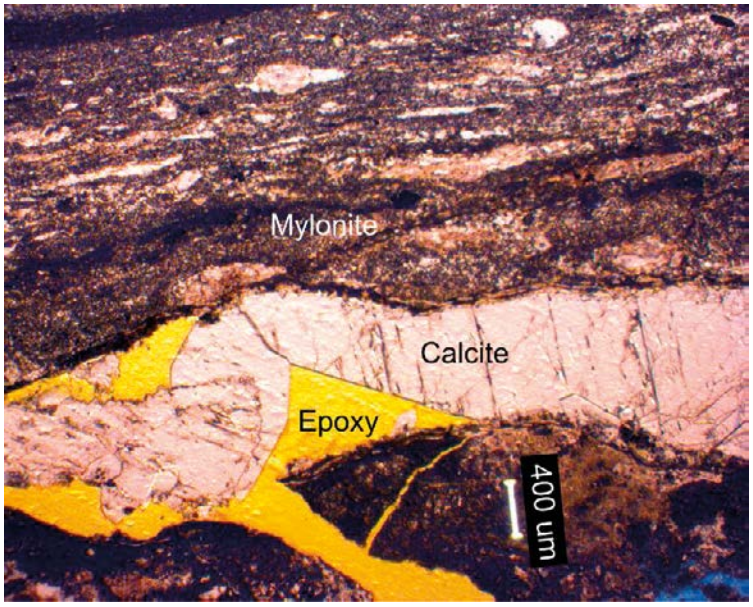

Figure 6-52. *Photomicrograph from sample 3:II:8 (KXTT4) of epoxy found within a porous calcite filling, which has cut through older mylonite. K-feldspar coats the calcite-filled fracture. Plane polarised light.*

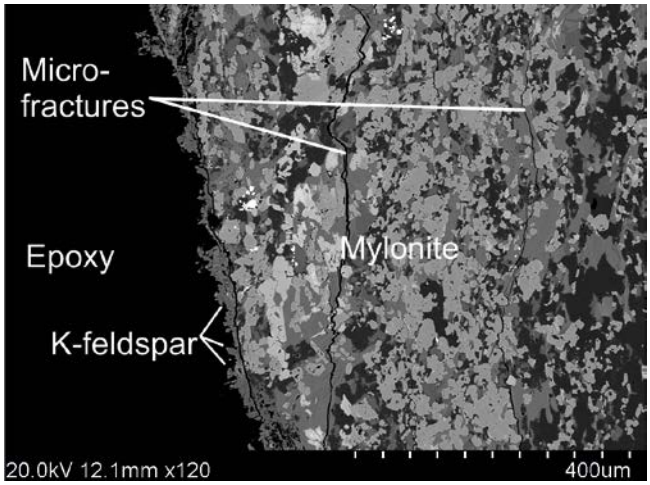

Figure 6-53. *Back-scattered SEM-image from sample 3:II:8 (KXTT4) of a K-feldspar coating between mylonite and the epoxy-coated main fracture.*

6.4.5 Sample 8:III:6 (Feature A')

This sample consists of a highly altered granitic rock, almost entirely mylonitized (Figure 6-54). The primary wall rock minerals only remain as small fragments in the mylonite, mostly as K-feldspar phenocrysts. Most of the Fe-Mg-rich minerals have re-crystallised to epidote and chlorite in the mylonite. Most of the mylonite bands are undulating and sub-parallel to the Feature A' fracture. At the fracture rim of this fracture, are also remnants of a fracture filling (consisting of e.g. calcite), which is younger than the mylonite, and formed in a brittle fracture. This shows that the fracture has been activated at several events. A partly open fracture parallel to the main fracture may also have been an active flow path.

Almost the entire thin section is made up of mylonite, which is dominantly medium-grained, greenish-grey in colour and epidote-quartz-chlorite-dominated (Figure 6-55). Euhedral, slightly altered magnetite is common as well (replaced to up to 10% by hematite).

Two of the edges of the rock featured in the thin section are in contact with the epoxy coating. One of these is bordered by a calcite filling of about 1 mm thick, parallel with the mylonite, present between the mylonite and the epoxy (calcite-epoxy contact shown in Figure 6-56). Related to this calcite is a fine-grained filling of mainly corrensite (euhedral). Small amounts of euhedral quartz and fluorite are found together with the corrensite. Calcite (dominantly) and corrensite forms the contact with the epoxy. The other epoxy-bordered edge is oriented perpendicular to the mylonite, and the fracture surface is very rough. Some micro-fractures have introduced epoxy from this fracture edge into the mylonite, maximum 0.8 mm into it, both perpendicularly and sub-parallel to the mylonite strata. Next to the calcite-filling, epoxy has penetrated 1.5 mm into the mylonite, in a 50 µm thick fracture, perpendicular to the mylonite foliation.

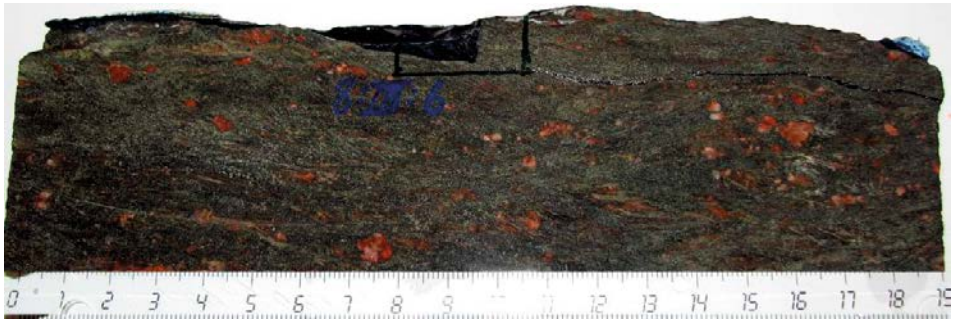

Figure 6-54. *Photograph of sample 8:III:6 (KXTT4), with the open fracture (Feature A') in the upper part of the sample. The location of the thin section is indicated by the markings. Black parts are epoxy attached to the fracture surface after drilling.*

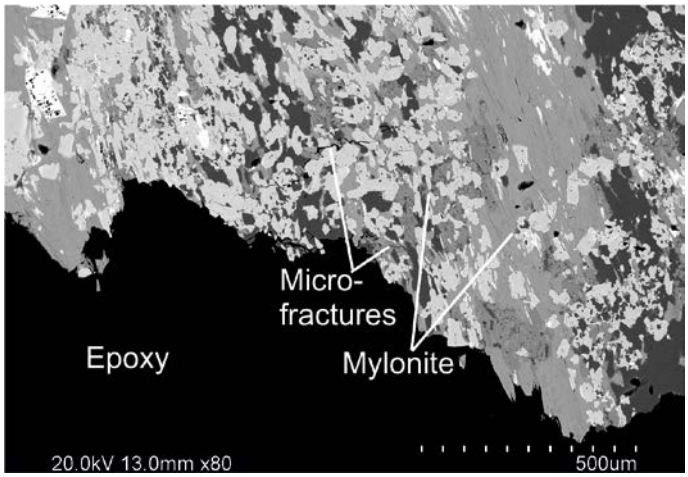

Figure 6-55. *Back-scattered SEM-image from sample 8:III:6 (KXTT4) of mylonite and epoxy bordering to mylonite and penetrating into some micro-fractures in the mylonite. The epoxy was added after drilling (reinforcement of fracture surface).*

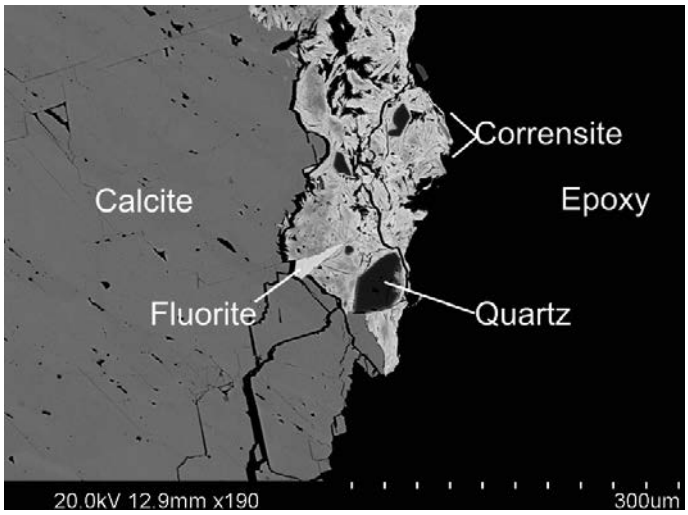

Figure 6-56. *Back-scattered SEM-image from sample 8:III:6 (KXTT4) of the outermost part of the calcite-corrensite(-fluorite-quartz) coating next to the epoxy-coated fracture. The epoxy was added after drilling (reinforcement of fracture surface).*

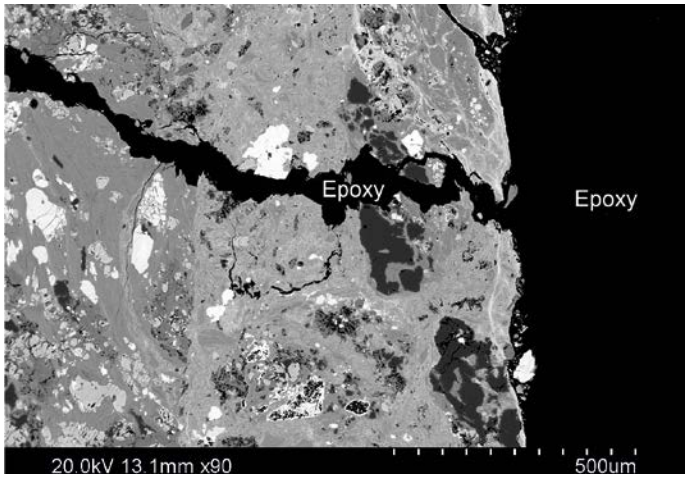

Figure 6-57. *Back-scattered SEM-image from sample 8:III:6 (KXTT4) showing epoxy intruding into the mylonite. The epoxy was added after drilling (reinforcement of fracture surface).*

6.4.6 Sample 8:III:7 (Feature A')

This sample consists of a strongly altered and deformed granitic rock, which is almost completely mylonitized (Figure 6-58). The primary wall rock minerals only remain as small fragments in the mylonite, mostly as K-feldspar phenocrysts. Most of the Fe-Mg-rich minerals have re-crystallised to epidote and chlorite. Most of the mylonitic bands are undulating and sub-parallel to the Feature A' fracture. An open fracture sub-parallel to the main fracture is also present (Figure 6-59), and the fracture surfaces of this fracture have been investigated using SEM-EDS and show:

The lower rim of the fracture includes the following minerals (not in order of formation):

- Chlorite, which dominates the fracture (see EDS spectra in Figure 6-60, and SEM-image in Figure 6-61),
- Clay minerals (mixed layer-clay, see EDS spectra in Figure 6-60), which are almost as common as chlorite,
- Quartz,
- Illite,
- Fe-oxide (< 25 µm crystals),
- Chalcopyrite (scattered anhedral crystal aggregates of up to 150 µm in size),
- Ti-oxide (5–25 µm crystals),
- Apatite.

Figure 6-58. *Photograph of 8:III:7 (KXTT4), with the open fracture (Feature A') in the upper part of the sample. Black parts are epoxy attached to the fracture surface after drilling.*

Figure 6-59. *Photograph of 8:III:7 (KXTT4), showing both of the fracture surfaces of the fracture parallel to the open Feature A' fracture.*

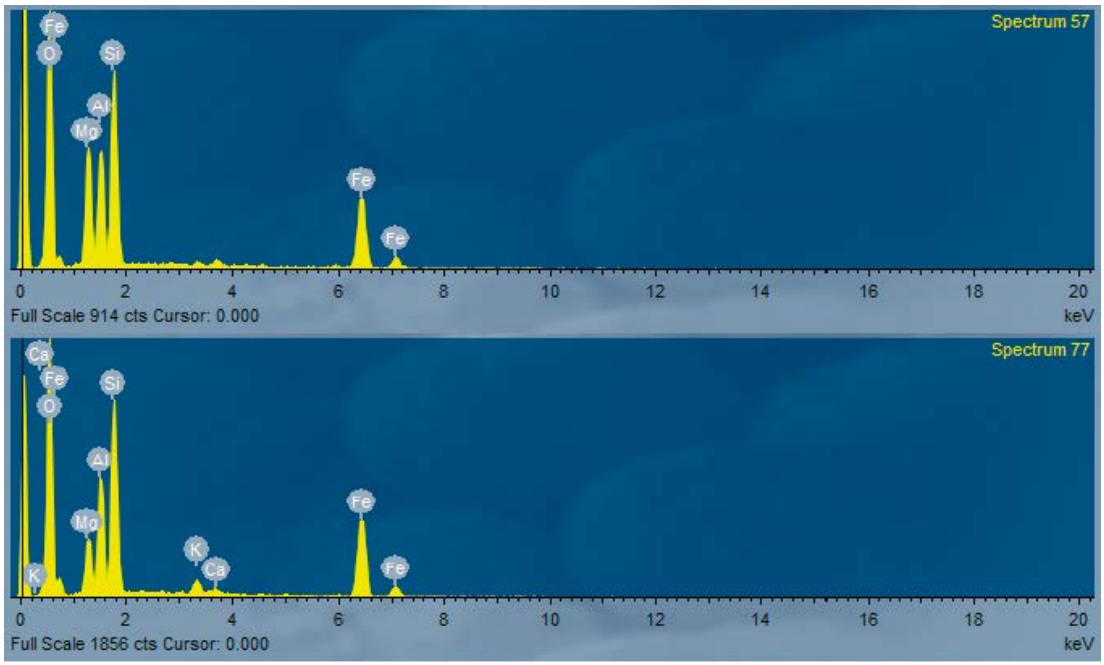

Figure 6-60. *EDS spectra from sample 8:III:7 (KXTT4) of chlorite and clay minerals.*

Figure 6-61. *Back-scattered SEM-image from sample 8:III:7 (KXTT4) of chlorite, commonly appearing as a smooth layer, but occasionally, platy irregular crystals make the surface rougher.*

At least ~80% of the surface is covered by chlorite and clay minerals. About 10–15% of the fracture surface is covered by clusters of fine-grained quartz, Fe-oxide, Ti-oxide, illite, and apatite etc. Wall rock is exposed in 5–10% of the fracture surface.

The surface is smooth. Fine-grained crystal aggregates are present and the individual crystals are commonly < 10 µm.

Upper rim of the fracture includes the following minerals (not in order of formation):

- Chlorite (see EDS spectrum 98 in Figure 6-62, and SEM-image in Figure 6-63) and clay minerals dominate. The clay minerals are mostly mixed layer-clay, sometimes of euhedral corrensite-type, with spherulitic aggregates with large surface area (see EDS spectrum 91 in Figure 6-62). The spherulitic corrensite aggregates are ~20–50 µm in diameter and are made up of numerous platy crystals with an individual thickness generally of about 0.5–2 µm (Figure 6-64),

- Quartz, euhedral crystals, up to 200 µm in size,
- Chalcopyrite, scattered anhedral aggregates of up to 150 µm in size (Figure 6-63),
- Fluorite, euhedral, up to 120 µm sized crystals, associated with corrensite and euhedral quartz,
- Sphalerite, is rare, and is found together with fluorite and corrensite.

About 50–60% (estimated) of the surface is covered by chlorite and clay minerals. Chalcopyrite is common and make up 5–10% of the fracture surface area. Rough parts where euhedral fluorite, corrensite, quartz etc. are found make up ~30–40% of the surface area.

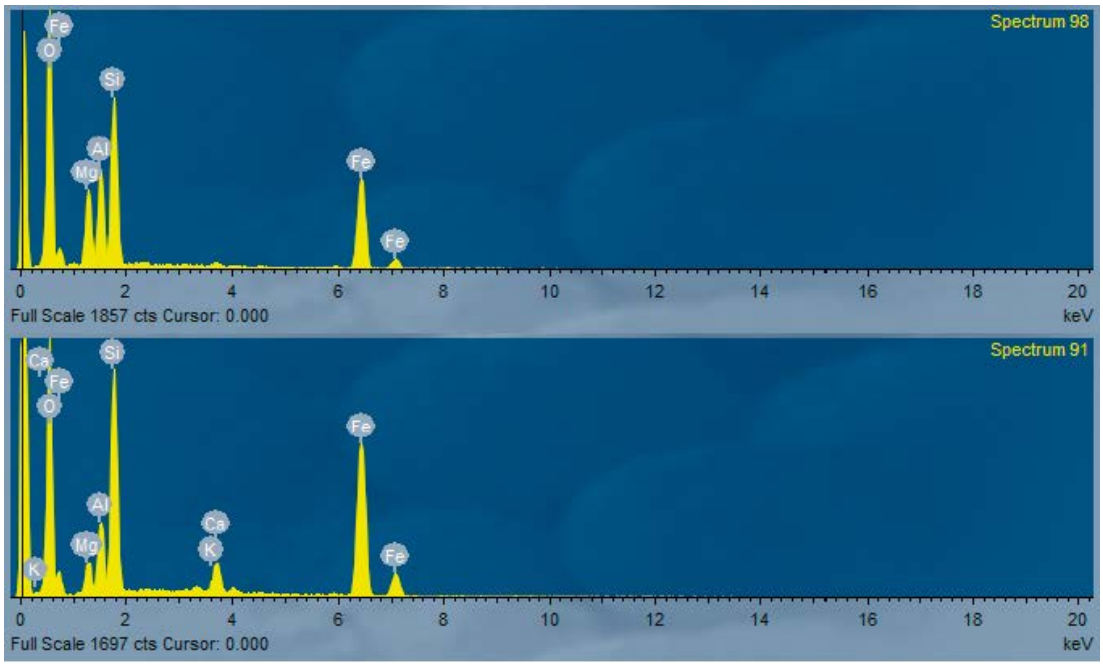

Figure 6-62. *EDS spectra from sample 8:III:7, KXTT4.*

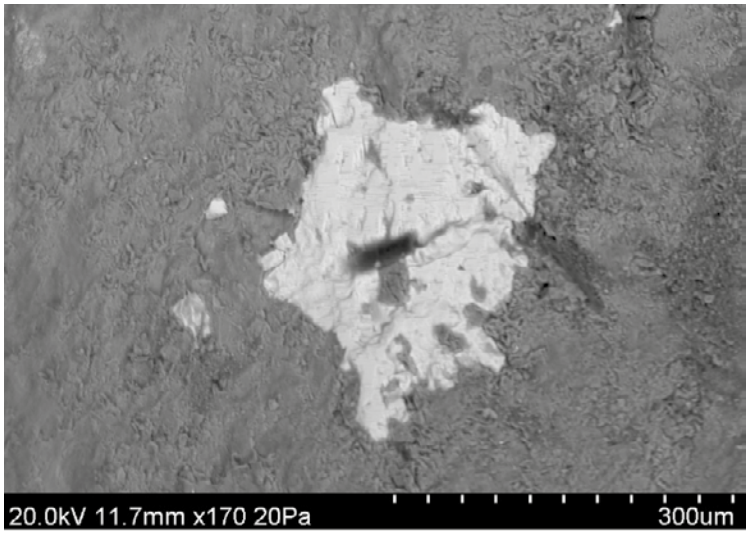

Figure 6-63. *Back-scattered SEM-image from sample 8:III:7 (KXTT4) of chlorite (dark) and chalcopyrite (bright). Chlorite commonly appears as a smooth layer, but occasionally platy, irregular crystals make the surface rougher, as shown in this image.*

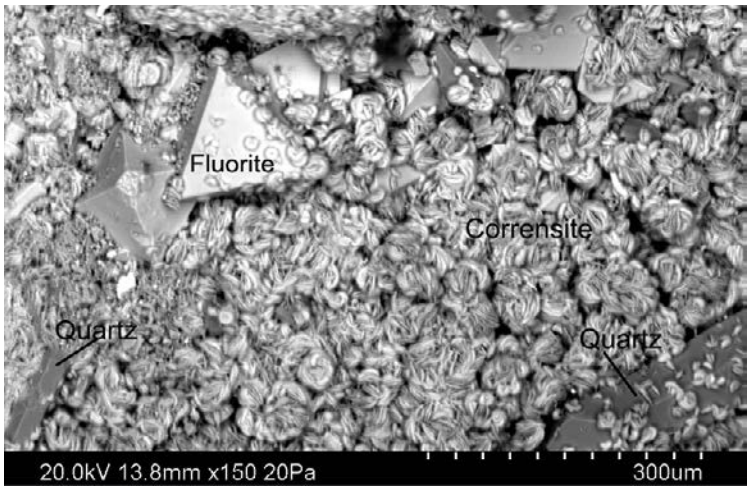

Figure 6-64. *Back-scattered SEM-image from sample 8:III:7 (KXTT4) of corrensite, fluorite and quartz.*

The fracture surface is mainly smooth, and the smooth parts are dominated chlorite and clay minerals. However, parts with spherulitic corrensite aggregates are rougher. Fine-grained crystal aggregates are present and the individual crystals are commonly < 10 µm. In parts where euhedral fluorite, corrensite, quartz etc. are found (~30% of the surface), the surface is very rough and the surface area of the individual crystals is very large, especially where corrensite is present.

6.4.7 Sample 11:I:5 (Feature A')

The sample consists of highly altered granitic rock, with up to centimetre-thick mylonite bands (Figure 6-65). One of the major mylonite bands runs parallel to the open Feature A' fracture. Another branch of this mylonite runs sub-parallel with the fracture, a couple of centimetres into the wall rock. The fracture surfaces of an open/partly open less permeable fracture at one centimetre distance from the Feature A' fracture has been investigated using SEM-EDS and shows that the minerals on the fracture surface are (not in order of formation):

- Clay minerals, which dominate. They are of mixed layer-clay type (see EDS spectrum 38 in Figure 6-66, and SEM-image in Figure 6-67). The maximum grain size of the individual crystals is about 40 µm. The main grain size is below 5 µm.
- Chlorite (see EDS spectrum 32 in Figure 6-66).
- K-feldspar (see EDS spectrum 35 in Figure 6-66).
- Illite.
- Quartz, fine-grained crystals < 25 µm.
- Fe-oxide, fine-grained < 25 µm crystals.

At least ~85% of the fracture surface is covered by clay minerals and chlorite. About 10–15% of the fracture surface is covered by clusters of fine-grained K-feldspar, quartz, Fe-oxide and other wall rock derived minerals. Clay minerals and chlorite are also present in these clusters.

The fracture surface is undulating but quite smooth, and mostly lacks euhedral single crystals or crystal aggregates on the smooth surface. If fine-grained crystal aggregates are present, individual clay mineral crystals are commonly < 10 µm.

Figure 6-65. *Photograph of sample 11:I:5 (KXTT4), with the open fracture (Feature A') in the upper part of the sample. Black parts have been epoxy-impregnated after drilling.*

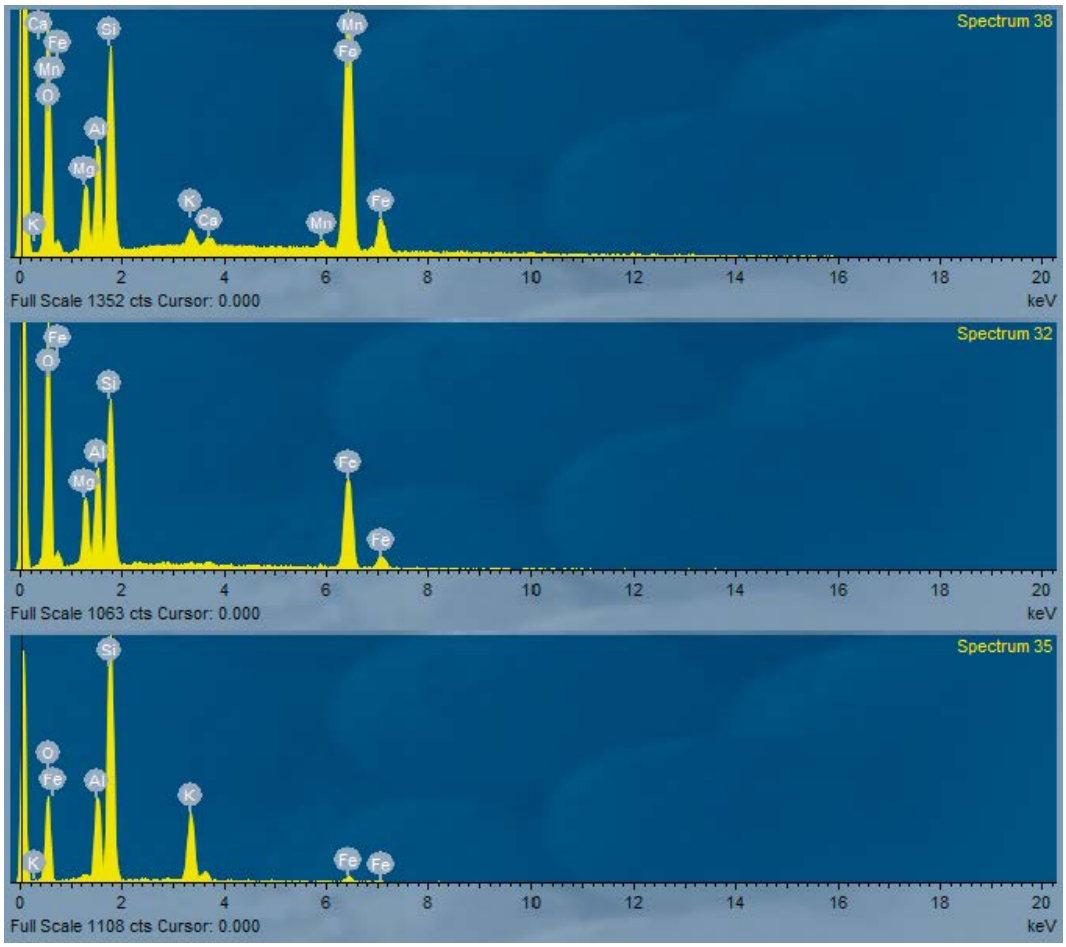

Figure 6-66. *EDS spectra from sample 11:I:5 (KXTT4).*

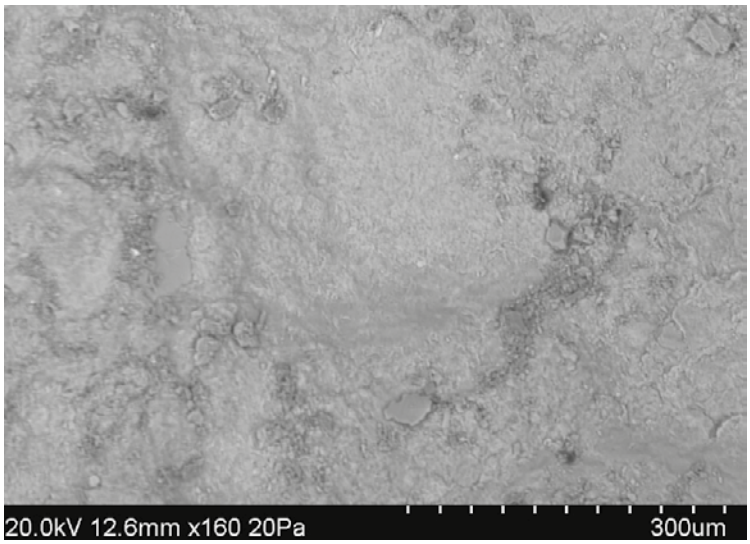

Figure 6-67. *Back-scattered SEM-image from sample 11:I:5 (KXTT4) of the smooth fracture coating, dominated by clay minerals and chlorite. Scattered individual clay mineral crystals make the coating rougher locally.*

6.4.8 Sample 11:III:4 (Feature A')

This sample consists of a highly altered granitic rock with several sub-parallel mylonite bands (Figure 6-68) of which the two most distinct bands are about 5 mm thick, sub-parallel and slightly undulating. One of them borders to the open fracture (Feature A), which has reactivated the mylonite. The mylonite has earlier been reactivated along the same fracture plane as Feature A', on at least one occasion, shown by the presence of calcite (seen in the photograph as a white coloured, calcite-dominated filling bordering the open fracture).

Almost the entire thin section is made up of mylonite, which is greenish-grey in colour and epidote-dominated. Chlorite is also common in the epidote-rich parts of the mylonite. Some brighter parts are dominated by crypto-crystalline quartz. Wall rock minerals can be seen as fragments in the mylonite, e.g. feldspars and magnetite, which both are partly replaced by the secondary minerals albite and hematite. There are two major mylonite bands in the thin section. The one closest to the open fracture runs parallel to fracture surface, whereas the other differs in orientation by up to 30°.

Figure 6-68. *Photograph of 11:III:4 (KXTT4), with the open fracture (Feature A') in the upper part of the sample. The location of the thin section is indicated by the markings. Black parts have been epoxy-impregnated after drilling.*

Fine-grained, cataclasite fillings of adularia, hematite and chlorite with a dark red to black colour, are up to 200 µm thick and are commonly present close to the fracture edge. The cataclasite cuts through the mylonite. The outermost coating is however made up of both a single elongated, anhedral, calcite crystal (up to 0.8 mm thick, Figure 6-72), which lines almost 50% of the fracture length, as well as by an up to 100 µm thick (commonly < 50 µm) corrensite coating, (with some related fluorite). The latter coats the rest of the fracture and is found underneath calcite, where present. Corrensite is euhedral and forms spherulitic aggregates (Figure 6-70, see also EDS spectrum in Figure 6-72). Partly, corrensite also coats the outermost part of the calcite crystal, and in these cases, it is the outermost part of the coating.

A less than 50 µm thick micro-fracture, running sub-parallel to the open fracture, is partly filled with epoxy about 0.4 mm into the wall rock/mylonite (Figure 6-73).

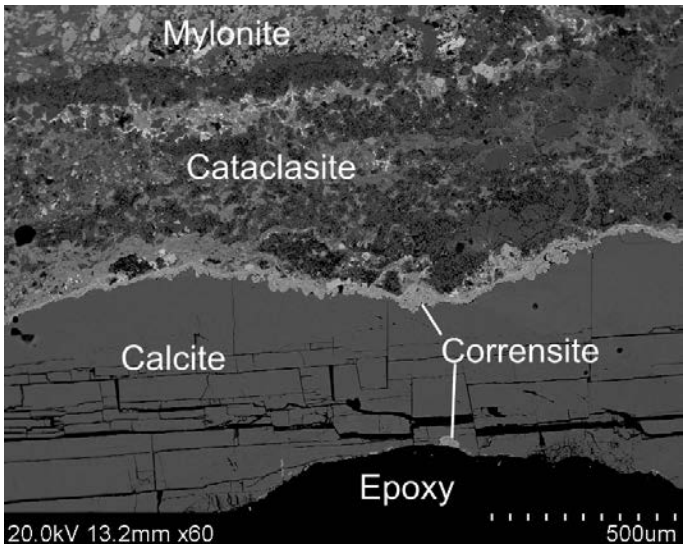

Figure 6-69. *Back-scattered SEM-image from sample 11:III:4 (KXTT4) of the outermost part of the coating next to the open fracture (coated by epoxy), in order: mylonite, at greatest distance from the fracture, cataclasite (which sometimes is in contact with epoxy), and the outermost minerals corrensite and calcite. The epoxy was added after drilling (reinforcement of fracture surface). Epoxy is not present in the micro-fractures in the interior of the calcite filling.*

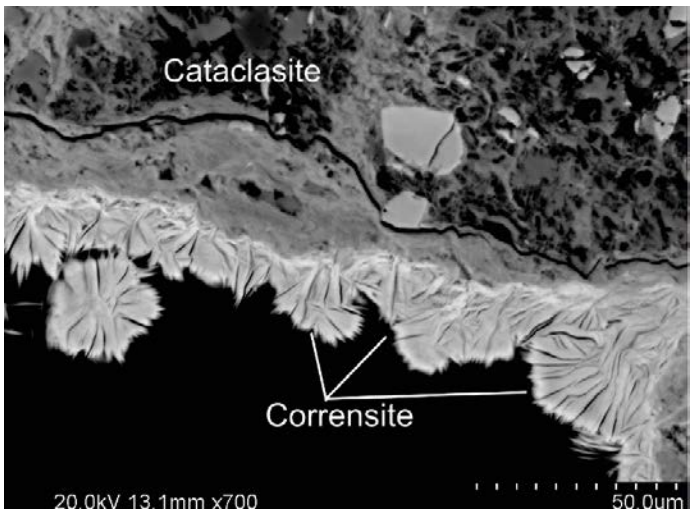

Figure 6-70. *Back-scattered SEM-image from sample 11:III:4 (KXTT4) of the outermost part of the coating next to the open fracture (coated by epoxy), with cataclasite coated by euhedral corrensite. The epoxy was added after drilling (reinforcement of fracture surface).*

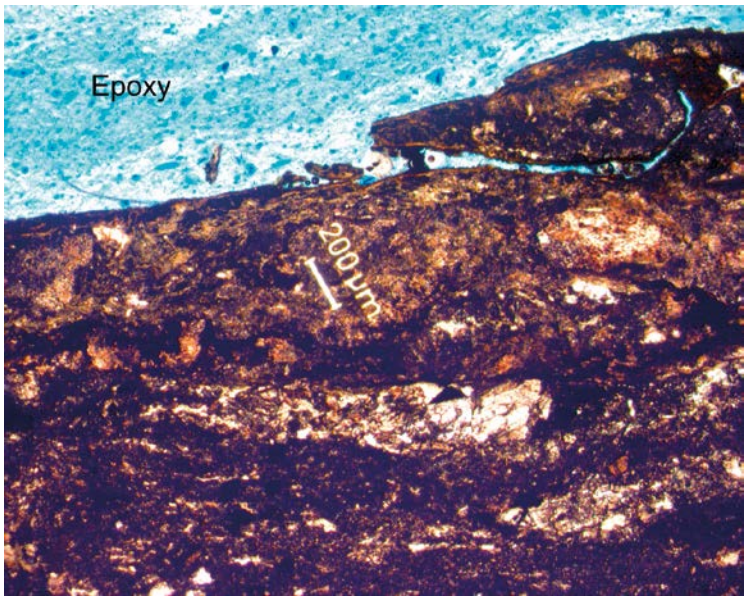

Figure 6-71. *Photomicrograph from sample 11:III:4 (KXTT4) of epoxy in contact with and partly intruding into mylonite. Plane polarised light. The epoxy was added after drilling (reinforcement of fracture surface).*

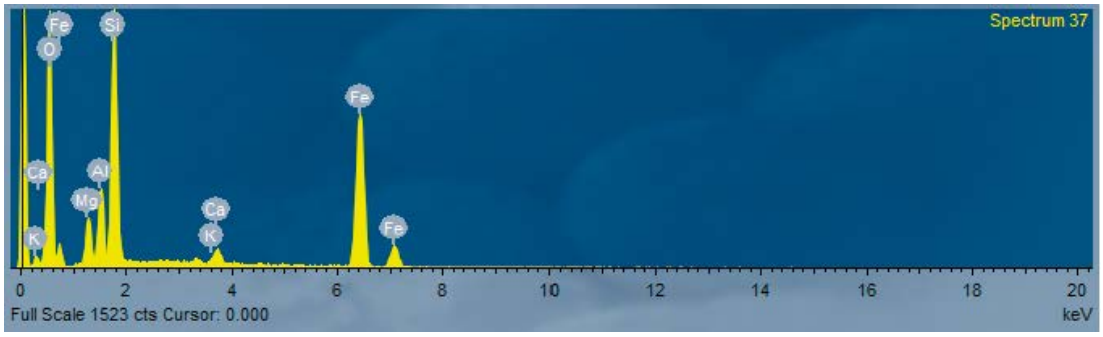

Figure 6-72. *EDS-spectrum from sample 11:III:4 (KXTT4) for corrensite.*

Figure 6-73. *Photograph of sample 11:III:6 (KXTT4), with the open fracture (Feature A') in the upper part of the sample. The location of the thin section is indicated by the markings. Black parts have been epoxy-impregnated after drilling.*

6.4.9 Sample 11:III:6 (Feature A')

This sample consists of a highly altered granitic rock with several sub-parallel mylonite bands (Figure 6-73). Only fragmented, and partly re-crystallized, K-feldspar phenocrysts remain of the primary wall rock minerals. The two most distinct mylonite bands are about 5–20 mm thick and are sub-parallel and slightly undulating. One of these bands is about ~5 mm thick and borders to the open fracture (Feature A').

The wall rock is in parts highly altered and has a foliation oriented about 45° from that of the fracture and the mylonite. Primary plagioclase and K-feldspar are fractured and largely replaced by secondary minerals. Quartz is re-crystallised. Biotite is altered to chlorite and subordinate titanite. Magnetite is euhedral, but is to a variable degree (25–75%) replaced pseudomorphically by hematite. Some fine-grained pyrite is also present. Primary titanite remains but it is sometimes fractured and fragmented. Fe-Mg-rich minerals are mostly fine-grained chlorite and epidote, but also euhedral magnetite, form dark bands of semi-ductile character in between the primary feldspars. Brighter bands are made up by crypto-crystalline quartz.

The mylonite next to the fracture is mainly made up of epidote. Numerous quartz crystals also exist and form occasional individual mylonite bands, which are not as dominant as the epidote-dominated bands. Reddish K-feldspar (adularia) is also present.

The outermost part of the mylonite, which is present very close to the epoxy-coated fracture, features high amounts of euhedral epidote. Close to the fracture the mylonite is cut by fine-grained cataclasite fillings consisting of adularia, hematite and chlorite, with a dark red to black colour (Figure 6-74). These fillings are up to 200 µm thick and are also present at the very edge of the fracture, i.e. between the epoxy and the mylonite, but they also cut through the mylonite. Green-coloured chlorite is spatially associated with these fillings. The outermost coating is mainly a thin corrensite-dominated coating, of about 10–50 µm thickness, found on top of the cataclasite (Figure 6-75). The corrensite crystals are euhedral, and coats about 50% of the main fracture in the thin section. One part of the coating also features euhedral 10–20 µm hematite crystals in contact with the epoxy, but this coating is only 200 µm thick.

Occasionally, very thin fractures (< 20 µm thick) cut through the adularia-hematite-chlorite-fillings. These fractures are calcite-filled, and at one part of the fracture (only about 0.4 mm), this calcite is the outermost part of the coating. None of the micro-fractures, running from the fracture into the wall rock contain any epoxy.

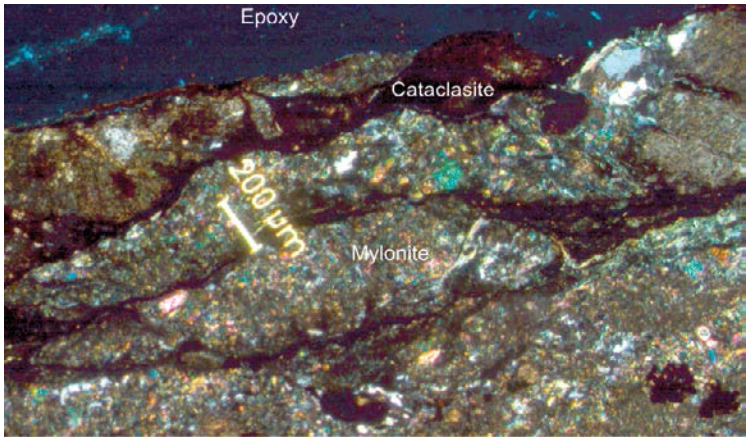

Figure 6-74. *Photomicrograph from sample 11:III:6 (KXTT4) of mylonite and younger dark red cataclasite next to the epoxy-coated main fracture. The epoxy was added after drilling (reinforcement of fracture surface).*

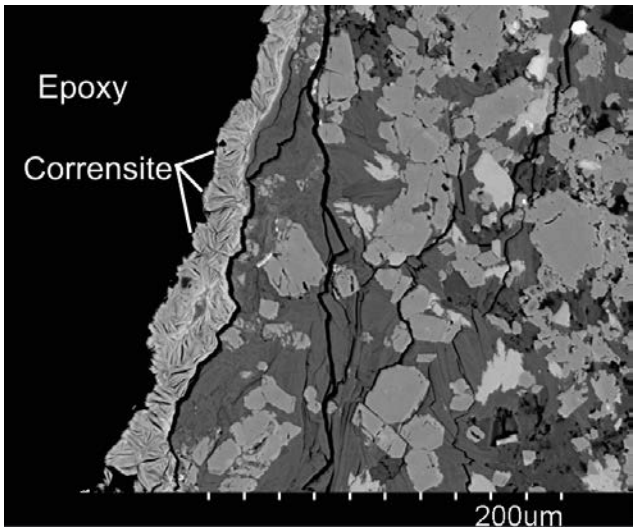

Figure 6-75. *Back-scattered SEM-image from sample 11:III:6 (KXTT4) of a corrensite coating on top of mylonite, next to the main fracture. The epoxy was added after drilling (reinforcement of fracture surface). Micro-fractures do not contain epoxy.*

6.4.10 Summary of KXTT4 sample characteristics

The KXTT4 samples feature several generations of fracture fillings/coatings, which once again supports that Feature A and Feature A' have been reactivated at several events and that these samples (KXTT4), in similarity with the KXTT3 samples, show that the features have been water-conducting for a very long time, although the detailed flow paths may have varied.

The oldest secondary minerals are in the numerous sub-parallel mylonite bands, which are characteristic for Feature A and Feature A', and are found in all of the samples. Younger cataclasite is also present in some of the samples. Fracture fillings of prehnite, quartz and K-feldspar are not as frequent as in the KXTT3 samples. The next generation, consisting dominantly of calcite, but also fluorite, pyrite, barite, quartz and clay minerals and some accessory minerals, e.g. some sulphide phases, is very common. The outermost coatings are often completely dominated by chlorite and clay minerals, but also by calcite and K-feldspar coatings and additional wall rock fragments. The fracture surfaces are not always covered by fracture minerals. Instead, the wall rock (or mylonite) is exposed. The clay mineral-chlorite fracture coatings are often very smooth, but may be rougher when euhedral minerals, such as spherulitic corrensite, cubic fluorite, euhedral K-feldspar, or wall rock fragments are abundant. Clay minerals are mainly of mixed-layer type, probably dominantly of chlorite/smectite type (corrensite). The mylonite in Feature A' seems to be a little bit thicker than the Feature A mylonite, in general roughly 5–20 mm bands (sometimes together comprising up to 5 cm in collective thickness) vs. 5–8 mm bands, respectively.

6.5 Summary of mineralogical investigations

The samples from the two drill cores KXTT3 and KXTT4 generally show the same type of fracture mineral assemblages and deformation (see summary in Table 6-1), and the variation within the samples is generally larger than the variation between the different samples. The numerous generations of fracture fillings/coatings, show that Feature A and Feature A' have been reactivated at several events and that they have been intermittently water-conducting for a very long time, although the detailed flow paths may have varied.

The fracture mineral generations in Feature A and Feature A' comprise five events (from oldest to youngest):

1. Mylonite (usually epidote-dominated, very fine-grained shear bands in the order of 15 mm thickness).
2. Cataclasite.
3. Prehnite, quartz, K-feldspar, chlorite and occasionally epidote. Hydrothermal precipitates in fractures that have formed due to brittle reactivation of the mylonite.
4. Calcite, fluorite, corrensite, quartz, K-feldspar and barite.
5. Chlorite and corrensite comprise the youngest fracture coating and in many cases constituting the surface (contact to the epoxy impregnation), sometimes together with calcite, K-feldspar and minor precipitates of sulphides.

The sequence of events listed above have earlier been observed and described in several studies from the area (e.g. at Laxemar and Simpevarp, summarised in Drake and Tullborg (2009a)), and Feature A and Feature A' can therefore be regarded as very representative for the area in this regard. The earliest deformation identified dates back to ductile/semi-ductile conditions with formation of mylonites (generation 1) and cataclasites (generation 2), which have been interpreted to be more than 1.4 Ga old (Drake and Tullborg 2009a). Along these zones of weakness, repeated activation in the brittle regime has occurred subsequently, such as by Proterozoic prehnite-quartz-chlorite-K-feldspar (generation 3), and by Palaeozoic calcite-fluorite-quartz-barite-clay mineral-chlorite fillings/coatings (generation 4). The former has been described in detail in studies from Laxemar, Simpevarp and Äspö (e.g. Stanfors et al. 1999, Drake and Tullborg 2005, 2009b, Drake et al. 2009) and the latter generation is also very common in the whole Laxemar-Simpevarp-Äspö (Drake and Tullborg 2009a) and the age is around 440–400 Ma (Drake and Tullborg 2009a). Earlier studies from Laxemar, Simpevarp, Äspö and Götemar, have shown that calcite of this generation has a very typical stable isotope composition (Tullborg 2003, Drake and Tullborg 2006, 2009a, b), e.g. indicating higher formation temperatures than the present. Stable isotope values of six Feature A calcites (Winberg 1996), match those earlier reported for this generation which is another example of that the characteristics of Feature A are representative for the area.

The outermost coatings are often dominated completely by chlorite and clay minerals (generation 5), and partly also by calcite, K-feldspar, fluorite, wall rock fragments and some scattered sulphides and sulphates. It has not been possible to draw any conclusions regarding the actual ages of these outermost mineral coatings, but a late Palaeozoic maximum age (~250 Ma) can be proposed and Quaternary ages (within the last 2 Ma) are possible for at least some of the minerals, based on earlier studies in the area (Drake and Tullborg 2009a). Minor parts of the fracture surfaces are in some cases not covered by any fracture minerals, and the wall rock (or mylonite) is exposed. The clay mineral-chlorite fracture coatings are often very smooth, but may be rougher when euhedral minerals, such as spherulitic corrensite aggregates, cubic fluorite, and euhedral K-feldspar, or wall rock fragments are abundant. Clay minerals are mainly of mixed-layer type, probably dominantly of chlorite/smectite type (corrensite).

In contrast to the studies summarised in Winberg et al. (2000) in which clay minerals could not be identified although they were interpreted to be present on the fracture coatings, based on retention results and modelling, the current investigation has detected clay minerals. This is mainly due to that the fracture zone was impregnated with epoxy prior to drilling, which has enabled preservation of the soft clay minerals. Another reason is that the core diameter is larger which has enabled sampling of larger samples. Therefore, the results presented in this report can be regarded to be more representative for Feature A than those reported in Winberg et al. (2000), where, in addition, the superior triple-tube drilling technique was not applied. Epoxy has generally not intruded far into the fracture coatings/fillings or wall rock. In a minority of the samples, epoxy has entered into porous parts of partly filled fractures and has fragmented the fracture filling, and may also sometimes include mylonite fragments from the fracture rim. If epoxy has entered into the wall rock it is either through micro-fractures running perpendicular to the main fracture (up to a couple of millimetres of intrusion), or it has, more commonly, entered through micro-fractures or fractures which are sub-parallel to the main fracture, and commonly runs along an older fracture filling generation.

The fact that Feature A has acted as a zone of weakness since the Proterozoic and that it has been a pathway for hydrothermal fluid during both Proterozoic and Palaeozoic events and remained water conducting probably since the late Palaeozoic is in accordance with observations from many other features studied during the site investigation at Laxemar/Simpevarp and at Äspö (Stanfors et al. 1999, Drake and Tullborg 2005, 2009a, b, Drake et al. 2009). The flow path follows the Feature A structure but it should be emphasised that the actual water conducting channels may have varied over time and it is shown by epoxy impregnation that the flow alternates between fractures filled or coated by different mineral assemblages within the zone, and several parallel fractures are sometimes impregnated showing the complexity of the structure. This is in accordance with observations made by Winberg et al. (2000) and Andersson et al. (2002c).

The thickness of the outermost coatings next to the epoxy varies from about 0.8 to 5 mm for calcite (minimum down to 40 μm, in comparison the mean calcite fracture coating thickness at the Laxemar site is ~0.25 mm (Löfgren and Sidborn 2010)) and from 10 to 500 μm for chlorite/clay minerals (mainly 50–100 μm). The size of individual crystals on the fracture coatings vary from about 10 μm in smooth chlorite/clay mineral coatings, but individual corrensite aggregates may be up to 50 μm. The epoxy thickness is generally 100–800 μm, although it may occasionally have a thickness of a couple of millimetres. (Particular analyses of the epoxy geometrical characteristics are presented in Chapter 5.) When epoxy has penetrated into the wall rock or fracture coatings it has reached from 0.4 mm up to a couple of centimetres depth in the studied samples.

Table 6-1. Summary of the fracture mineral observations in the KXTT3 and KXTT4 samples.

		Fracture mineral generations					Outermost coating
Drill core	**Sample**	**Mylonite**	**Cataclasite**	**Pre-qz-kfs-chl-(ep)**	**cc-fl-co-qz-kfs-ba**	**chl/co**	**Minerals**
KXTT3	25 (Fracture 1)	x		x	x	x	myl, cc, (ba, chl/co)
KXTT3	26 (Fracture 1)	x	x	x		x	catacl+chl, qz, kfs, pl, MLC (sm/chl)
KXTT3	Part of piece 31 (Fracture 1 and 2)	x	x	x		x	chl, ep, qz, kfs, (pl), MLC (sm/chl)
KXTT3	X (close to piece 29)			(x)	(x)	x	chl, qz, kfs, pl, MLC (sm/chl)
KXTT3	Feature A - fragments			(x)	x	x	chl, qz, kfs, pl, ill, MLC (sm/chl), cc, fl, ba, (qz)
KXTT3	Fragments from Fracture 3 at 14.08–14.11 m				x	x	co/chl, cc, kfs
KXTT4	1:I:0	x			x	x	chl/co, (py, qz, ep, Fe-ox, ga, sph), WR-frag
KXTT4	1:III:6	x	x	(x)	x	x	cc,fl,kfs,ba,qz,chl,myl
KXTT4	2:5	x			x	(x)	myl, (+cc, chl/co, adu)
KXTT4	3:II:8	x		(x)	x	x	cc,fl,ba,qz,py,kfs
KXTT4	8:III:6	x			x	x	mylonite, cc, co,
KXTT4	8:III:7	x			(x)	x	chl/co, (cpy, fl, qz, Ti/Fe-ox, ill, WR-frag).
KXTT4	11:I:5	x				x	chl/co, (WR-frag)
KXTT4	11:III:4	x	x		x	x	cc, co (+fl)
KXTT4	11:III:6	x	x			x	co, catacl, (Fe-ox)

myl = mylonite, catacl = cataclasite, cc = calcite, ep = epidote, ba = barite, chl = chlorite, co = corrensite, qz = quartz, kfs = K-feldspar, pl = plagioclase, MLC = mixed-layer clay, sm = smectite, ill = illite, fl = fluorite, Fe-ox = Fe-oxide, Ti-ox = Ti-oxide, ga=galena, sph = sphalerite, WR-frag = wall rock fragments, py = pyrite, cpy = chalcopyrite, pre = prehnite. Minerals in brackets are minor minerals.

7 Analysis of Cs-137 on surfaces

7.1 Methodology for Cs-137 analyses

7.1.1 Background

The fractures connecting the borehole sections KXTT4:T3 and KXTT3:S3 was used for tracer experiment in June 1996 (Sorbing Tracer Test 1, STT1) and in June 1997 (STT2) (Winberg et al. 2000). In the first experiment a cocktail of radiotracers were injected among which Cs-137 ($t_{½}$=30.2 years), Ba-133 ($t_{½}$=10.5 years), Na-22 ($t_{½}$=2.6 years) and H-3 ($t_{½}$=12.3 years) are long-lived enough to still be measurable today. In the STT2 tracer experiment, the same tracers were used, except for Cs-137 which was replaced by Cs-134 ($t_{½}$=2.06 years). The mass recoveries (i.e., the part of the injected tracers that was pumped out from the fracture) were high for the most the tracers, except for the comparatively strongly sorbing Cs tracers for which only less than 38% and 24% (STT1 and STT2, respectively) were recovered.

During the time period after the pumping of the STT2 tracer experiment was finished in the end of 1998, the borehole section has for most of the subsequent duration been closed without any water extraction. However, several short time pumping tests have been performed from that time until now of which the CEC test (Nordqvist et al. 2015), injection of high chemical concentrations of non-radioactive Cs in the flow path of the STT1 and STT2 tracer experiment, is the one that one could be associated with the highest release of adsorbed radioactive Cs tracer. Nevertheless, a total amount of only 40 kBq of Cs-137 could be measured in the pumped water of the CEC experiment. This should be compared to the 4.4 MBq of Cs-137 which was not recovered in the tracer experiments performed 10 years before the performance of the CEC experiment and therefore expected to remain in the surrounding of in the fracture system. This comparison therefore gives that less than 1% of the tracer was desorbed in the CEC experiments. One could thus anticipate a significant amount of radioactive tracers, especially in the injection section of borehole KXTT4, to remain and be measurable on the fracture surfaces of Feature A and A' of the overcored rock. Such measurements should therefore provide information on the sorption characteristics.

7.1.2 Experimental

Four different measurement campaigns were performed for the measurement of traces of radioactivity on the overcored rock material in the surroundings of the Feature A fracture system.

Contamination monitoring

Directly after the overcoring process, the drill core was measured qualitatively using a portable contamination monitor (plastic scintillation monitor), a detector that give response Cs-137 in the range of > 500 Bq. It was only for the Feature A' surface in KXTT4 that the scintillation monitor indicated presence of radioactivity.

Autoradiography

An attempt to visualise the spatial distribution of the sorption of radioactive tracers on the fracture surfaces was performed, i.e. a photographic film (KODAK BioMax MR film) was placed on the fracture surfaces and the obtained blackening should therefore be able to be used as verification of the presence of radioactive tracer in this particular area. The applied procedure is described in Figure 7-1.

However, the results showed no blackening at all, cf. Figure 7-2. The explanation to this may be that this technique could not ensure that the films came close enough to the surfaces to enable interaction with the beta radiation from the Cs-137 tracer, or the Cs-137 may have been transported elsewhere in the system. It could also have been transported into the porous structures of the coatings where radiation would be somewhat shielded. One therefore instead had to rely on the gamma spectrometry measurements to obtain the spatial distribution of the radioactive tracers.

a. The drill cores were placed with the fracture surfaces up, here illustrated with Feature A', lower surface (sample# 11).

b. The autoradiography film was put on top of the fracture surfaces.

c. A slight pressure (using rice bags) was applied in order to position the film as close to the fracture surface as possible, but still minimizing the mechanical damages (scratches, etc) on the film.

Figure 7-1 a–c. *Illustration of the procedure applied for autoradiography. Of course, all these measures were performed in darkness, the figures are just illustrations of the actual process. The films were exposured for one day after which the films were developed.*

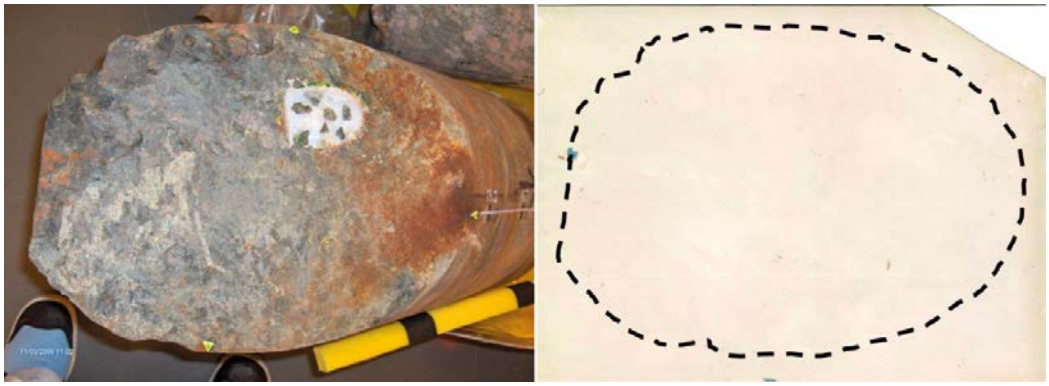

Figure 7-2. *Photography (left) and corresponding autoradiography (right) of the lower surface of Feature A´ (sample#11). No blackening whatsoever was obtained and the shape of the sample has thus been marked on the autoradiography.*

Gamma-spectrometry

In order to quantify the amount of radioactive tracers on the different samples, gamma-spectrometry measurements were employed. This procedure was performed at BASLAB CLAB using a HPGe-detector (35% relative efficiency) and the GammaVision 5.31 software for evaluation. Measurements were performed using both slices (typically 10x5x1 cm size, cf. Figure 3-3a) and rods (typically 1x1x2 cm, cf. Figure 3-3b) and calibration was performed as follows:

Rods: Samples were put directly on top of the detector with the fracture surface facing downwards and the calibration was thus performed using a concrete sample in a 1.6x1.6x0.3 cm sample casted with a known amount of QCY44 (Perkin Elmer) mixed radionuclide standard. The reason for using a 0.3 cm sample instead of the actual sample thickness of ~1cm was based on the assumption that the majority of the Cs tracer was expected to be found in very low thickness of the samples (cf. Byegård et al. 1998, Nilsson et al. 2010), i.e., the 3 mm sample was anticipated to give a good representation of the actual tracer distribution of the samples.

Slices: Samples were, as for the rods, put on top of the detector and measured. Due to sample irregularities and, most probably, heterogeneous distribution of tracers, preparation of calibration samples with the same geometry would not be meaningful. Instead, the samples that were measured both as slices and as rods were studied separately. A calibration was established by comparing the counting rate of the sum of the rod samples with the counting rate of the corresponding slice, according to:

$$A_{slice} = \sum A_{rods} \frac{R_{slice}}{\sum R_{rods}} = k \cdot R_{slice} \qquad (7.1)$$

An individual geometry factor, k, was thus identified for all 35 slices that had also been measured after they had been sawed into rods. Ideally, the factor should be identical. However, and not surprisingly given the irregularity of sample geometries, a standard deviation of ~60% was observed for the k and one thus has to address a considerable uncertainty for the results of the measurements of the slices.

In the evaluation of measurement, attempts were made to identify and quantify all γ-emitting tracers with half-lifes long enough to possibly remain in the samples, i.e., Na-22, Cs-134, Cs-137 and Ba-133. However, no identification of Na-22 and Ba-133 was obtained for any of the samples. Cs-134 was (as expected due to its rather shorter half-life) only found in very low activities in a low number of samples and the results for this isotope has therefore not been a subject to an elaborate evaluation and result summary. Addressing the Cs-134 activity would have demanded a more than 10 times longer measurement time which was not considered realistic within the project frames.

The results from the gamma-spectrometry measurements are summarised in the following sections and, based on the discussions above, only the Cs-137 activity are addressed from now on.

7.2 Results from Feature A in KXTT3

No thorough address of the KXTT3 samples has been made. A short measurement consisting of a large number of rod samples put in the detector simultaneously gave no indication of any activity present in these samples. Since the KXTT3 was used as the pumping borehole during the experiment, no measureable activity was expected due to the fact that activities in the range of only 1–2 Bq per litre had been found in the pumped water prior to overcoring.

7.3 Results from Feature A in KXTT4

The results of the measurements of Cs-137 in the Feature A are illustrated in Figure 7-3. Comparisons are made with the corresponding photography (Figure 7-4) and for the lower side of the fracture (Surface #3, i.e. the surface sitting on core piece 3) a comparison of the Cs-137 distribution to the distribution of epoxy during the epoxy injection is made (Figure 7-5). It is obvious that the concentration of Cs-137 is highest in the samples closest to the borehole, otherwise a comparatively homogeneous distribution is observed in the sample. Presence of Cs-137 can thus be observed in almost all samples, however with some exceptions for samples mostly located at the longest distance from the borehole. The direction towards the KXTT3 borehole (the pumping borehole in the previously performed tracer experiment) is to the left of each figure and some indications are obtained of increased activity in samples located in a presumed flow path. It is nevertheless shown that Cs-137 covers a large surface; far much more surface than a single thin flow path.

Given the discussion in Section 5.2 it is not easy, based on the overview photographs, to make any correlation between the observed distribution of Cs-137 and the thickness of epoxy. However, for Feature A in KXTT4 it may be concluded that both the epoxy and the Cs-137 seem to cover the whole sample surfaces.

A comparison between concentration of Cs-137 and the fracture classification types (cf. Section 5.2) is presented in Figure 7-6. As can be seen there is no obvious correlation between fracture classification and Cs-137 distribution; given the variation within the fracture classification groups, no difference can be seen whatsoever. An exception is the E group (Fault zone, complex geometry) which is much lower that the other groups; however, an observation of questionable value due to only two measured samples.

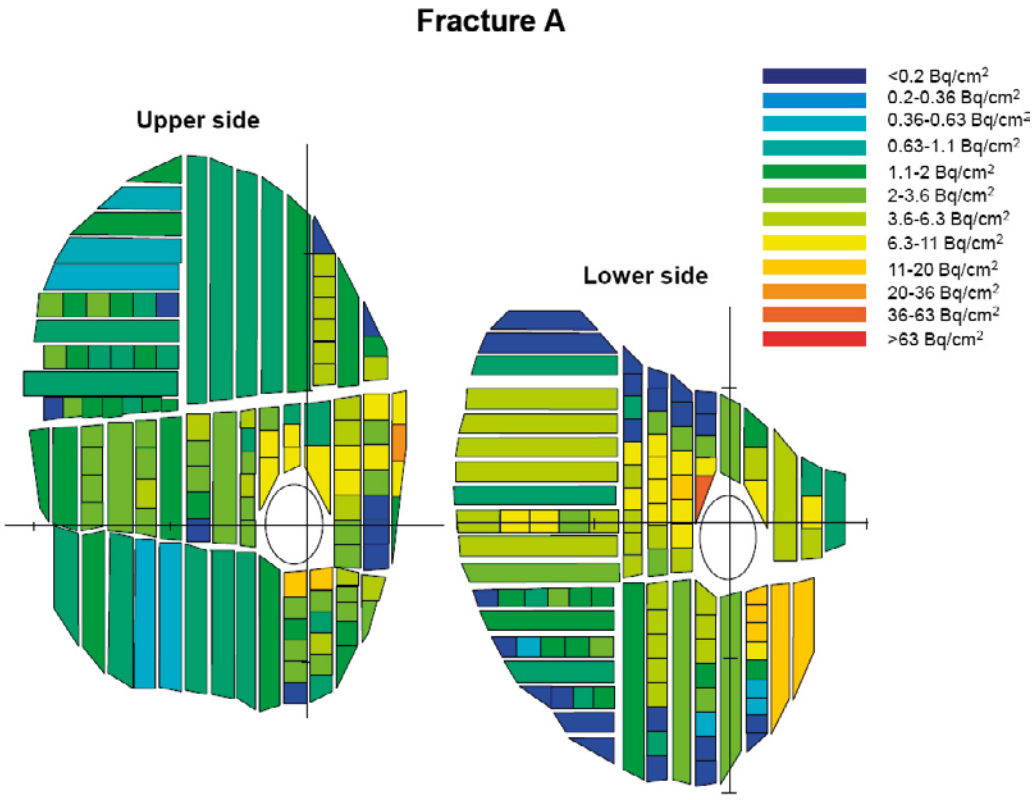

Figure 7-3. *Illustration of the Cs-137 distribution related to the upper and lower side of the Feature A fracture in KXTT4. The oval form of the picture is a result of the fact that a non-perpendicular cross section of the drill core and the fractures was obtained during the drilling, cf. Figure 7-2. The coordinate systems are given with the same coordinates for the two fractures; the distance between each tic mark on the scale is 10 cm. The uncertainties for the Cs-137 measurements are in the range of 60% for the slice samples and in the range of 10% for the rod samples (generally somewhat higher for the cases of lower activity).*

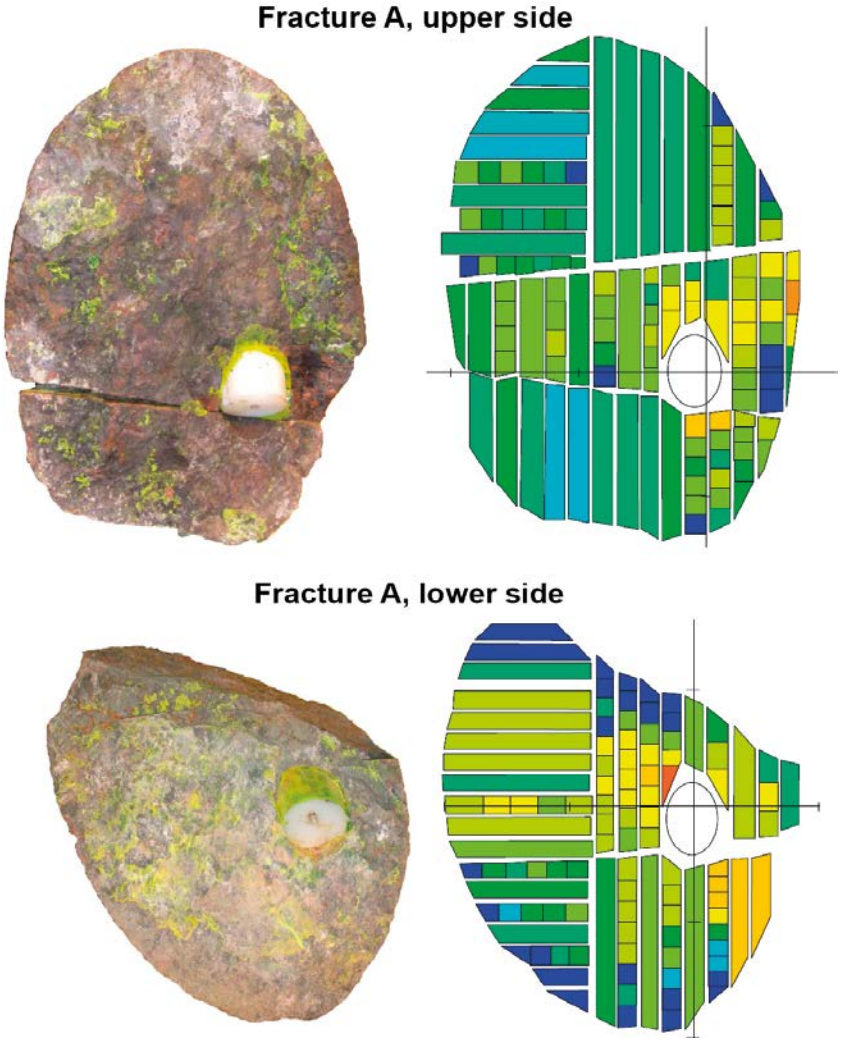

Figure 7-4. *Photography (left) and an illustration of the Cs-137 distribution (right) on the Feature A surface samples in KXTT4. One can observe for the lower samples that the photography was obtained in a different angle compared to the illustration of the Cs-137 distribution, which causes a slight mismatch of the figures.*

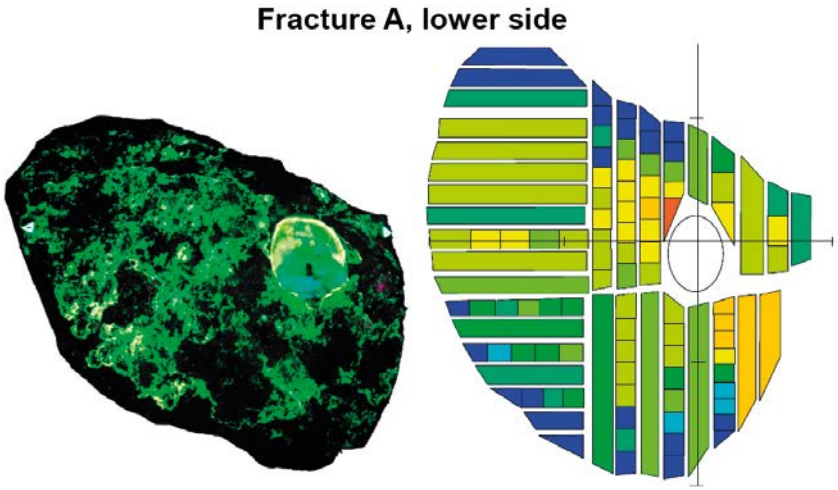

Figure 7-5*. Epoxy distribution (Fluorescence induced by UV-light) and Cs-137 distribution on the lower side of the Feature A surface in KXTT4. One can observe that the photography of the epoxy distribution was obtained in a different angle compared to the illustration of the Cs-137 distribution, which causes a slight mismatch of the figures.*

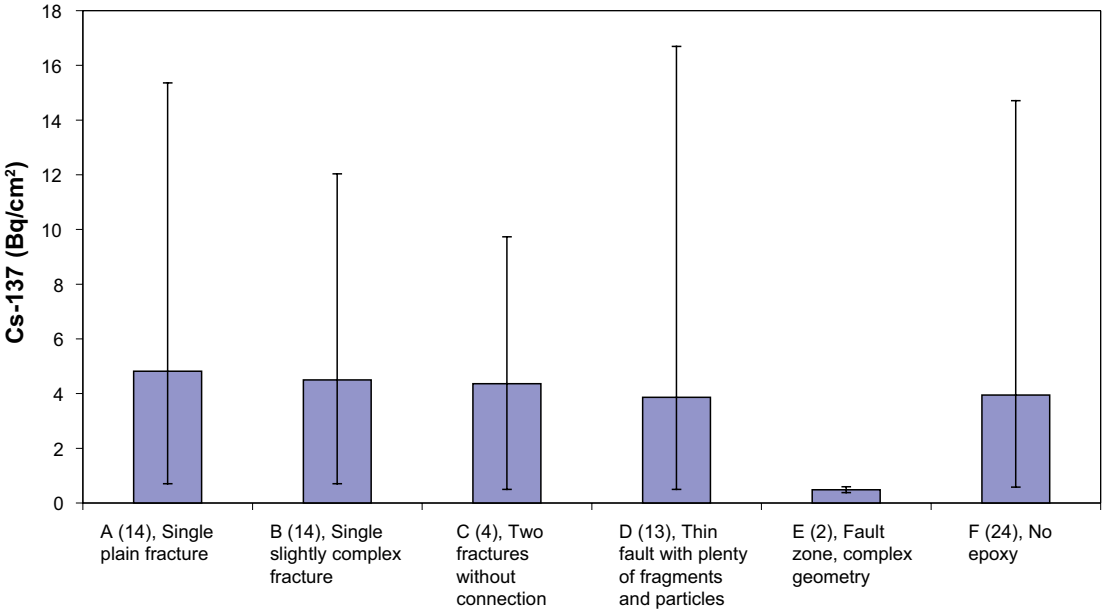

Figure 7-6. *Average values for the Cs concentration for the different fracture classification types identified in the Feature A. The error bars represents the min-max values and the number of measured samples within each group is given within the parenthesis.*

7.4 Results from Feature A' in KXTT4

The results of the measurements of Cs-137 in the Feature A' are illustrated in Figure 7-7. Comparisons are made with the corresponding photography (Figure 7-8) and for the lower side of the fracture (Surface #11) a comparison of the Cs-137 distribution to the distribution of epoxy during the epoxy injection is made (Figure 7-9). It is obvious that the concentration of Cs-137 is highest in the samples closest to the borehole and that (contrary to the situation for the Feature A surface) the major part of the sample rock surface is devoid of any presence of Cs-137. The direction to the KXTT3 borehole is to the left of each figure and a flow path in this direction may be inferred.

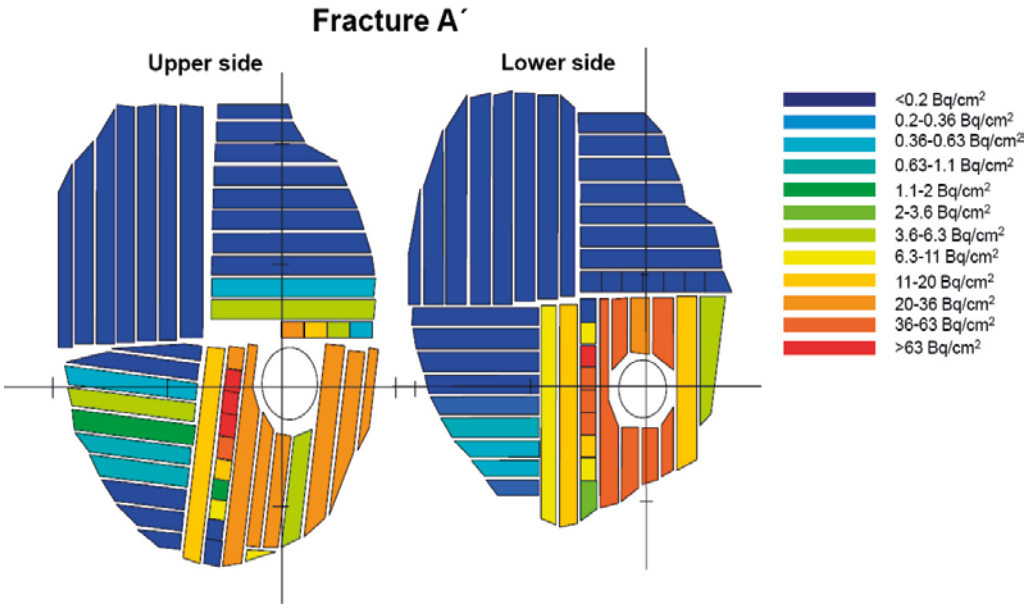

Figure 7-7. *Illustration of the Cs-137 distribution in the upper and lower side of the Feature A' fracture in KXTT4. The coordinate systems are given with the same coordinates for the two fractures; the distance between each scale unit is 10 cm. The uncertainties for the Cs-137 measurements are in the range of 60% for the slice samples and in the range of 10% for the rod samples (generally somewhat higher for the cases of lower activity).*

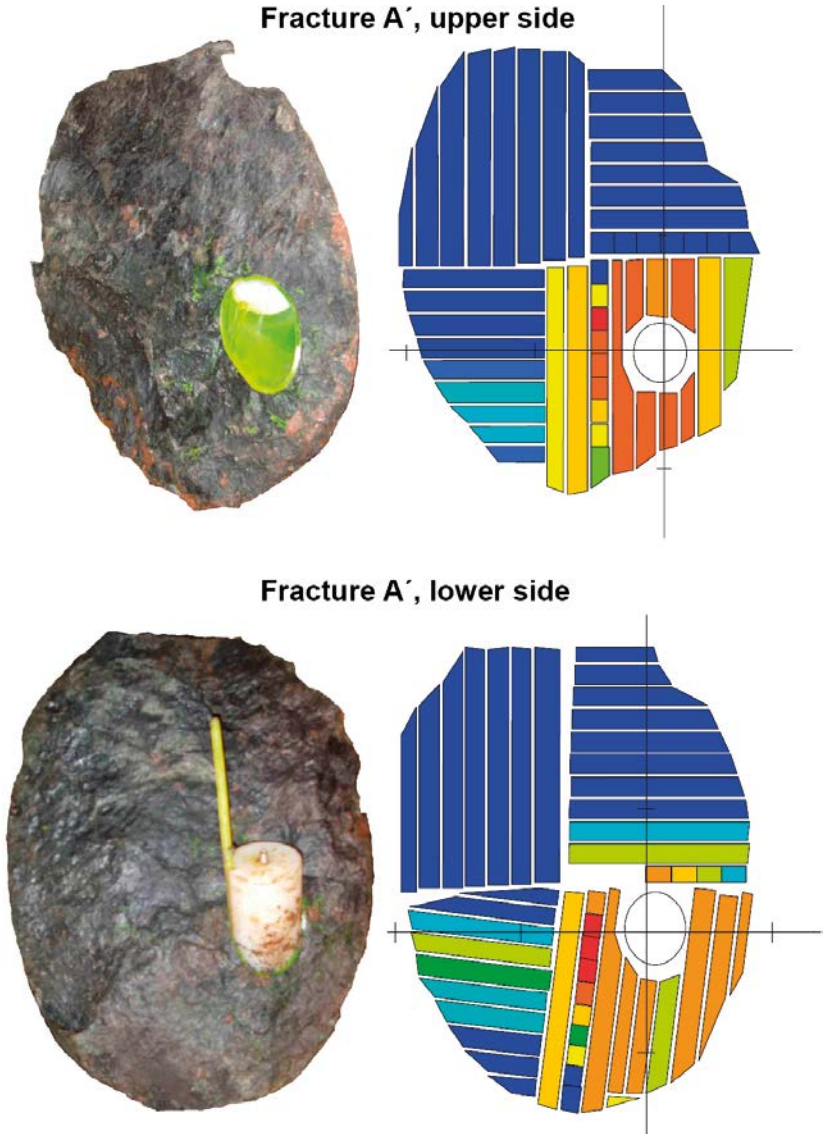

Figure 7-8. *Photography (left) and an illustration of the Cs-137 distribution (right) on the Feature A surface samples in KXTT4.*

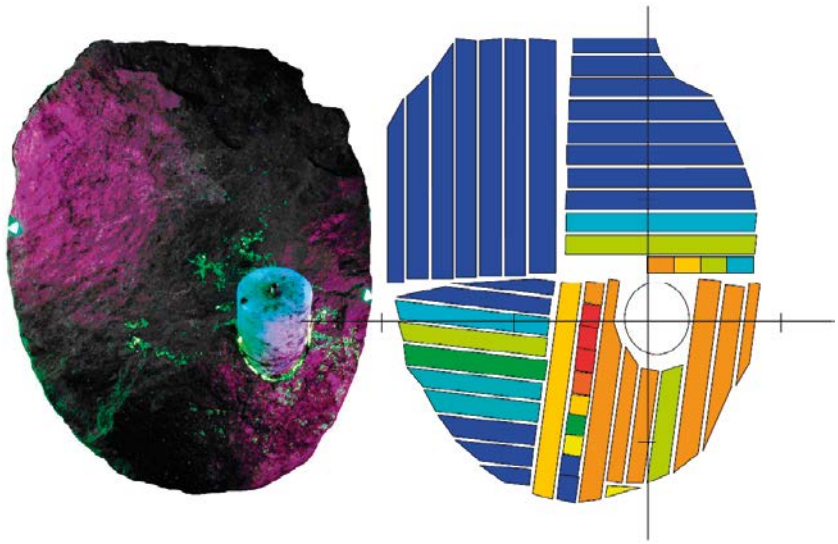

Figure 7-9. *Epoxy distribution (Fluorescence induced by UV-light) and Cs-137 distribution on the lower side of the Feature A' surface in KXTT4.*

7.5 Discussion of the Cs analysis

The total amount of Cs 137 found on the sample surfaces (Table 7-1), is 3 kBq for Feature A and 9 kBq for Feature A'. It is notable that the amount on the mating sides of the fractures is quite similar. Further, it can be concluded that the total amount of Cs-137 measured at the two sampled surfaces at the injection borehole was only 0.29% of the Cs-137 not recovered during the STT1 tracer experiment. This could be an indication that there could be high amounts of Cs-137 distributed on the surfaces (or underlying rock matrix) of the fractures between the two boreholes. However, with a rough approximation of that a total fracture surface of 6 +6 = 12 dm^2 = 0.12 m^2 has been measured in this experiment, one would "need" a 0.12/0.0029 ≈ 40 m^2 fracture with an average surface concentration as given by the measurements closest to the injection borehole. Actually, that amount of fracture would correspond to a circle with the radius of 3.6 m, which can be compared with the fact that the Euclidean distance between the boreholes is only 4.6 m. Such an explanation is, however, contradicted by the absence of Cs in the surfaces in the surrounding of the pumping borehole.

However, one should acknowledge the possibility that the tracer transport may have taken place in several subparallel fractures, or splays to the main fracture plane, which is supported to some extent by the mapping of the drill cores from the site (see Figure 2-2). Apart from the main fracture plane in Feature A, Fracture 1, there also exist Fracture surfaces 2–4 and minor surfaces on which no measurements of Cs-137 have been made. Nevertheless, it is difficult from the results of the measurement of the surfaces to produce a good proposal for the location of the non-recovered Cs tracer.

The amount of radioactivity found on the Feature A' surfaces was approximately three times higher compared with that found on Feature A surfaces, 8.9 kBq versus 3.1 kBq. A very good agreement of the upper versus the lower surfaces was obtained.

The most striking observation is, however, the agreement between the epoxy injection characteristics and the distribution of the Cs-137 tracer. The Feature A fracture seems to have been conductive enough to allow a significant inflow of epoxy resin which can be interpreted to be in agreement with the relatively homogeneous distribution of Cs-137 tracer. On the other hand, Feature A' is more or less non-conductive to inflow of epoxy resin which is in agreement with the low amount of surface that, according to the results of the Cs-137 measurements, seem to have been in contact with the flowing water. These observations are interesting to compare with the results of especially the STT2 experiment (Andersson et al. 1999) where the breakthrough curve showed characteristics indicating transport in a double pathway.

Table 7-1. Total amounts of Cs-137 found on the different surface samples in the KXTT4 surface. The amounts presented are also compared to the total amount of tracer injected in the STT1 experiment and a comparison is also made to the part of the Cs-137 tracer that was not recovered during the pumping phase of the experiment.

Total amount Cs-137 injected in the STT1 experiment: 6,400 kBq
Non-recovered amount in the STT1 experiment: 4,200 kBq

Borehole	Fracture	Side	[Cs-137] kBq	Part of total injected	Part of non-recovered
KXTT4	Feature A	Upper surface	1.5±0.1	0.02%	0.04%
		Lower surface	1.6±0.2	0.02%	0.04%
		Sum, Feature A	3.1±0.2	0.05%	0.07%
	Feature A'	Upper surface	4.4±0.7	0.07%	0.11%
		Lower surface	4.5±0.7	0.07%	0.11%
		Sum, Feature A'	8.9±1.0	0.14%	0.21%
		Sum, KXTT4	12.0±1.1	0.19%	0.29%

8 Conclusions

The objective of this study was to characterise the water-bearing feature referred to as Feature A, which was the main conductive structure investigated by the TRUE-1 tracer experiments. A characterisation was performed, using samples from two large diameter overcores along KXTT3 and KXTT4, with regards to pore space geometry, mineralogy and Cs-137 sorbed to the fracture surfaces.

The method developed to study pore volume geometry using injection of fluorescent epoxy followed by overcoring, sampling and image analysis, has proved to work satisfactory in this study. The mineralogical investigations included scanning electron microscope investigations as well as X-ray diffractometry. Also the applied methodology for quantifying the distribution of sorbed Cs-137 on rock fracture surfaces using γ-spectrometry worked out well.

All samples from Feature A have a main fracture plane showing clear indications of shearing, although parallel fracture planes and/or sub-parallel branching or splay fractures, also of significant aperture, are present. If the pore space geometrical character is simplified into three classes: 'single plane', 'single but slightly complex' and 'thin fault with plenty of fragments and particles', the studies show that roughly one third of the Feature A fracture plane belongs to each of these geometrical classes.

Several generations of fracture fillings, or coatings, show that Feature A has been reactivated at several events and that it has been intermittently water-conducting for a very long time. These characteristics agree with what is found in previous studies at Äspö, and Feature A can therefore be regarded as representative for water-bearing structures in the area from a mineralogical point of view.

The thickness of the outermost coatings next to the epoxy varies from about 0.8 to 5 mm for calcite (minimum down to 40 µm) and from 10 to 500 µm for chlorite/clay minerals (mainly 50–100 µm). The size of individual crystals on the fracture coatings varies from about 10 µm in smooth chlorite/clay mineral coatings, but individual corrensite aggregates may be up to 50 µm in size.

Since the samples from KXTT4 are related to the injection hole for the radioactive tracer and the samples from KXTT3 are related to the pumping borehole used in the tracer experiments, a major difference between the samples with respect to radiation was to be expected, and accordingly no Cs-137 was measured in samples related to KXTT3. For samples of Feature A at KXTT4 the total amount of Cs-137 measured was 3 kBq, while for samples of Feature A' in KXTT4 the total amount was about 9 kBq. The surface coverage of Cs-137 is however much smaller in the case of Feature A'.

The two sample, as a whole, from Feature A intersection with KXTT3 and KXTT4, generally show the same mineralogical and pore space characteristics, although the point wise mineral occurrence and the point wise aperture varies quite strongly. These results imply that the character of Feature A remains similar over the area that was involved in the tracer experiments.

The repeated activation of the Feature A, as evidenced by the mineralogical analysis, together with the fairly large mean cumulative aperture (around 0.45 mm), both indicated that this structure has much larger extent than the size of the TRUE-1 test site. The aperture correlation distances for both KXTT3 and KXTT4 are in the order of 5–9 cm, and this is in agreement with what may be expected from a fracture of this mean cumulative aperture, based on previous studies (e.g. Hakami 1995). Also, the mineralogical studies show that the variations within the samples are larger than between the samples. These are all conditions that support the conclusion of constant characteristics, including the described complexity and variability, over the whole extent of Feature A at the TRUE-1 site.

References

SKB's (Svensk Kärnbränslehantering AB) publications can be found at www.skb.se/publications.

Andersson P, Wass E, Byegård J, Johansson H, Skarnemark G, 1999. Äspö Hard Rock Laboratory. TRUE 1st tracer test programme. Tracer tests with sorbing tracers, STT-2. Experimental description and preliminary evaluation. SKB IPR-99-15, Svensk Kärnbränslehantering AB.

Andersson P, Byegård J, Dershowitz B, Doe T, Hermanson J, Meier P, Tullborg E-L, Winberg A (ed), 2002a. Final report of the TRUE Block Scale project. 1. Characterisation and model development. SKB TR-02-13, Svensk Kärnbränslehantering AB.

Andersson P, Byegård J, Winberg A, 2002b. Final report of the TRUE Block Scale project. 2. Tracer tests in the block scale. SKB TR-02-14, Svensk Kärnbränslehantering AB.

Andersson P, Wass E, Gröhn S, Holmqvist M, 2002c. Äspö Hard Rock Laboratory. TRUE-1 continuation project. Complementary investigations at the TRUE-1 site – Crosshole interference, dilution and tracer tests, CX-1–CX-5. SKB IPR-02-47, Svensk Kärnbränslehantering AB.

Andersson P, Byegård J, Billaux D, Cvetkovic V, Dershowitz W, Doe T, Hermanson J, Poteri A, Tullborg E-L, Winberg A (ed), 2007. TRUE Block Scale Continuation Project. Final Report. SKB TR-06-42, Svensk Kärnbränslehantering AB.

Brindley G W, Brown G (eds), 1984. Crystal structures of clay minerals and their X-ray identification. London: Mineralogical Society.

Byegård J, Johansson H, Skålberg M, Tullborg E-L, 1998. The interaction of sorbing and non-sorbing tracers with different Äspö rock types. Sorption and diffusion experiments in the laboratory scale. SKB TR-98-18, Svensk Kärnbränslehantering AB

Byegård J, Widestrand H, Nilsson K, Gustafsson E, Kronberg M, 2010. Long-term Sorption Diffusion Experiment (LTDE-SD). Performance of main in-situ experiment and results from water phase measurements. SKB IPR-10-10, Svensk Kärnbränslehantering AB.

Drake H, Tullborg E-L, 2005. Oskarshamn site investigation. Fracture mineralogy and wall rock alteration. Results from drill cores KAS04, KA1755A and KLX02. SKB P-05-174, Svensk Kärnbränslehantering AB.

Drake H, Tullborg E-L, 2006. Oskarshamn site investigation. Fracture mineralogy of the Götemar granite. Results from drill cores KKR01, KKR02 and KKR03. SKB P-06-04, Svensk Kärnbränslehantering AB.

Drake H, Tullborg E-L, 2009a. Fracture mineralogy Laxemar. Site-descriptive modelling, SDM-Site Laxemar. SKB R-08-99, Svensk Kärnbränslehantering AB.

Drake H, Tullborg E-L, 2009b. Paleohydrogeological events recorded by stable isotopes, fluid inclusions and trace elements in fracture minerals in crystalline rock, Simpevarp area, SE Sweden. Applied Geochemistry 24, 715–732.

Drake H, Tullborg E-L, Page L, 2009. Distinguished multiple events of fracture mineralisation related to far-field orogenic effects in Paleoproterozoic crystalline rocks, Simpevarp area, SE Sweden. Lithos 110, 37–49.

Drever J I, 1973. The preparation of oriented clay mineral specimens for X-ray diffraction analysis by a filter-membrane peel technique. American Mineralogist 58, 553–554.

Hakami E, 1995. Aperture distribution of rock fractures. PhD thesis. Department of Civil and Environmental Engineering, Division of Engineering Geology, Royal Institute of Technology, Stockholm, Sweden.

Hakami E, Wang W, 2005. Äspö Hard Rock Laboratory. TRUE-1 continuation project. Fault rock zones characterisation. Characterisation and quantification of resin-impregnated fault rock pore space using image analysis. SKB IPR-05-40, Svensk Kärnbränslehantering AB.

Jasmund K, Lagaly G (eds), 1993. Tonminerale und Tone: Struktur, Eigenschaften, Anwendungen und Einsatz in Industrie und Umwelt. Darmstadt: Steinkopff Verlag.

Löfgren M, Sidborn M, 2010. Statistical analysis of results from the quantitative mapping of fracture minerals in Laxemar. Site descriptive modelling - complementary studies. SKB R-09-31, Svensk Kärnbränslehantering AB.

Nilsson K, Byegård J, Selnert E, Widestrand H, Höglund S, Gustafsson E, 2010. Äspö Hard Rock Laboratory. Long Term Sorption Diffusion Experiment (LTDE-SD). Results from rock sample analyses and modelling. SKB R-10-68, Svensk Kärnbränslehantering AB.

Nordqvist R, Byegård J, Hjerne C, 2015. Complementary tracer tests – SWIW, CEC and multi-hole reciprocal cross flow tests at the TRUE-1 site. TRUE-1 Continuation project. TRUE-1 Completion. SKB P-11-27, Svensk Kärnbränslehantering AB.

Poteri A, Billaux D, Dershowitz W, Gómez-Hernández J-J, Cvetkovic V, Hautojärvi A, Holton D, Medina A, Winberg A (ed), 2002. Final report of the TRUE Block Scale project. 3. Modelling of flow and transport. SKB TR-02-15, Svensk Kärnbränslehantering AB.

Sigurdsson O, Hjerne C, 2014. Overcoring of resin-impregnated boreholes KXTT3 and KXTT4 at the TRUE-1 site. TRUE-1 Completion. SKB P-11-21, Svensk Kärnbränslehantering AB.

Stanfors R, Rhén I, Tullborg E-L, Wikberg P, 1999. Overview of geological and hydrogeological conditions of the Äspö Hard Rock Laboratory site. Applied Geochemistry 14, 819–834.

Tullborg E-L, 2003. Palaeohydrogeological evidences from fracture filling minerals – Results from the Äspö/Laxemar area. In Oversby V M, Werme L O (eds). Scientific basis for nuclear waste management XXVII: symposium held in Kalmar, Sweden, 15–19 June 2003. Warrendale, PA: Materials Research Society. (Materials Research Society Symposium Proceedings 807), 873–878.

Widestrand H, Byegård J, Börjesson S, Berglien A, Wass E, 2006. Äspö Hard Rock Laboratory. LTDE Long-term Diffusion Experiment. Functionality tests with short-lived radionuclides 2005. SKB IPR-06-05, Svensk Kärnbränslehantering AB.

Widestrand H, Byegård J, Selnert A, Skålberg M, Höglund S, Gustafsson E, 2010. Long-term Sorption Diffusion Experiment (LTDE-SD). Supporting laboratory program – Sorption diffusion experiments and rock material characterisation, with supplement of adsorption studies on intact rock samples for the Forsmark and Laxemar site investigations. SKB IPR-10-11, Svensk Kärnbränslehantering AB.

Winberg A (ed), 1996. First TRUE stage – Tracer Retention Understanding Experiments. Descriptive structural-hydraulic models on block and detailed scales on the TRUE-1 site. SKB ICR-96-04, Svensk Kärnbränslehantering AB.

Winberg A, Andersson P, Hermanson J, Byegård J, Cvetkovic V, Birgersson L, 2000. Äspö Hard Rock Laboratory. Final report of the first stage of the tracer retention understanding experiments. SKB TR-00-07, Svensk Kärnbränslehantering AB.

Winberg A, Andersson P, Byegård J, Poteri A, Cvetkovic V, Dershowitz W, Doe T, Hermanson J, Gómez-Hernández J J, Hautojärvi A, Billaux D, Tullborg E-L, Holton D, Meier P, Medina A, 2003. Final report of the TRUE Block Scale project. 4. Synthesis of flow, transport and retention in the block scale. SKB TR-02-16, Svensk Kärnbränslehantering AB.

Appendix 1

Overview images on core pieces

This appendix shows the overview images of the selected surfaces studied, with ordinary and UV light.

A1.1 KXTT3 – Overview photos

Figure A1-1. *KXTT3, Feature A, core piece 15. Upper surface of Fracture 1, the quarter that lies underneath core piece 30 in the upper left corner (see Figure A1-2) is the upper surface of Fracture 3, see Figure 2-2.*

Figure A1-2. *KXTT3, Feature A, core piece 15 (see also Figure A1-1) and 30 (upper surface of Fracture 1, see Figure 2-2) in ordinary lighting. The big piece is core piece 15 and the smaller is core piece 30.*

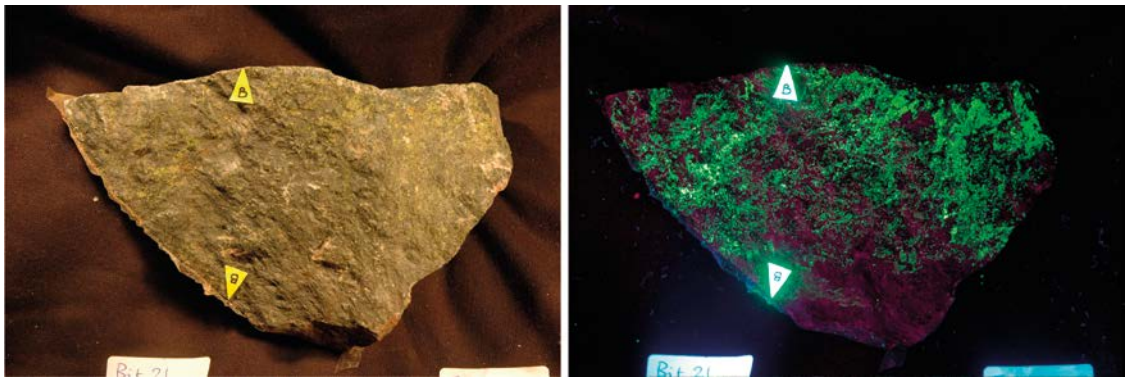

Figure A1-3. *KXTT3, Feature A, core piece 21 (upper surface of Fracture 3, see Figure 2-2) in a) ordinary lighting and b) UV lighting.*

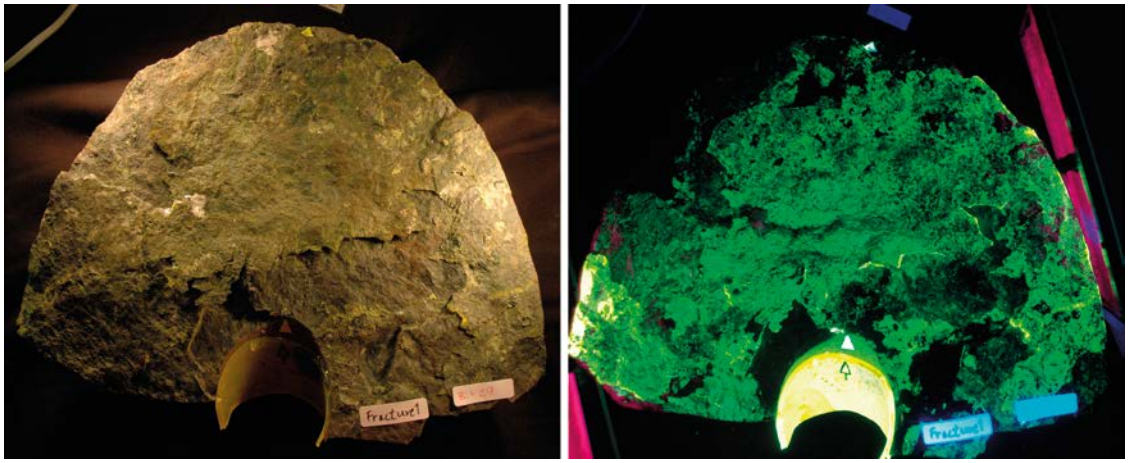

Figure A1-4. *KXTT3, Feature A, core piece 29 (lower surface of Fracture 1, see Figure 2-2) in a) ordinary lighting and b) UV lighting.*

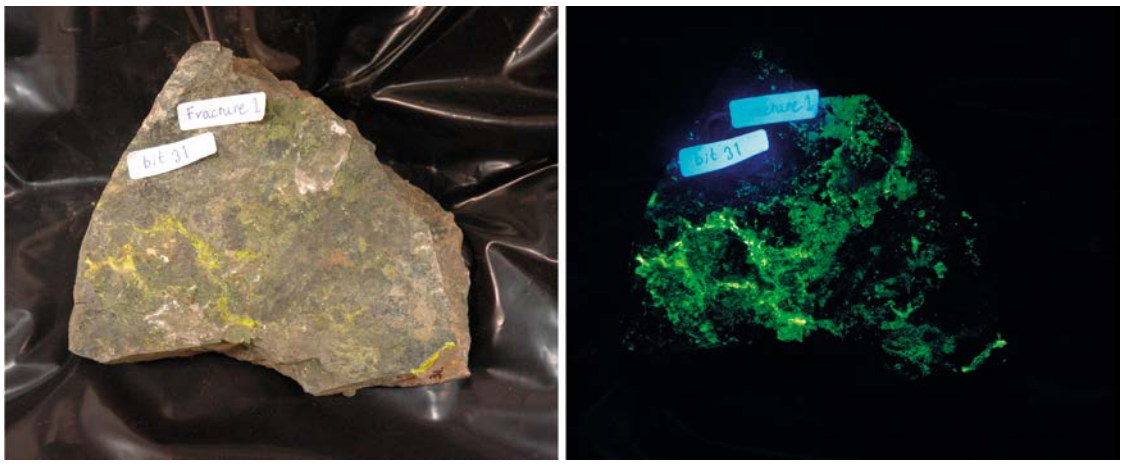

Figure A1-5. *KXTT3, Feature A, core piece 31 (lower surface of Fracture 1, see Figure 2-2) in a) ordinary lighting and b) UV lighting. The other side of this core piece is seen in Figure A1-6.*

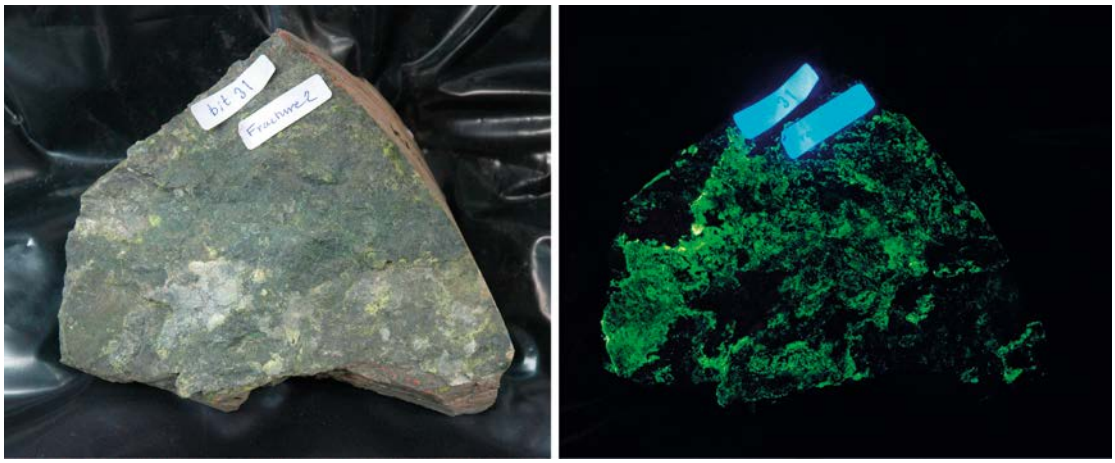

Figure A1-6. *KXTT3, Feature A, core piece 31 (upper surface of Fracture 2, see Figure 2-2) in a) ordinary lighting and b) UV lighting.*

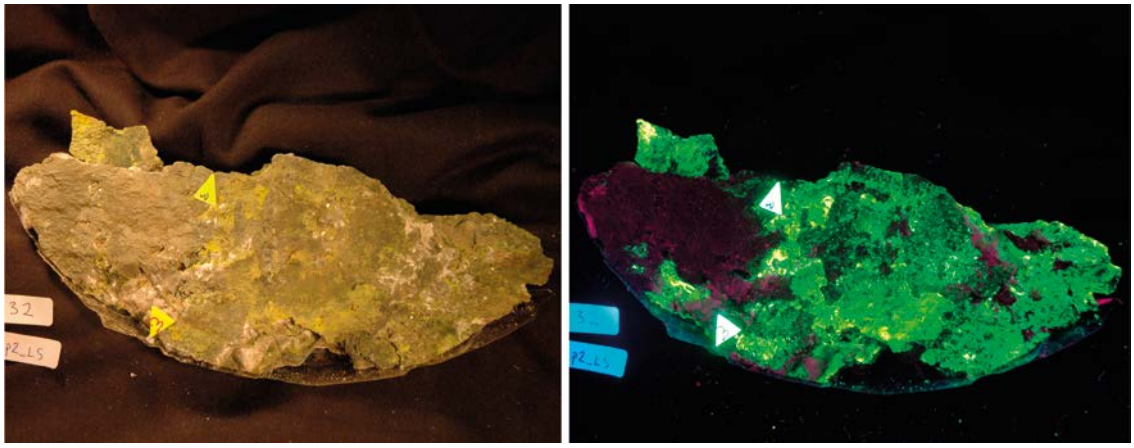

Figure A1-7. *KXTT3, Feature A, core piece 32 (lower surface of Fracture 1, see Figure 2-2) in a) ordinary lighting and b) UV lighting.*

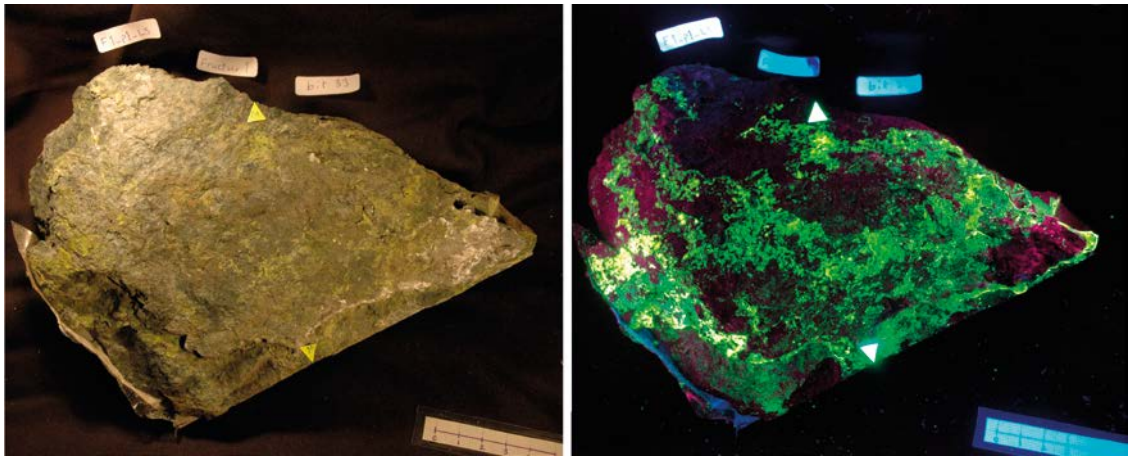

Figure A1-8. *KXTT3, Feature A, core piece 33 (lower surface of Fracture 1, see Figure 2-2) in a) ordinary lighting and b) UV lighting.*

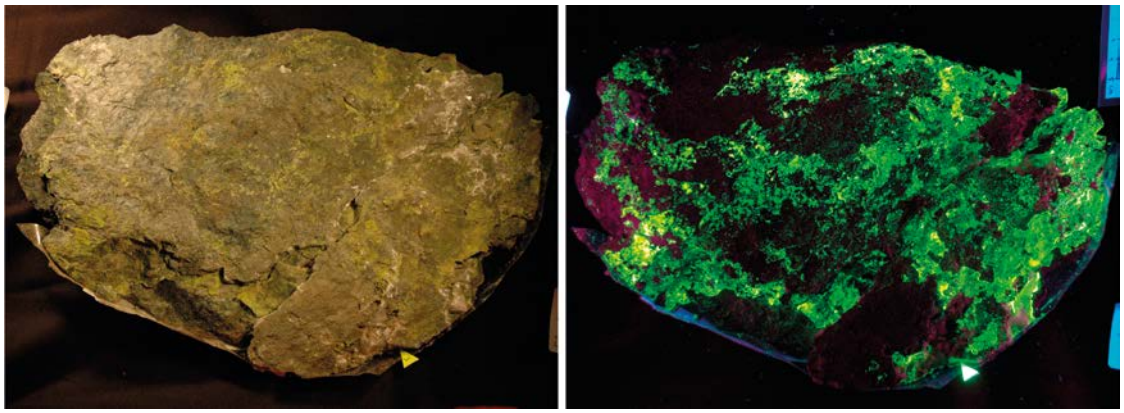

Figure A1-9. *KXTT3, Feature A, core pieces 32 (see Figure A1-7) and 33 (see Figure A1-8) (lower surface of Fracture 1, see Figure 2-2) in a) ordinary lighting and b) UV lighting. The smaller piece on the right is core piece 32 and the larger is core piece 33.*

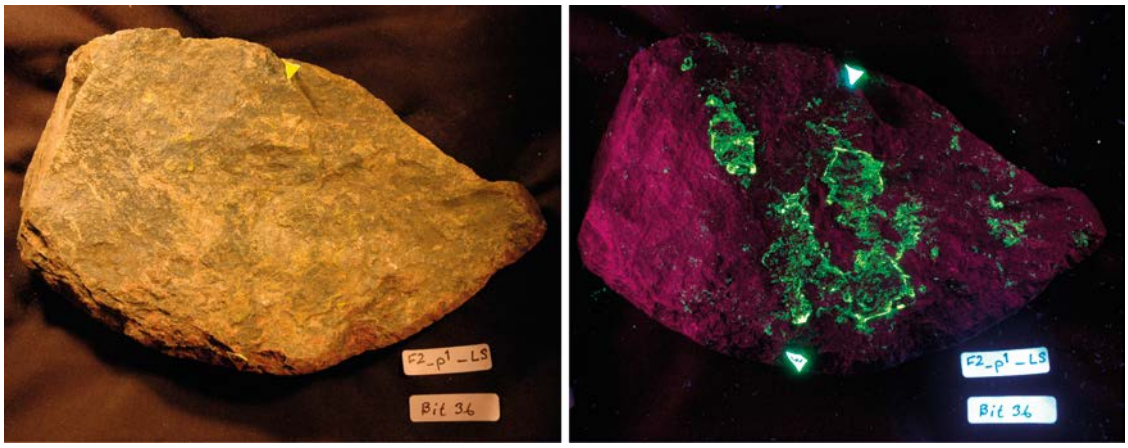

Figure A1-10. *KXTT3, Feature A, core piece 36 (lower surface of Fracture 2, see Figure 2-2) in a) ordinary lighting and b) UV lighting.*

A1.2 KXTT4 – Overview photos

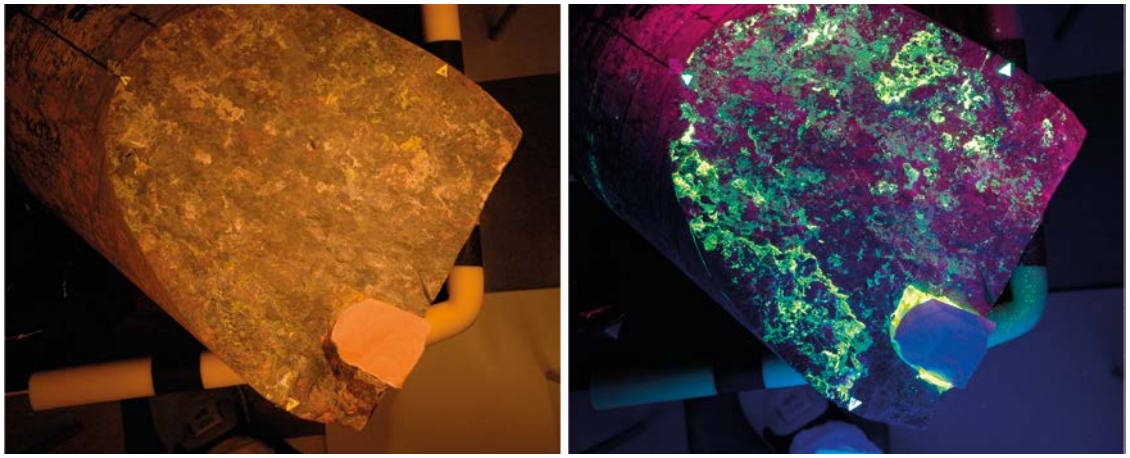

Figure A1-11. *KXTT4, Feature A, core piece 1 (see Figure 2-1) in a) ordinary lighting and b) UV lighting.*

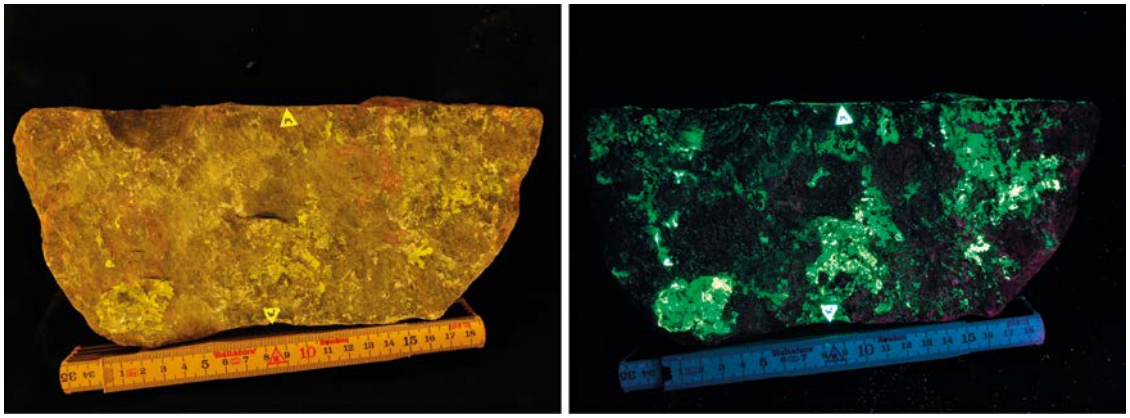

Figure A1-12. *KXTT4, Feature A, core piece 2 (see Figure 2-1) in a) ordinary lighting and b) UV lighting.*

Figure A1-13. *KXTT4, Feature A, core piece 1(Figure A1-11) with core piece 2 (Figure A1-12) on top, as these pieces fit together. The surfaces are in this picture reinforced with a layer of dark blue epoxy. This is made before further cutting to keep the surfaces intact.*

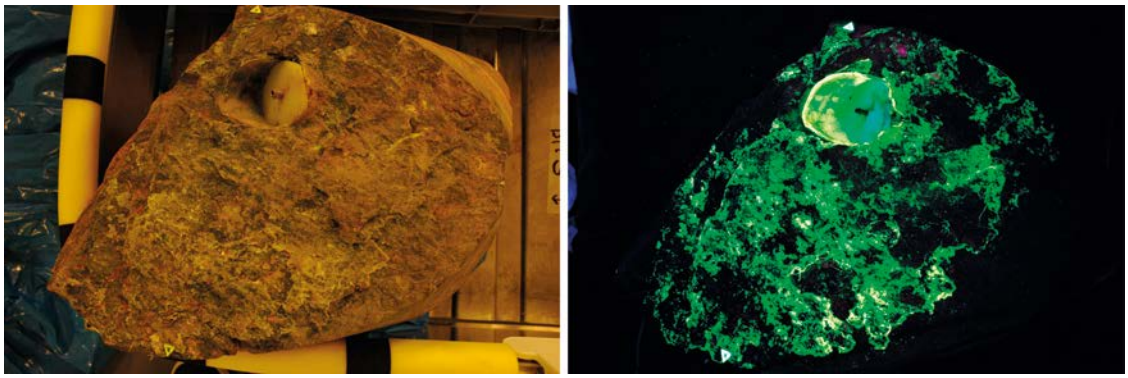

Figure A1-14. *KXTT4, Feature A, core piece 3 (see Figure 2-1) in a) ordinary lighting and b) UV lighting.*

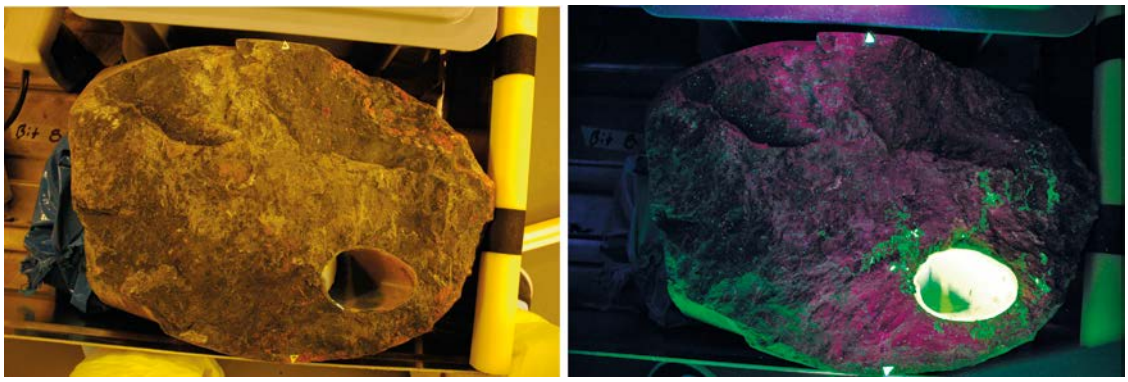

Figure A1-15. *KXTT4, Feature A', core piece 8 (see Figure 2-1) in a) ordinary lighting and b) UV lighting.*

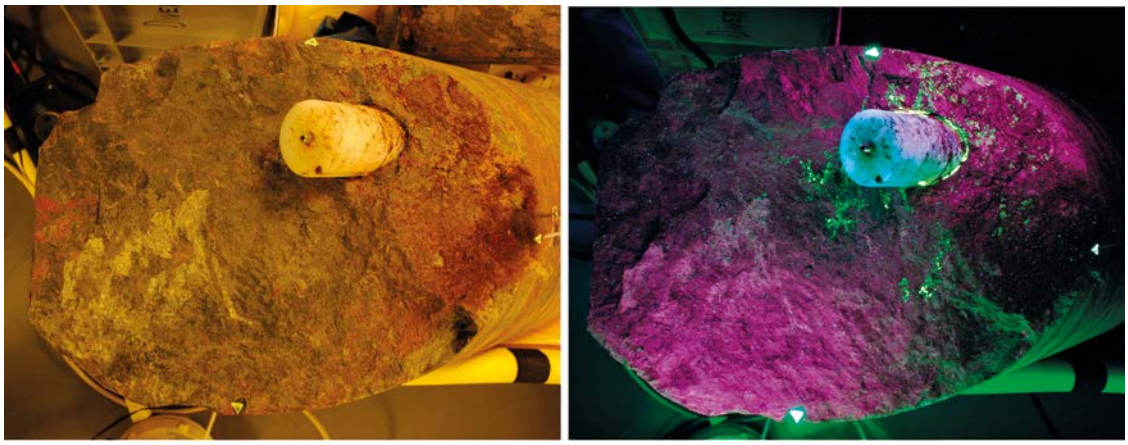

Figure A1-16. *KXTT4, Feature A', core piece 11 (see Figure 2-1) in a) ordinary lighting and b) UV lighting.*

Appendix 2

Overview images of stacks of slices

This appendix shows the stack images of the slices in UV light.

A2.1 KXTT3

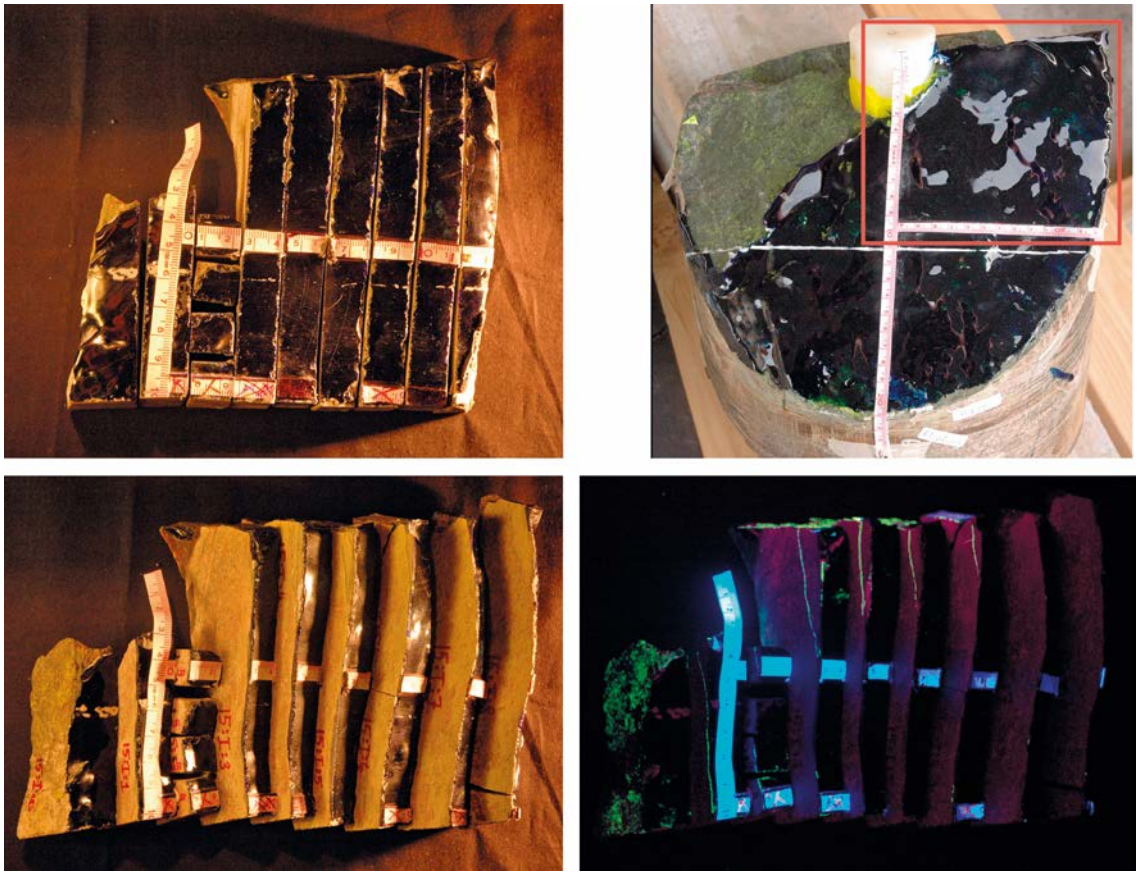

Figure A2-1. *Core piece 15.I. Slices 15.I.0 to 15.I.8, Slice 15.I.2 has been cut into rods for Cs analysis.*

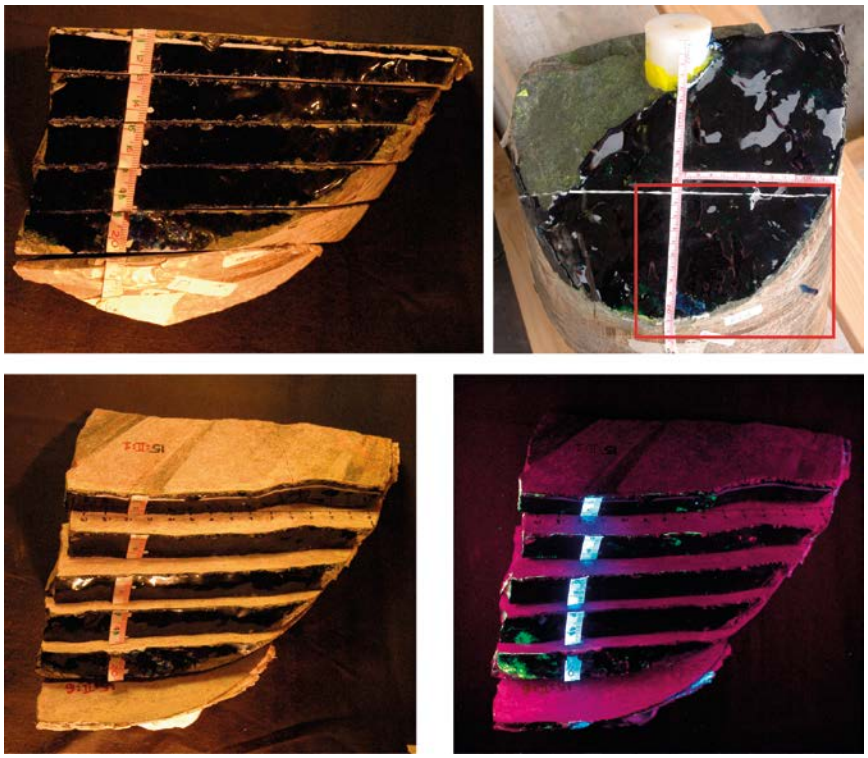

Figure A2-2. *Core piece 15.II. Slices 15.II.1 to 15.II.6.*

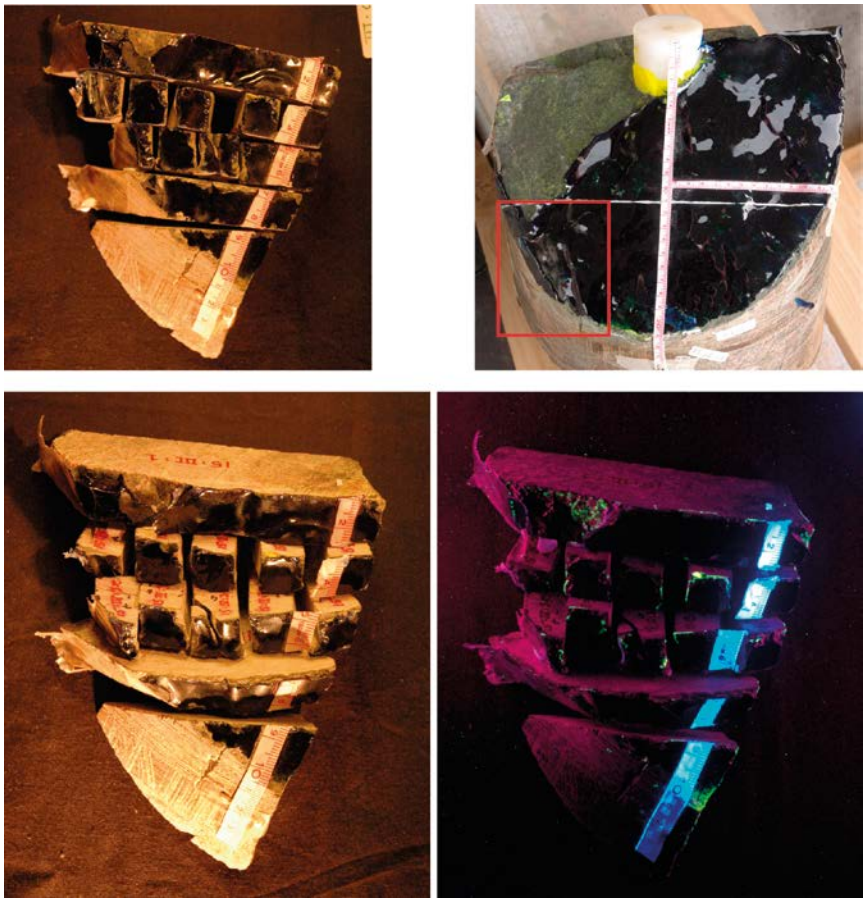

Figure A2-3. *Core piece 15.III. Slices 15.III.1 to 15.III.5, Slices 15.III.2 and 15.III.3 has been cut into rods for Cs analysis.*

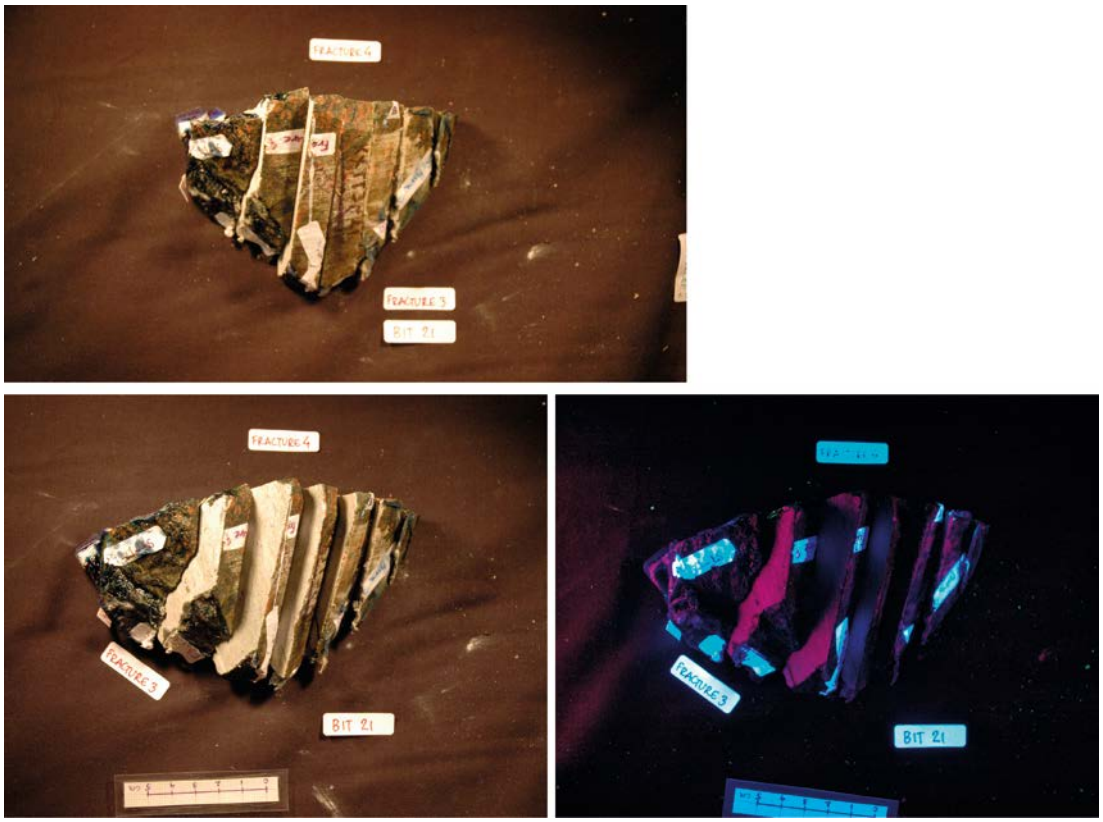

Figure A2-4. *Core piece 21. Slices 21.1 to 21.7, Slices 21.2 and 21.4 has been cut into rods for Cs analysis.*

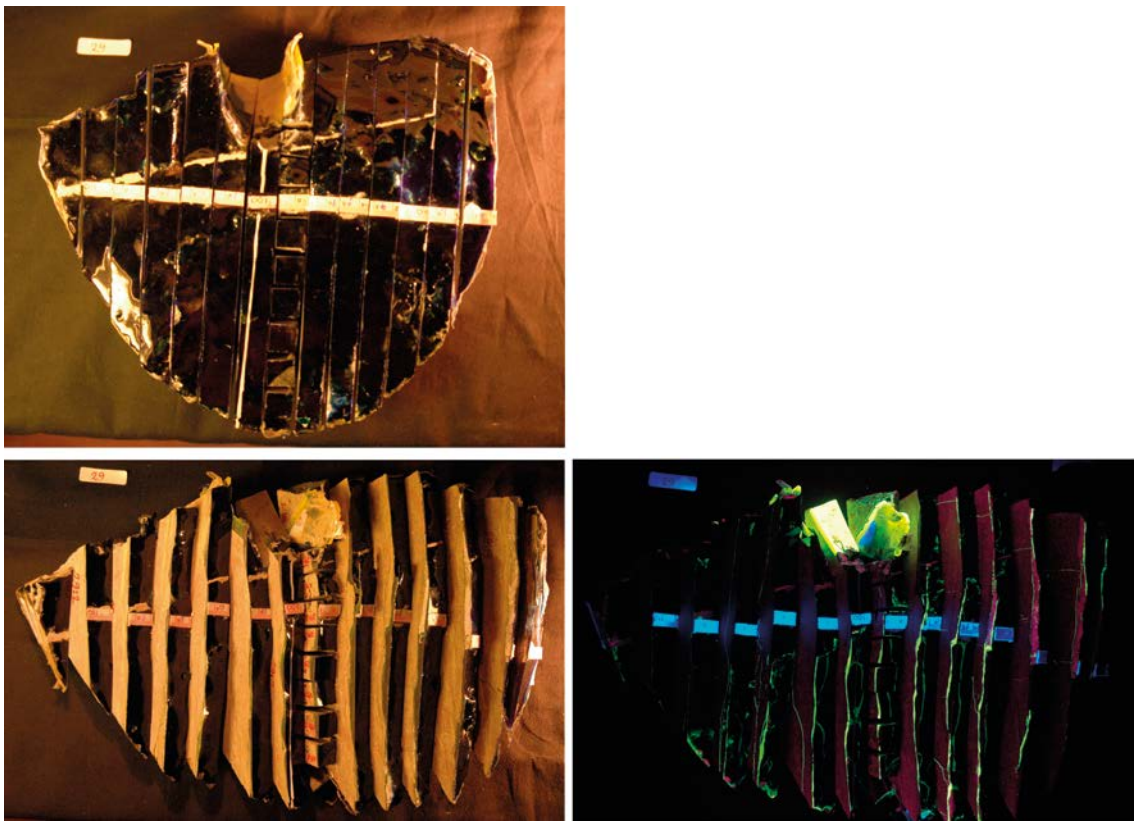

Figure A2-5. *Core piece 29. Slices 29.1 to 29.14, Slice 29.8 has been cut into rods for Cs analysis. The white line in the first image is wrongly placed according to the coordinate system, it should be placed 11.5 degrees counter clock wise (in the picture) in the outer rim (the inner point, near the injection hole, is correct).*

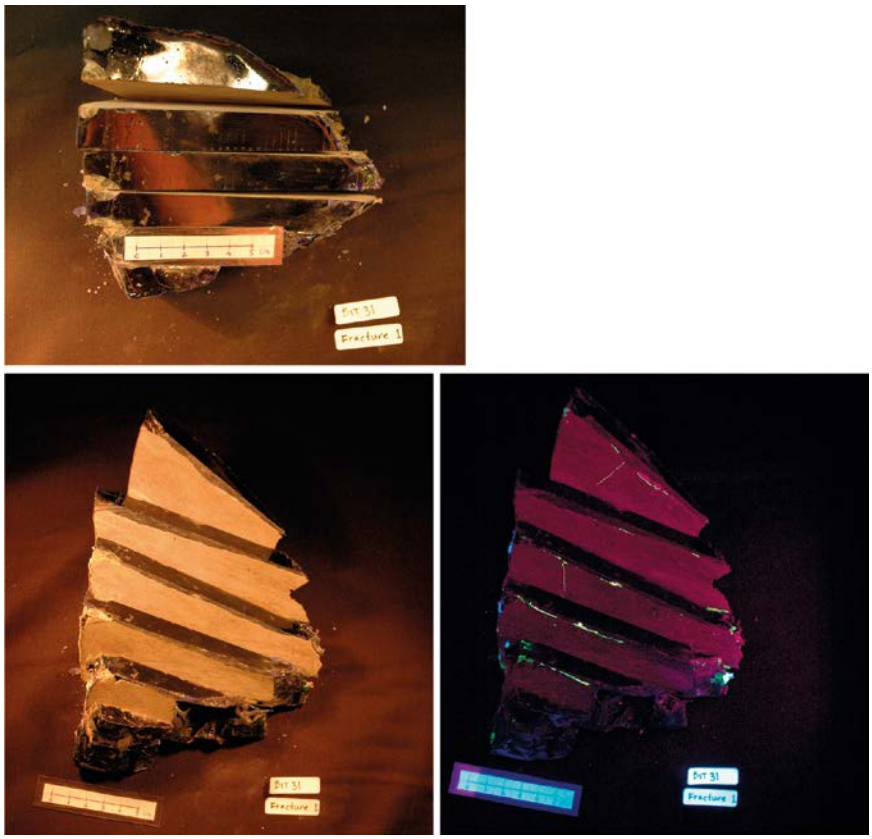

Figure A2-6. *Core piece and fracture plane 31 Fracture 1. Slices 31.1 to 31.6.*

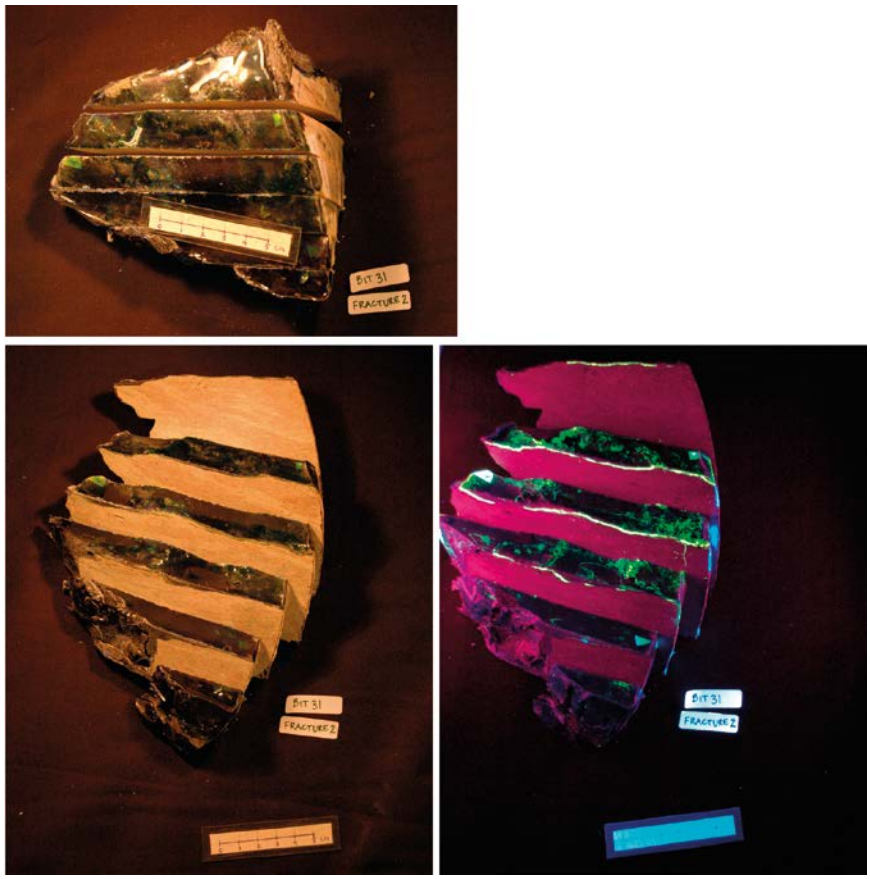

Figure A2-7. *Core piece and fracture plane 31 Fracture 2. Slices 31.1 to 31.6. Slice 31.5 has been cut into rods for Cs analysis.*

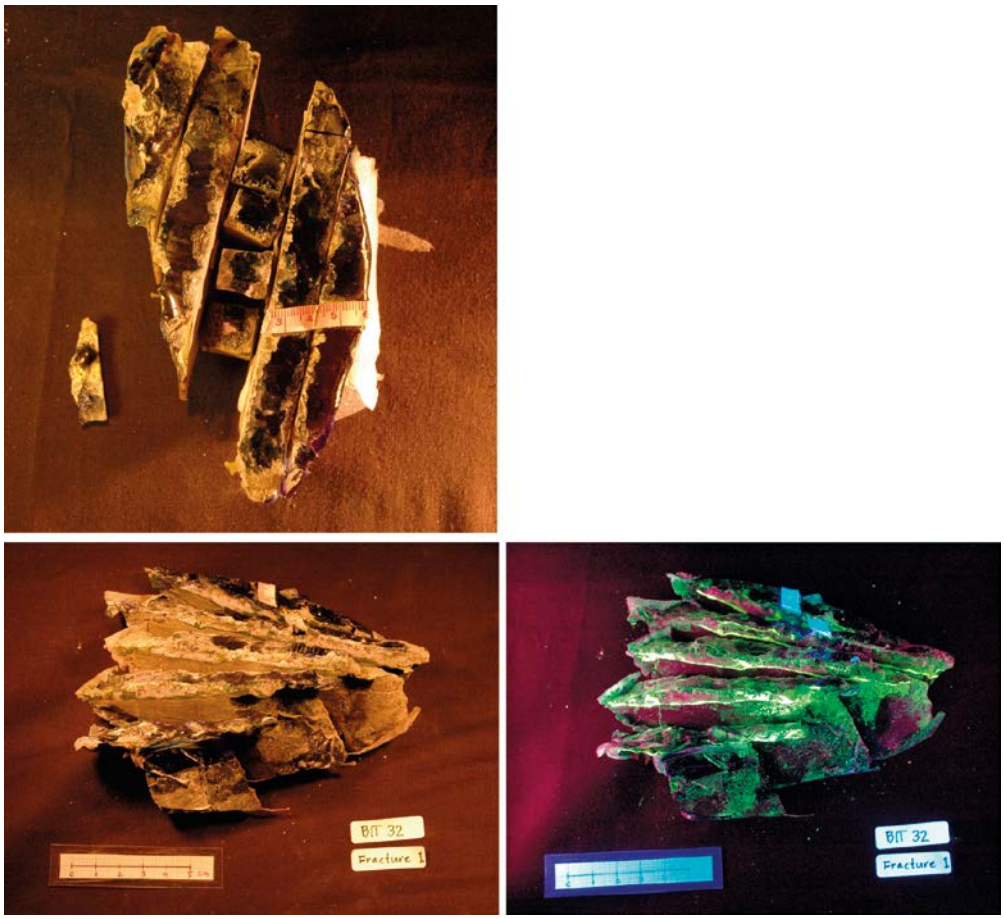

Figure A2-8. *Core piece 32. Slices 32.1 to 32.5, Slice 32.3 has been cut into rods for Cs analysis.*

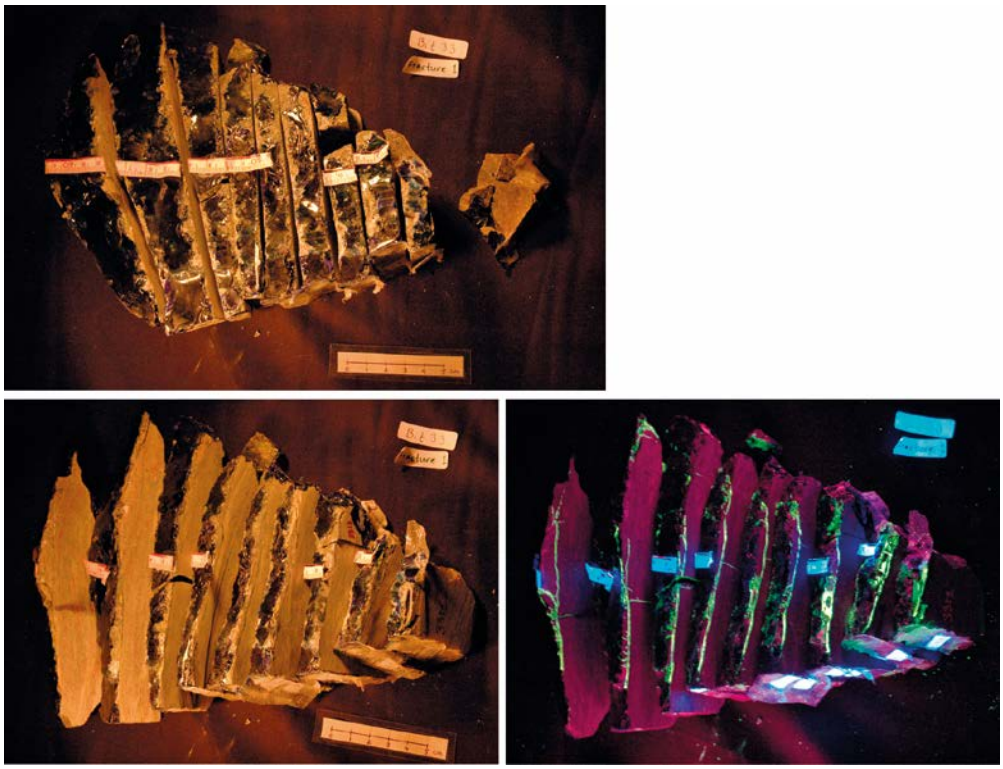

Figure A2-9. *Core piece 33. Slices 33.1 to 33.9 and on the upper picture a broken corner also is shown. Slices 33.1 to 33.6 has been cut into rods for Cs analysis.*

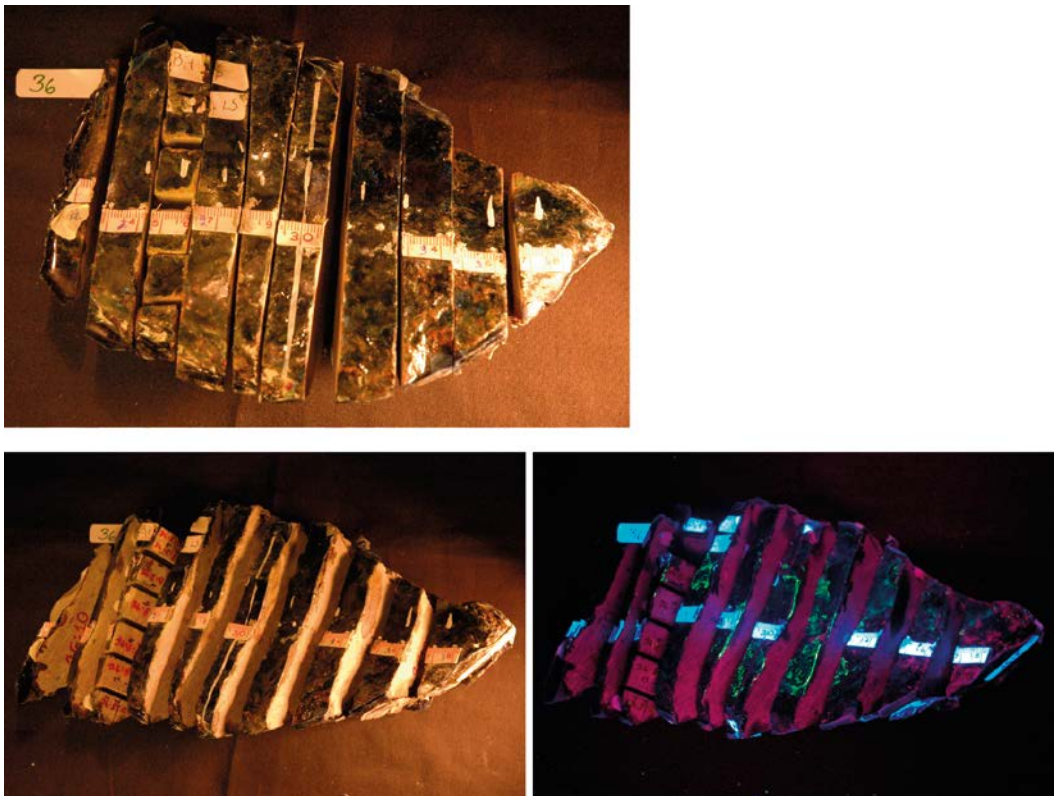

Figure A2-10. *Core piece 36. Slices 36.1 to 36.10 and on the upper picture a broken corner also is shown. Slice 36.8 has been cut into rods for Cs analysis.*

A2.2 KXTT4

Figure A2-11. *Feature A, core piece 1.I. Slices 1.I.0 to 1.I.14. Slices 1.I.2, 1.I.4, 1.I.6 and 1.I.8 to 1.I.14 have been cut into rods for Cs analysis.*

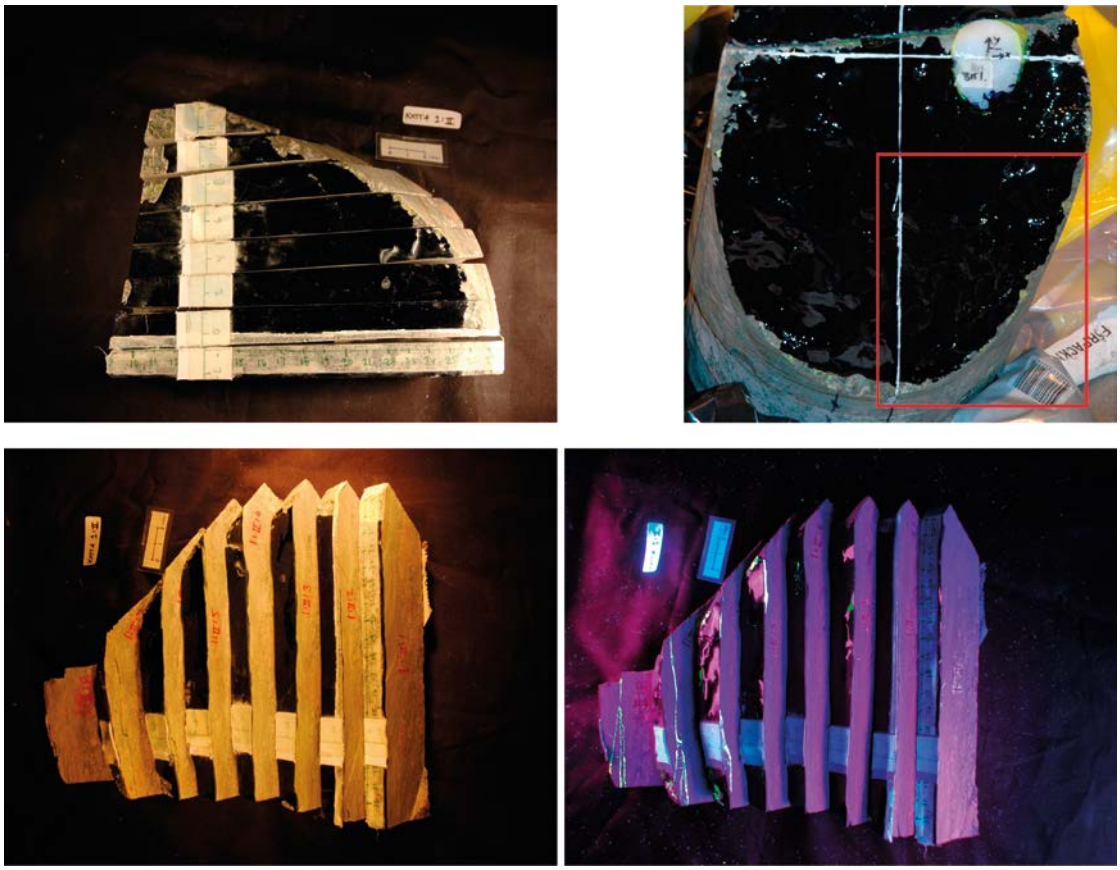

Figure A2-12. *Feature A, core piece 1.II. Slices 1.II.1 to 1.II.8. Slices 1.II.6 and 1.II.8 have been cut into rods for Cs analysis.*

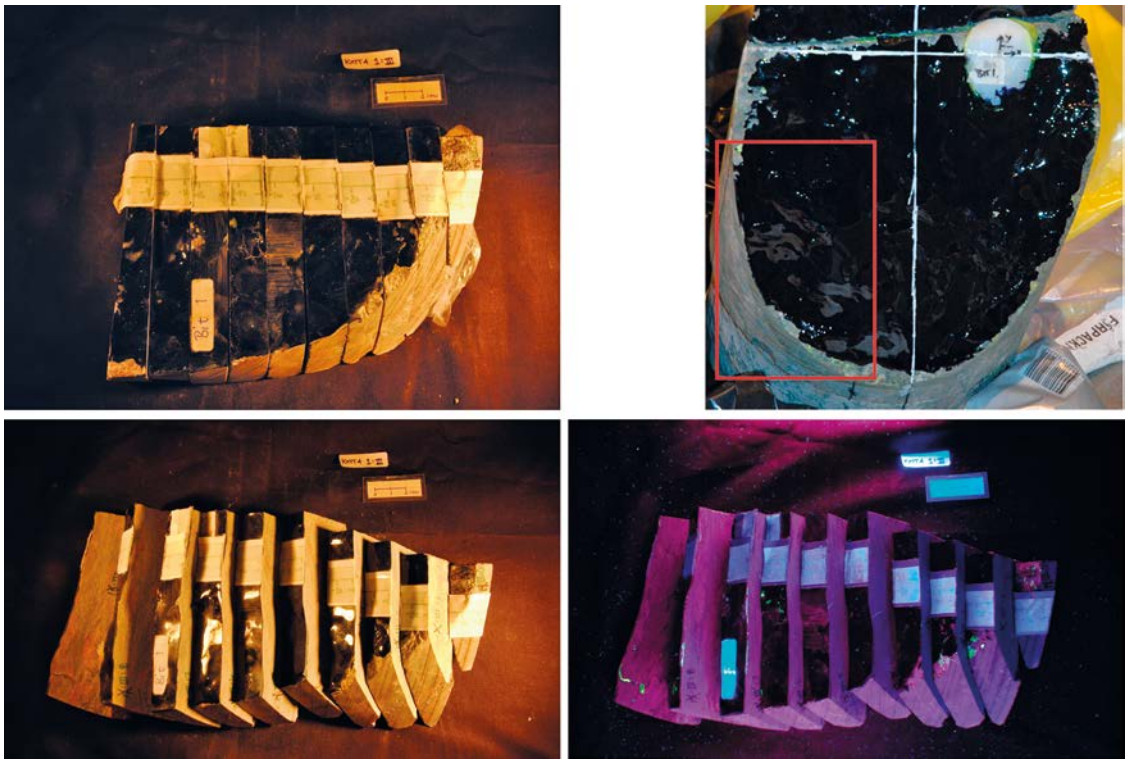

Figure A2-13. *Feature A, core piece 1.III. Slices 1.III.0 to 1.III.9. Slices 1.III.5, 1.III.7 and 1.III.9 have been cut into rods for Cs analysis.*

Figure A2-14. *Feature A, core piece 2. Slices 2.0 to 2.13. Slices 2.9 to 2.12 have been cut into rods for Cs analysis.*

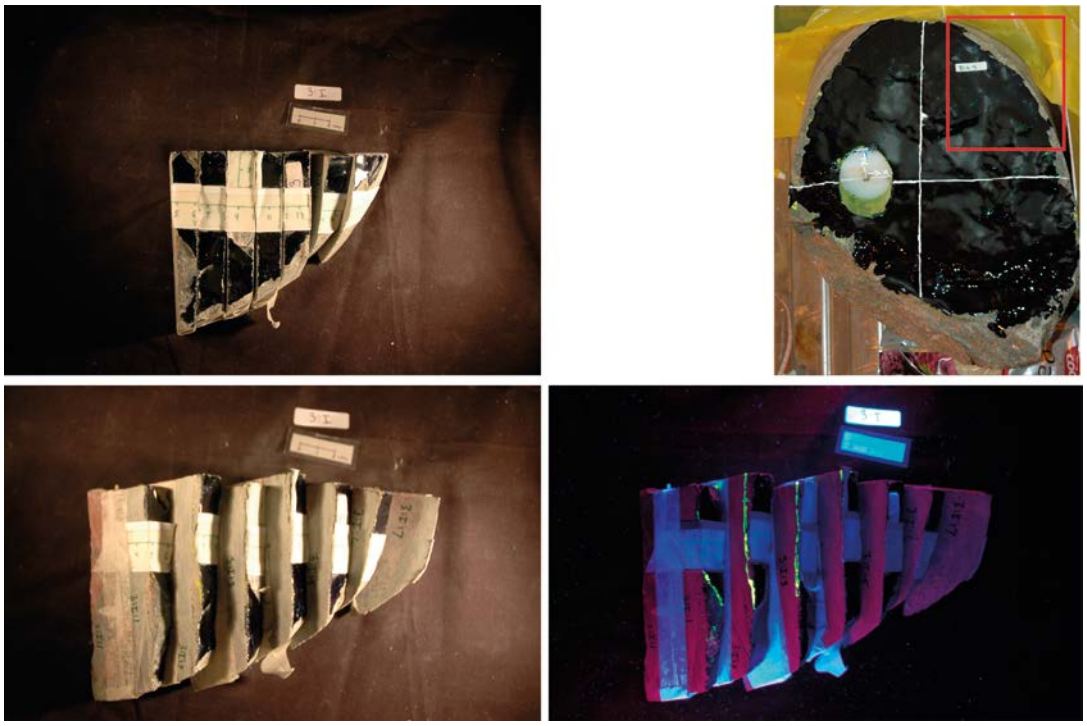

Figure A2-15. *Feature A, core piece 3.I. Slices 3.I.1 to 3.I.7. Slices 3.I.1, 3.I.3 and 3.I.5 have been cut into rods for Cs analysis.*

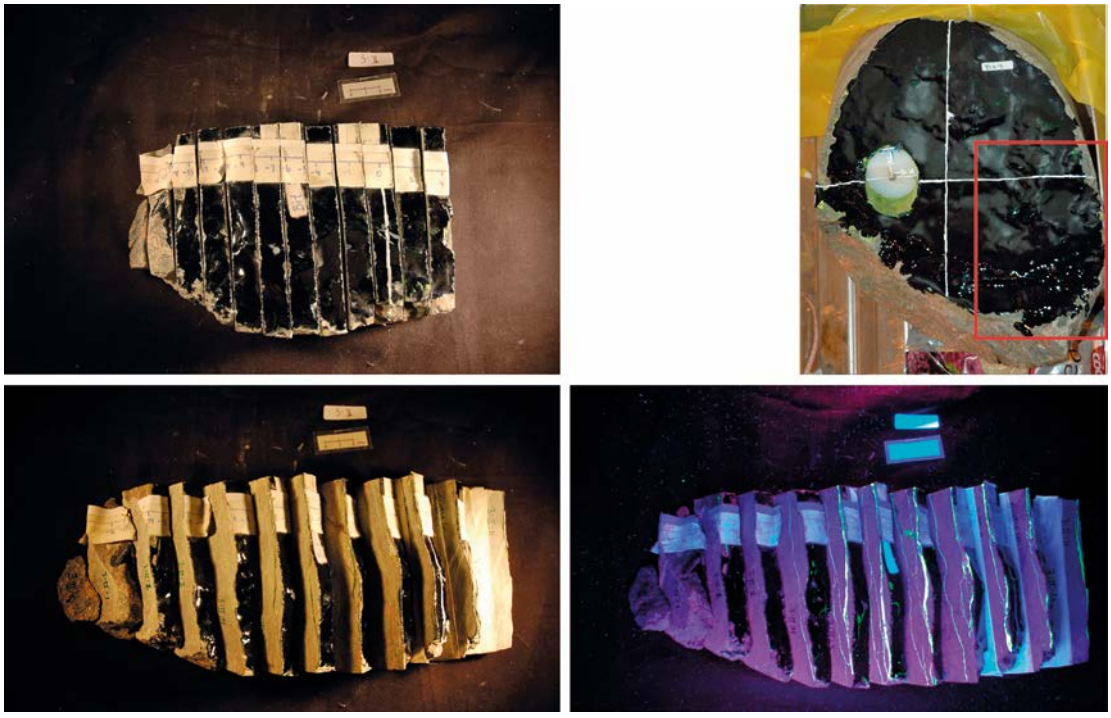

Figure A2-16. *Feature A, core piece 3.II. Slices 3.II.0 to 3.II.11. Slice 3.II.9 has been cut into rods for Cs analysis.*

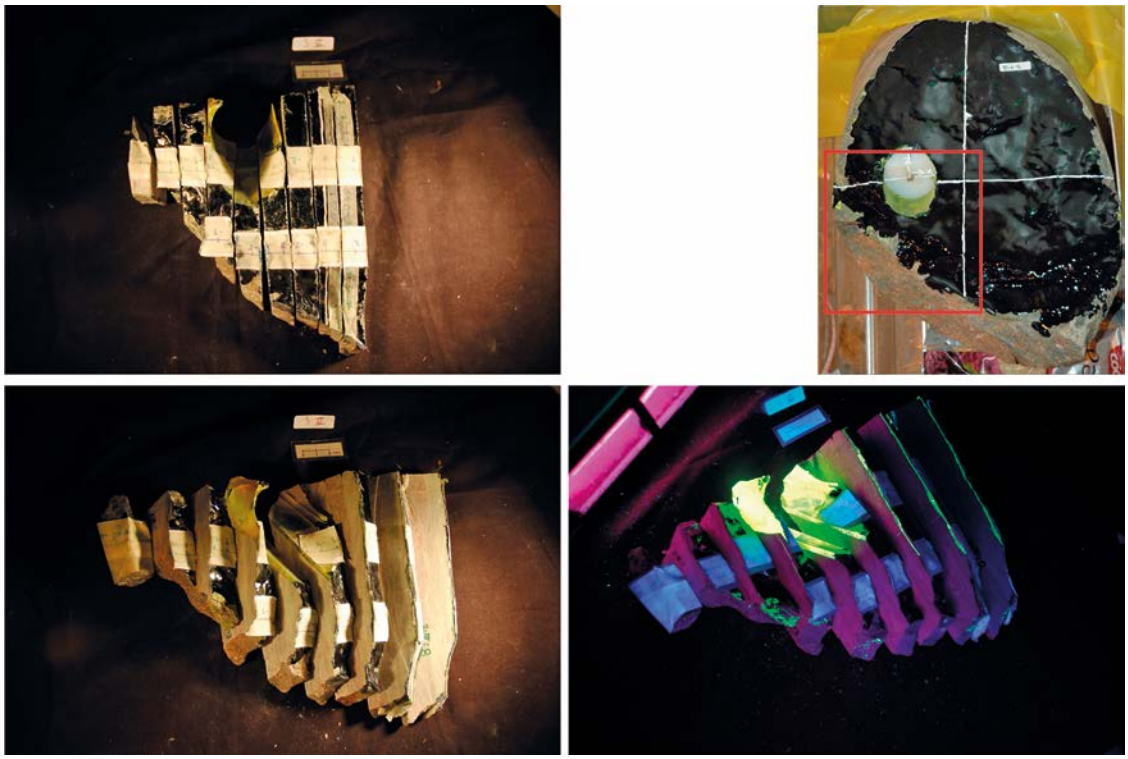

Figure A2-17. *Feature A, core piece 3.III. Slices 3.III.1 to 3.III.8. Slices 3.III.1, 3.III.3 and 3.III.5 to 3.III.8 have been cut into rods for Cs analysis.*

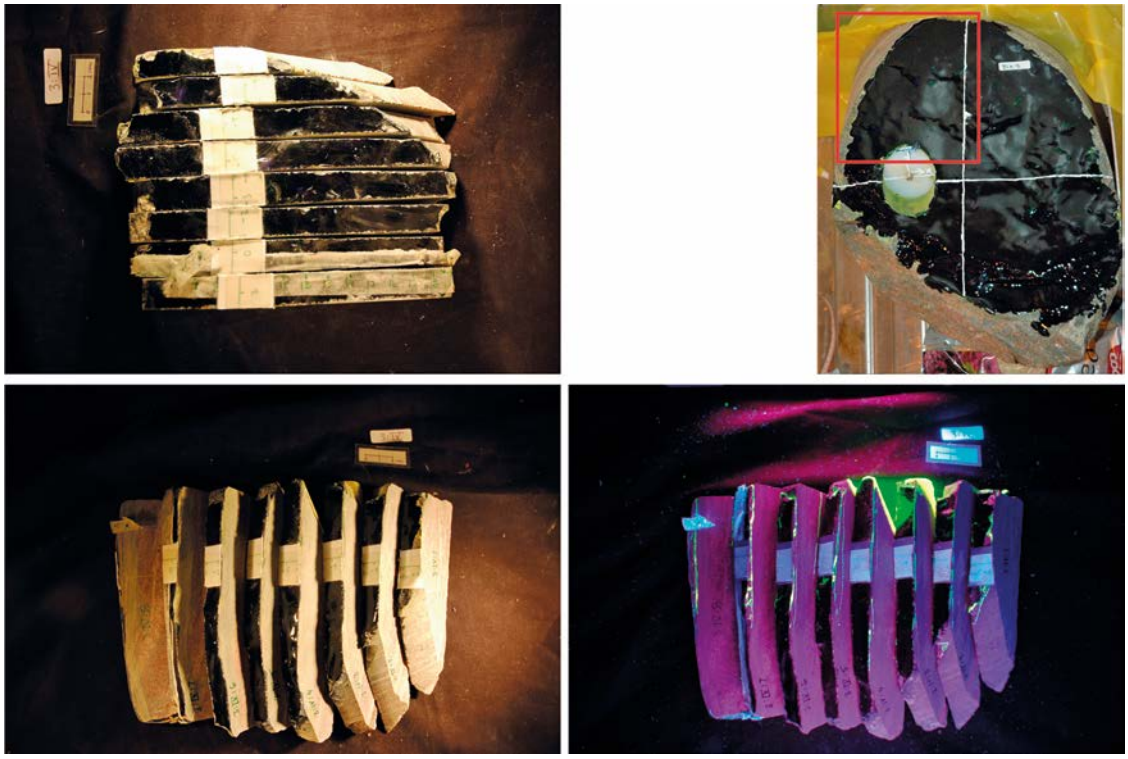

Figure A2-18. *Feature A, core piece 3.IV. Slices 3.IV.1 to 3.IV.8. Slices 3.IV.3, 3.IV.5, 3.IV.7 and 3.IV.8 have been cut into rods for Cs analysis.*

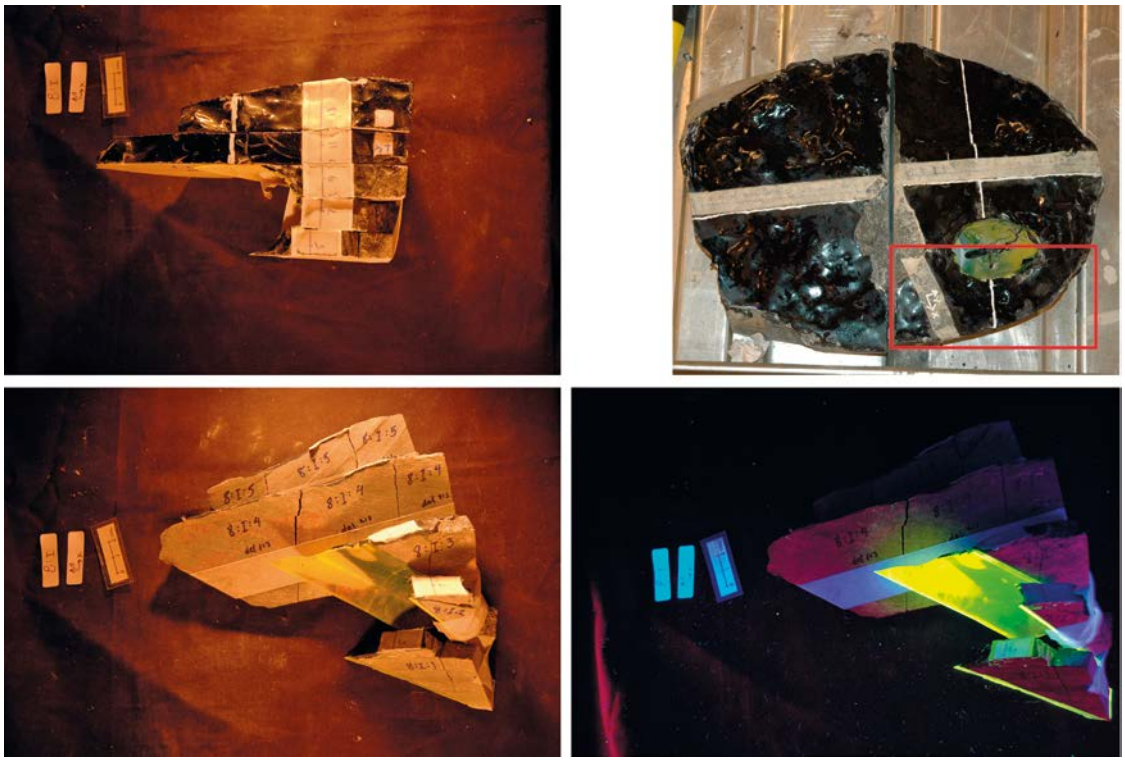

Figure A2-19. *Feature A', core piece 8.I. Slices 8.I.1 to 8.I.5.*

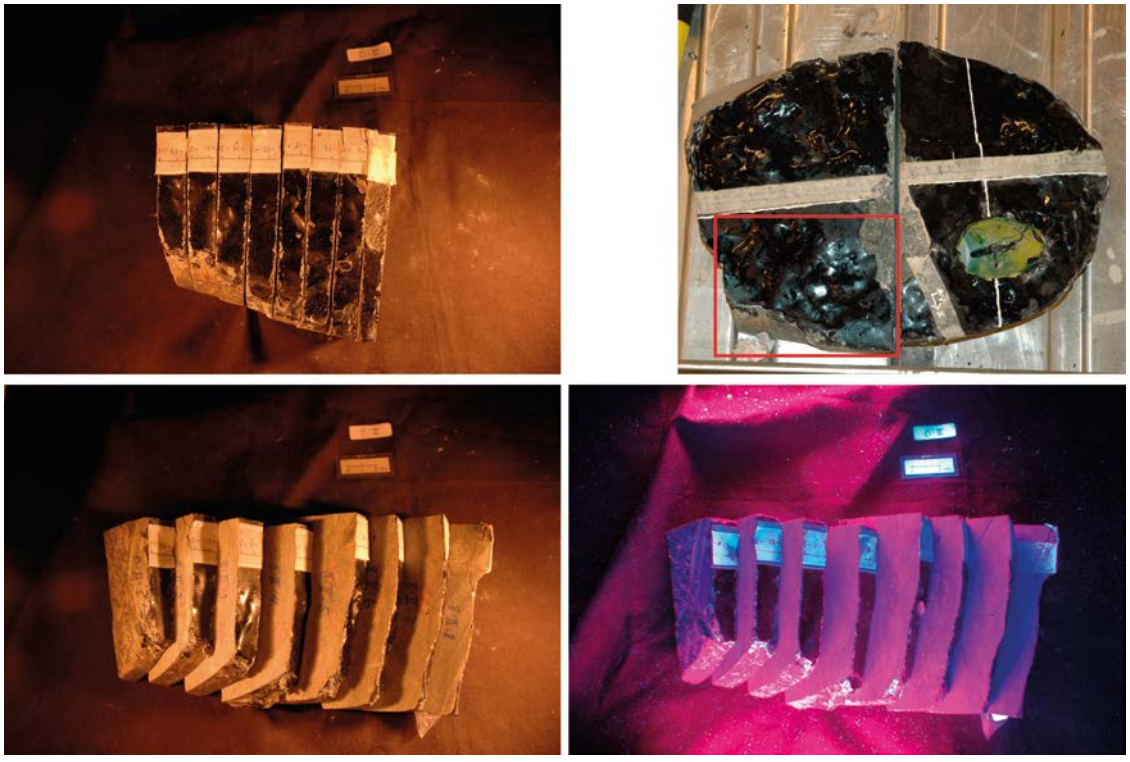

Figure A2-20. *Feature A', core piece 8.II. Slices 8.II.1 to 8.II.8. Slice 8.II.8 has been cut into rods for Cs analysis.*

Figure A2-21. *Feature A', core piece 8.III. Slices 8.III.1 to 8.III.8.*

Figure A2-22. *Feature A', core piece 8.IV. Slices 8.IV.1 to 8.IV.9.*

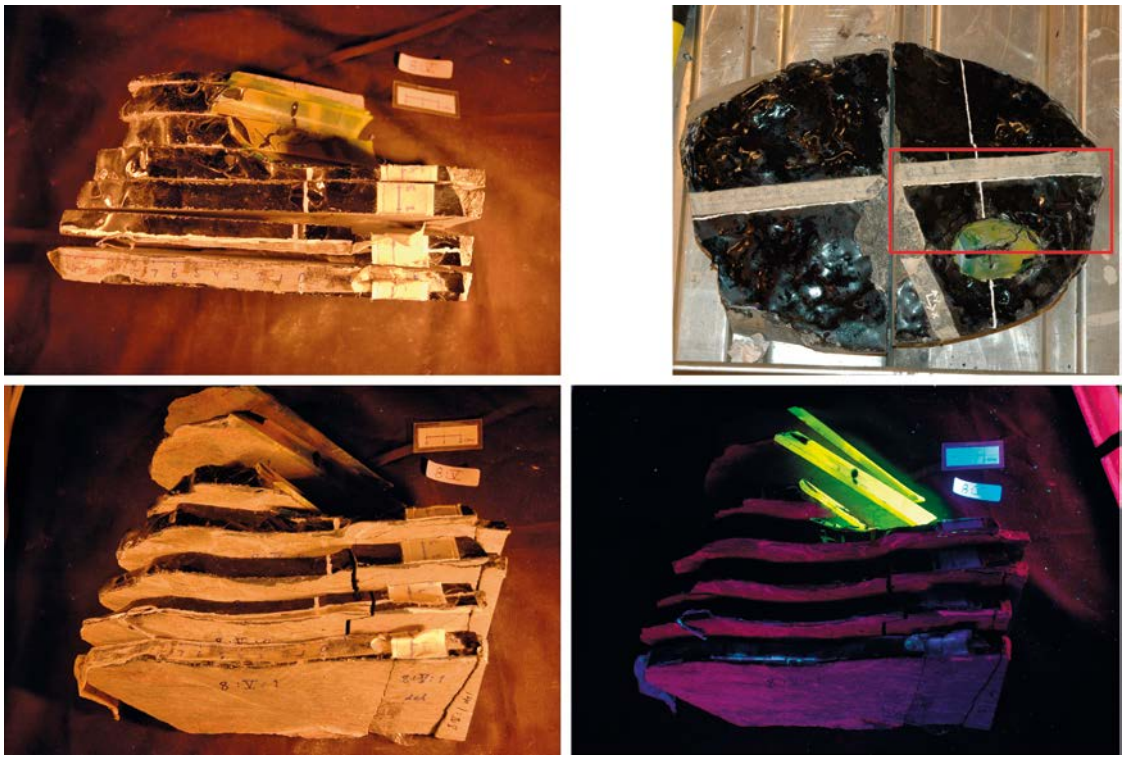

Figure A2-23. *Feature A', core piece 8.V. Slices 8.V.0 to 8.V.7. Slice 8.V.3 has been cut into rods for Cs analysis.*

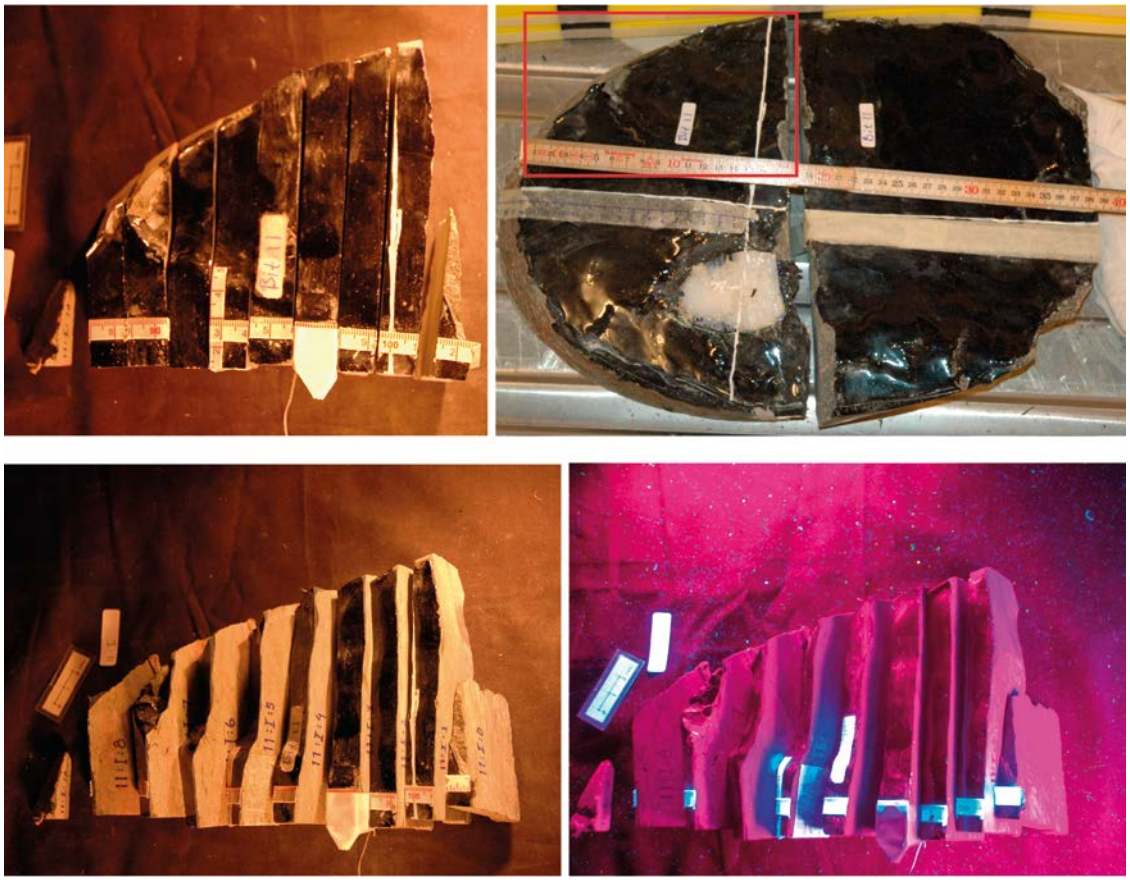

Figure A2-24. *Feature A', core piece 11.I. Slices 11.I.0 to 11.I.10.*

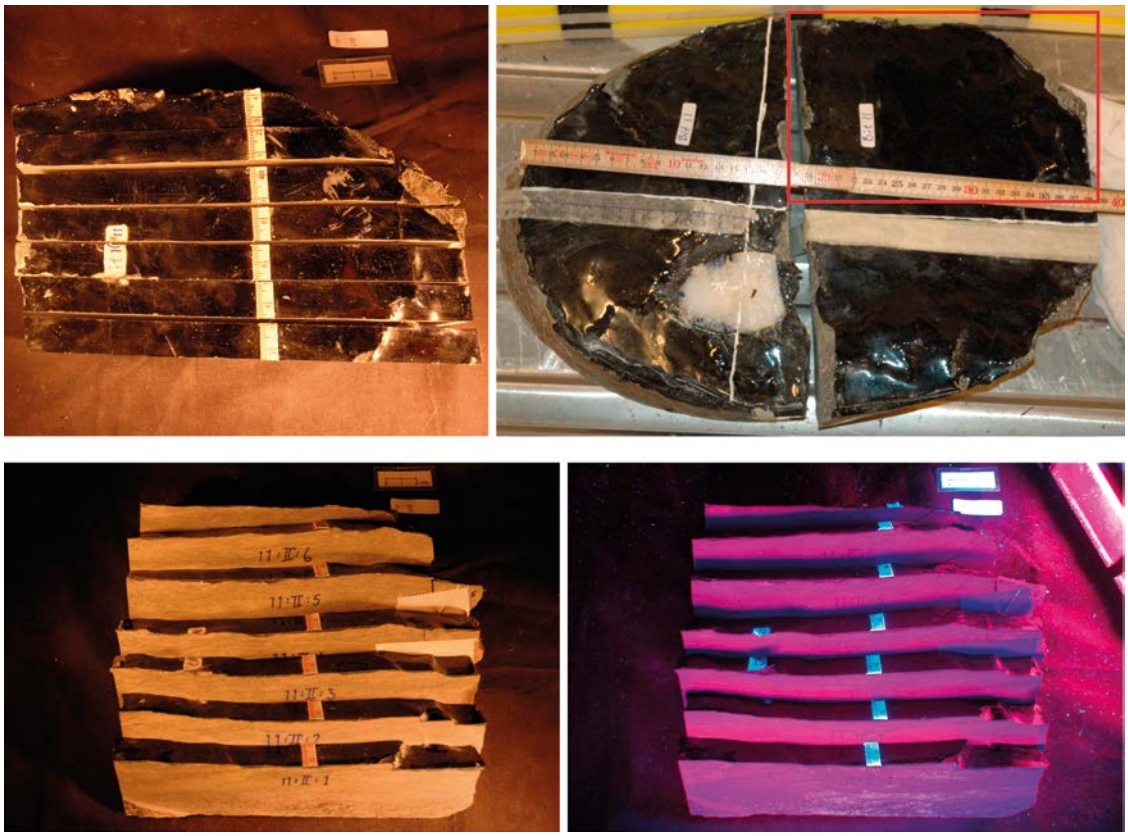

Figure A2-25. *Feature A', core piece 11.II. Slices 11.II.1 to 11.II.7.*

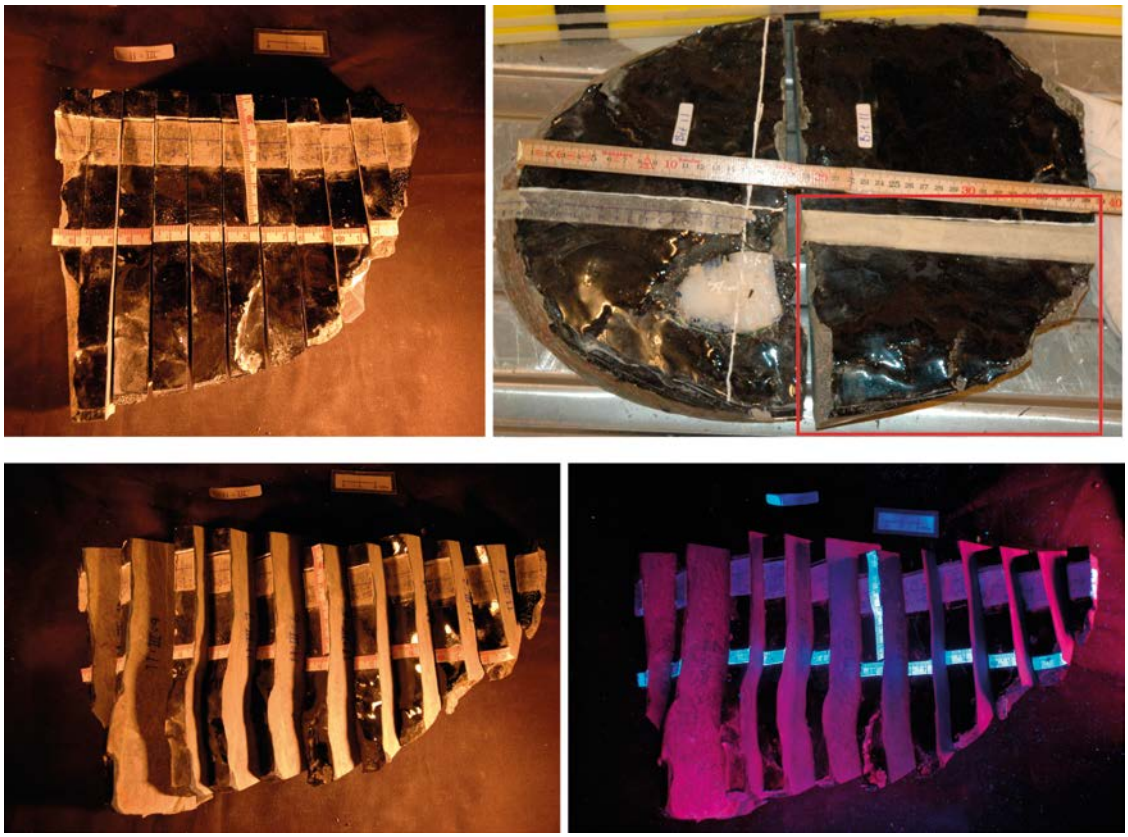

Figure A2-26. *Feature A', core piece 11.III. Slices 11.III.0 to 11.III.10. Slice 11.III.10 has been cut into rods for Cs analysis.*

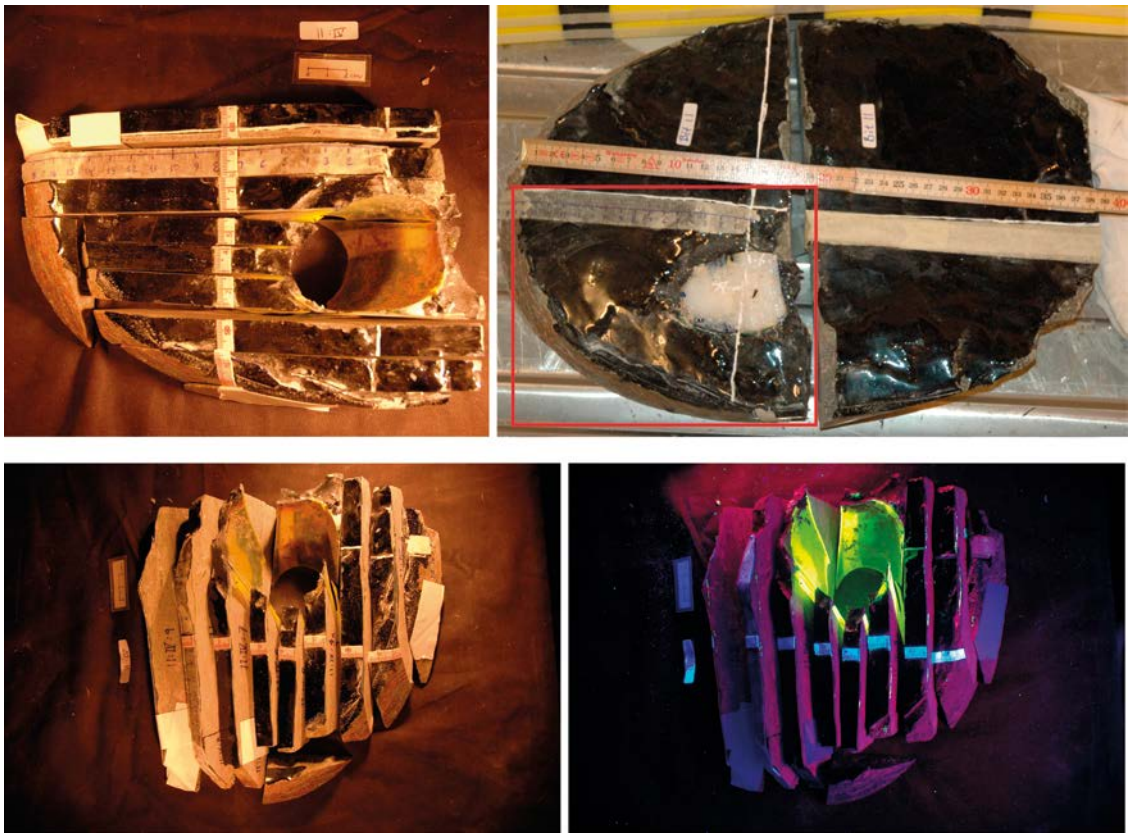

Figure A2-27. *Feature A', core piece 11.IV. Slices 11.IV.1 to 11.IV.9. Slice 11.IV.8 has been cut into rods for Cs analysis.*